universität wien

DISSERTATION / DOCTORAL THESIS

Titel der Dissertation /Title of the Doctoral Thesis

„Characterization of Dust Storms in West Asia“

verfasst von / submitted by

Seyed Omid Nabavi

angestrebter akademischer Grad / in partial fulfilment of the requirements for the degree of

Doktor der Naturwissenschaften (Dr.rer.nat.)

Wien, 2017 / Vienna 2017

Studienkennzahl lt. Studienblatt / degree programme code as it appears on the student record sheet:	A 796 605 452
Dissertationsgebiet lt. Studienblatt / field of study as it appears on the student record sheet:	Geographie
Betreut von / Supervisor:	ao. Univ.-Prof. Mag. Dr. Leopold Haimberger Univ.-Prof. Dr. Cyrus Samimi

This doctoral thesis was prepared at the Department of Meteorology and Geophysics at the University of Vienna from 03/2013 until 01/2018 and was supervised by ao. Univ.-Prof. Mag. Dr. Leopold Haimberger and Prof. Dr. Cyrus Samimi.
This is a full reprint of the dissertation submitted to obtain the academic degree of Doctor of Natural Sciences (Dr. rer. nat) and approved by the Faculty of Earth Sciences, Geography, and Astronomy of the University of Vienna.

Date of submission: 31.10.2017

Acknowledgements

First, I wish to express my sincere gratitude and appreciation to Leopold Haimberger for his tremendous guidance, genuine caring, and enthusiasm. As my supervisor, he gave me the freedom to pursue my sketchy ideas for growing as a research scientist. Since my first day in his research group, in spring 2015, he patiently taught me how to investigate a research problem, test possible causes, and finally evaluate and publish the results. Despite his busy schedules, he was always available to clarify my doubts. Thank You, Prof. Dr. Leopold Haimberger. My thanks also go to my co-supervisor Prof. Dr. Samimi who helped me, as an Iranian student, cut through red tape for starting my career at the University of Vienna. His insightful comments have been always remarkable for the compilation of my papers and Ph.D. thesis.

Words cannot express how grateful I am to my beloved wife, Reyhaneh, who was also my amicable tutor. I have continuously benefited from her up-to-date information for better understanding of statistical methods critical for accomplishing my thesis. I am particularly thankful to my office mates Dr. Michael Blaschek and Dr. Michael Mayer for all their support during my time at IMGW. Sincere thanks to the anonymous reviewers of the papers as well as all scientists involved in the production of freely available earth observation products, in particular, ECMWF, KNMI, NASA, and NCEP. This dissertation would not have been possible without funding support from the EU 7th framework program ERA-CLIM (No. 265229) and the Austrian Science Funds FWF (Projects P25260-N29).

Last but not the least, I would also like to thank my wonderful family for their sacrifices in tough days and for incenting me throughout conducting this research work. Their affection was worth more than I can express on paper.

Abstract

Extensive dust storms forming in arid areas adversely affect local inhabitants. It is well proven that constituents of dust storms such as salt, sulfur, and heavy metals cause serious respiratory diseases. Intense dust storms also shut down air and road traffic by reducing visibility or reduce crop yields by burial of agricultural fields under storm deposits. Despite the fact that the long-term characterization of dust storms is essential for providing any dust mitigation plan, until this study, it remained unclear in West Asia. In addition, this region undergoes significant degradation of agricultural fields, successive droughts, and the mismanagement of water resources. They all escalate desertification processes and, subsequently, expand the extent of dust-prone areas. Needless to say, because of this, the distribution of dust sources in West Asia needs to be reconsidered. The literature review also discloses that there were few attempts to forecast West Asian dust storms using locally evaluated model. Hence, this study aims to identify the long-term frequency of dust storms in West Asia, to designate the potential of dust emission at each grid point within the study area, known as dust source function, and to evaluate the performance of numerical models and Machine Learning Algorithms (MLAs) in the region.

In order to study the long-term, coarse scale variations of dust storms in the region, Aerosol Index (AI), from the Total Ozone Mapping Spectrometer (TOMS) and Ozone Monitoring Instrument (OMI), is examined during 1980 and 2014. Subsequently, Moderate Resolution images of Imaging Spectroradiometer (MODIS) Deep Blue (DB) Aerosol Optical Depth (AOD), from 2003 to 2014, is used to determine the severity of dust source points in a local scale. As expected, findings indicate that eastern deserts of Saudi Arabia embrace numerous dust sources which are emitting at least from 1980 onward. Further examinations have revealed that the northwest of Iraq is the main source of newly intensified dust storms entering western Iran and Persian Gulf countries since the beginning of the current century.

At the second step, previously determined dust source function, called West Asia source function (WASF), has been compared with the Ginoux Source Function (GSF). The latter is the most commonly used dust source function in

dust models. The comparison of these source functions is done by implementing them in three dust schemes used for Weather Research and Forecasting model coupled with Chemistry (WRF-chem). Resulting predictions are also compared against the simulations of Monitoring Atmospheric Composition and Climate (MACC) and Dust Regional Atmospheric Model (DREAM). Findings show that WRF-chem performance is significantly improved (Spearman correlation coefficient (SCC) increased by 12–16 percent points) after the implementation of WASF. Modified run (with WASF) even outperformed MACC and DREAM over main dust sources.

At the final step of the study, the performance of two deterministic dust models (DMs) and five MLAs is investigated to determine the most efficient dust model(s) in West Asia. Due to the lack of ground-based observations, monthly MODIS DB AOD is taken as the representative of the response variable, dust quantity. Six features including albedo, Dust Uplift Potential (DUP), Normalized Difference Vegetation Index (NDVI), soil moisture (SM), precipitation, and dust source function (SF) are selected to build MLAs using three types of Feature Selection Criteria (FSC). Results show that SF is a key feature for setting up MLAs and that MLAs, especially MARS and SVM outperformed DMs. MLA simulations have SCC of ≥ 0.76 while it is lower than 0.65 for DMs which yield high prediction error and bias (RMSE ≥ 0.2 and bias > 2) over dust sources and affected areas, respectively. Both DMs and MLAs have underestimated DB AOD peaks which is mainly attributed to the infrequency of extreme values, omission of some unknown features, and/or remaining deficiencies in source function specification. The high bias of DM simulations over dust receptors is linked to their failure in resolving the effect of the Zagros Mountains which prevent the transportation of dust to the east of the study area.

Abstrakt

Häufige Staubstürme in trockenen Gebieten beeinträchtigen die Lebensqualität der lokalen Bevölkerung. Es ist erwiesen, dass Bestandteile von Staubstürmen wie Salz, Schwefel und Schwermetalle zu schweren Atemwegserkrankungen führen. Starke Staubstürme können auch den Luft- und Straßenverkehr zum Erliegen bringen, indem sie die Sichtbarkeit verringern, und sie können Ernteerträge durch Staubablagerungen reduzieren. Trotz der Tatsache, dass die langfristige Charakterisierung von Staubstürmen für die Bereitstellung eines Staubminderungsplans unerlässlich ist, war sie bis zu dieser Studie in Westasien praktisch nicht vorhanden. Darüber hinaus verschlechtert sich in dieser Region die Qualität der landwirtschaftlichen Felder erheblich, auch wegen aufeinanderfolgenden Dürren und der Misswirtschaft der Wasserressourcen. Sie verstärken die Desertifikationsprozesse und vergrößern die Fläche der staubanfälligen Gebiete. Deshalb muss die Verteilung der Staubquellen in Westasien neu kartiert werden. Die Literaturübersicht offenbart auch, dass es kaum Versuche gab, westasiatische Staubstürme mit lokal evaluierten Modellen zu prognostizieren. Ziel dieser Studie ist es daher, die langfristige Häufigkeit von Staubstürmen in Westasien zu identifizieren, das Potenzial von Staubemissionen an jedem Gitterpunkt innerhalb des Untersuchungsgebiets, bekannt als Staubquellenfunktion, zu bestimmen und die Leistung von numerischen Modellen und Machine Learning Algorithmen (MLAs) in der Region einzuschätzen.

Um die langfristigen, grobskaligen Variationen von Staubstürmen in der Region zu untersuchen, wird der so genannte Aerosol Index (AI) aus dem Total Ozone Mapping Spectrometer (TOMS) und dem Ozone Monitoring Instrument (OMI) aus den Jahren 1980 und 2014 untersucht . Moderate Resolution Bilder von Imaging Spektroradiometer (MODIS) Deep Blue (DB) Aerosol optische Tiefe (AOD), von 2003 bis 2014, werden verwendet, um die Stärke der Staubquellen auf der lokalen Skala zu bestimmen. Wie erwartet, deuten die Ergebnisse darauf hin, dass die östlichen Wüsten Saudi Arabiens zahlreiche Staubquellen enthalten, die mindestens seit 1980 emittieren. Weitere Untersuchungen haben ergeben, dass der Nordwesten des Iraks seit Beginn des aktuellen Jahrhunderts eine neue Hauptquelle für verstärkte Staubstürme in den westlichen Iran und die Golfstaaten darstellt.

Im zweiten Schritt wurde die vorher festgelegte Staubquellenfunktion, die als West-Asien-Quellenfunktion (WASF) bezeichnet wird, mit der Ginoux-Quellenfunktion (GSF) verglichen. Letztere ist die am häufigsten verwendete Staubquellenfunktion in Staubmodellen. Der Vergleich dieser Quellenfunktionen erfolgt durch Implementierung in drei Staubschemata, die für das Wetterforschungs- und Vorhersagemodell in Verbindung mit Chemie (WRF-chem) verwendet werden. Die resultierenden Vorhersagen werden auch mit den Analysen des Monitoring Atmospheric Composition and Climate (MACC) Projekts und Vorhersagen mit dem Dust Regional Atmospheric Model (DREAM) verglichen. Die Ergebnisse zeigen, dass die WRF-Chem-Leistung nach der Implementierung von WASF signifikant verbessert wurde (der Spearman-Korrelationskoeffizient (SCC) stieg um 12-16 Prozentpunkte). Ein modifizierter Lauf (mit WASF) übertraf MACC und DREAM sogar gegenüber den Hauptstaubquellen.

Im letzten Schritt der Studie wird die Vorhersagequalität von zwei deterministischen Staubmodellen (DMs) und fünf MLAs untersucht, um das effizienteste Staubmodell (Modelle) in Westasien zu bestimmen. Aufgrund des Fehlens bodengebundener Beobachtungen wird die monatliche MODIS DB AOD als repräsentativ für den Prädiktanden Staubmenge genommen. Sechs Merkmale wie Albedo, Staubanhebungspotenzial (Dust Uplift Potential DUP), Normalisierter Differentieller Vegetationsindex (NDVI), Bodenfeuchtigkeit (Soil Moisture SM), Niederschlag und Staubquellenfunktion (Source Function SF) werden ausgewählt, um MLAs mit drei Arten von Merkmalauswahlkriterien (Feature Selection Criteria FSC) zu erstellen . Die Ergebnisse zeigen, dass SF ein Schlüsselmerkmal für die Optimieung von MLAs ist und dass MLAs, insbesondere MARS und SVM, DMs übertreffen. MLA-Simulationen haben einen SCC von ≥ 0,76, während sie für DMs niedriger als 0,65 sind, was einen hohen Vorhersagefehler und Bias (RMSE ≥ 0,2 und Bias> 2) über Staubquellen bzw. betroffenen Gebieten ergibt. Sowohl DMs als auch MLAs haben DB AOD-Peaks unterschätzt, was hauptsächlich auf die Seltenheit extremer Werte, das Fehlen einiger unbekannter Merkmale und / oder verbleibende Mängel in der Spezifikation der Quellenfunktion zurückzuführen ist. Der große systematische Fehler von DM-Simulationen über Staubrezeptoren hängt mit der Unterschätzung

der Wirkung des Zagros-Gebirges zusammen, das den Transport von Staub in den Osten des Untersuchungsgebiets großteils verhindert.

Preface

The abrupt increase of dust storms in West Asia is the main motivation of current research work. It tries to investigate this phenomenon from three different aspects: the description of dust storms behavior during last decades, the illustration of possible changes in the severity and extent of dust sources and the identification of most efficient dust modeling system. After the preparation and official approval of proposal between March 2013 and December 2014, Ph.D. candidate joined Prof. Dr. Leopold Haimberger's research group from January 2015. Since then, various types of remotely sensed datasets, ground-based observations, and dust models were used to answer aforementioned problems. The main outcomes of this attempt are three peer-reviewed papers, namely "**Climatology of dust distribution over West Asia from homogenized remote sensing data**", "**Sensitivity of WRF-chem predictions to dust source function specification in West Asia**", and "**Prediction of Aerosol Optical Depth in West Asia using Dust Models and Machine Learning Algorithms**". These studies were financially supported by the EU 7th framework program ERA-CLIM (No. 265229) and the Austrian Science Funds FWF (Projects P25260-N29).

I hereby declare that I have written this PhD thesis using only resources stated. Whenever a source is cited after the last full stop in a paragraph the citation concerns the whole paragraph (besides the other sources cited therein).

Wien, 11/12/2017

---------- ----------

Place, Date Signature

Contents

List of figures

Acronyms

AOD	Aerosol Optical Depth
AERONET	AErosol RObotic NETwork
AFWA	Air Force Weather Agency
ANN	Artificial Neural Networks
AVHRR	Advanced Very High-Resolution Radiometer
BF	Basis Function
CALIPSO	Cloud-Aerosol Lidar and Infrared Pathfinder Satellite Observations
DB	Deep Blue
DMs	Deterministic Models
DOD	Dust Optical Depth
DREAM	Dust Regional Atmospheric Model
DSF	Dust Source Function
DUP	Dust Uplift Potential
ECMWF	European Centre for Medium-Range Weather Forecasts
EMs	Embedded-type methods
ESA-CCI	European Space Agency Climate Change Initiative
FSC	Feature Selection Criteria
FoO	Frequency of Occurrence
FMs	Filter-type methods
FT	Fixed Threshold
GCV	Generalized Cross-Validation
GIMMS	Global Inventory Modeling and Mapping Studies
GPCC	Global Precipitation Climatology Centre
GOCART	Goddard Chemistry Aerosol Radiation and Transport
GSF	Ginoux Source Function
MACC	Monitoring Atmospheric Composition and Climate
MARS	Multivariate Adaptive Regression Splines
MI	Mutual Information
MISR	Multi-angle Imaging SpectroRadiomete
MLAs	Machine-Learning Algorithms
MLR	Multiple Linear Regression
MODIS	Moderate Resolution images of Imaging Spectroradiometer

MSE	Mean Squared Error
NCL	NCAR Command Language
NDVI	Normalized Difference Vegetation Index
OMI	Ozone Monitoring Instrument
OOB	Out-Of-Bag
PCC	Pearson Correlation Coefficient
POCD	Probability Of Correct positive Detection
POFD	Probability Of False positive Detection
PSS	Peirce Skill Score
RF	Random Forest
RFE	Recursive Feature Elimination
RMSE	Root Mean Square Error
RSS	Residual Sum of Squares
SeaWIFS	Sea-viewing Wide Field-of-view Sensor
SF	Source Function
SPEI	Standardised Precipitation-Evapotranspiration Index
SCC	Spearman Correlation Coefficient
SVM	Support Vector Machines
TOMS	Total Ozone Mapping Spectrometer Aerosol Index
VT	Varying Threshold
WASF	West Asia Source Function
WMs	Wrapper-type methods
WRF-chem	Weather Research and Forecasting model coupled with Chemistry

PART I: RESEARCH FRAMEWORK

1 Objectives and research questions

Dust storms are known as a natural phenomenon through which eroded soil particles may be lifted to a very high altitude and be transported over long distances. The disastrous consequences of dust storms in West Asia necessitate the investigation of the dust cycle at a climatology time scale. However, the lack of ground-based observations, particularly in Iraq and Syria, have hindered the regular monitoring and characterization of dust events. In spite of some limitations, remote sensing techniques provide an unprecedented capability to study the frequency and origins of dust clouds on a daily basis since the 1980s. In addition, dust modeling systems are widely being used to complement remotely sensed datasets by the 3D simulation of past events (hindcast) and to assist mitigation plans by the prediction of forthcoming dust storms (forecast). Hence, this study uses long dust-related records from different satellite platforms and sensors to provide a clearer picture of the spatio-temporal distribution of dust storms in West Asia during past decades. Subsequently, the most currently used numerical dust models are compared with new statistical counterparts to identify the most efficient strategy for dust forecast in the region. The first part (I) of this thesis discusses existing studies regarding 1- the application of remote sensing datasets in the long-term characterization of dust storms in West Asia, 2- the most commonly used methods for the specification of dust source function (SF), and 3- the prediction (estimation) of dust using numerical dust models (DMs) and machine learning algorithms (MLAs). These studies are then summarized to provide an outline of state of the art research gaps which explain the necessity of presented study. They also lay the path for forming research questions and hypotheses. At the end of this part, materials and methods that are applied to reach research goals are discussed. In Part II, three peer-reviewed articles, building the core of this dissertation, elucidate the main research activities. The formatting of the corresponding journals is maintained. Part III finally presents results in a synthesis and provides an outlook.

1.1 Introduction

Dust storms result from turbulent winds which raise large quantities of dust particles into the atmosphere and reduce visibility to less than 1000 m (McTainsh and Pitblado, 1987). With respect to the severity of dust entrainment, the extent of affected area, and characteristics of dust-laden atmospheric circulations, this phenomenon can be also called blowing dust (Novlan, 2007), dust haze (Adefolalu, 1984), dust devil (Lorenz et al., 2016), and Haboob (Vukovic et al., 2014). Blowing dust can cause a significant decrease in visibility but not as intense as a dust storm. Dust haze consists of very tiny suspended particles left from a passing dust storm. Dust devil results from atmospheric instability over strongly heated surfaces in local scale. It appears as a column of dust with a length between 30 m and 300 m. The Haboob is the result of descending cold air in front of thunderstorms which form dense clouds of dust in a larger scale comparing to a dust devil. Not to be confused with a dust storm, a sandstorm occurs when sand-sized particles are lifted to low altitudes by very strong winds and fall out of the air faster than finer particles of a dust storm (Ahrens, 2011, Goudie and Middleton, 2006). In this study, all aforementioned phenomena are considered as dust storm since they are not differentiable in regional scale through existing instruments.

The initiation of soil particle movement, the minimum wind velocity needed for erosion (erosion threshold), depends on the surface properties including soil texture and moisture and surface roughness (Ginoux et al., 2001). As wind velocity exceeds the erosion threshold soil particles are transported in three physical regimes: suspension (< ~70 μm diameter), saltation (~70 – 500 μm diameter), and creep (> ~500 μm diameter) (Kok et al., 2012). Large erodible particles are first to be moved (creeping) and/or ejected from the surface. Lifted particles (~70 – 500 μm diameter) follow a ballistic trajectory (saltation) and cause the saltation bombardment of the surface downwind and ejection of new particles. In fact, aerodynamic forces are mostly not strong enough to overcome interparticle cohesive forces and to induce direct entrainment of soil particles. Instead, sandblasting hit the surface and eject soil particles with a wide range of sizes that follow a similar saltating motion or remain in the atmosphere up to several weeks (Bagnold, 2012, Kok et al., 2012, Marticorena, 2014, Shao, 2008, UNCCD, 2001).

Dust storms mainly form over regions which undergo intense desertification caused by climate change and human activities (Kadomura, 2009). Reciprocally, dust can intensify desertification through soil erosion and transport known as land degradation (Middleton and Kang, 2017). Seasonal, local dust storms are known as typical events in West Asia (Shao et al., 2011b). They can be seen throughout the region especially over alluvial plains in Syria and Iraq. High-speed Shamal winds, with northwest-southeast direction, increase the intensity of these dust storms during summer months that used to affect only the downwind transport regions in the southeast of Iraq and Kuwait. The simultaneous increase of dust cases and the expansion of affected areas to Iran and the Persian Gulf countries have recently raised the attention of scientist (Azizi et al., 2012, Boloorani et al., 2013). The concentration of dust storms entering Iran is so severe that Ahwaz, located in the southwest of Iran, was announced as the most air-polluted city in the world in 2011 (Time Magazine, 2011). Interestingly, three other cities in western Iran including; Sanandaj, Kermanshah, and Yasuj have been also named in the list of 10 most air-polluted cities of this year (Figure 1).

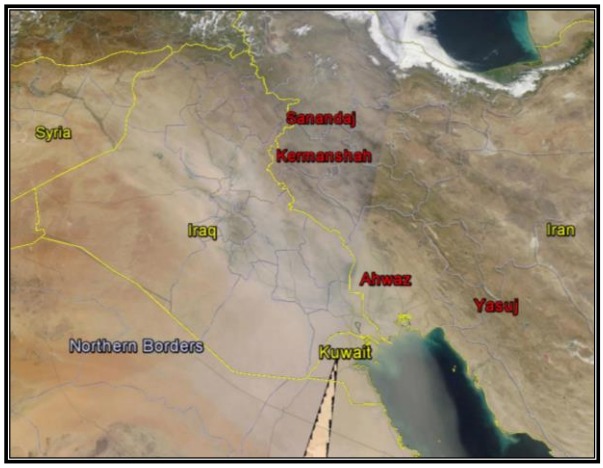

Figure 1 dust storm formed in Iraq and Syria is heading western Iran on 10/06/ 2013. Dust image is acquired from MODIS and is stacked in Google Earth.

Regarding the purposes of this study, the research background will be discussed in the next subsection from three different perspectives including 1. Long-term spatio-temporal characteristics of dust storms, 2- the specification of dust source function (map) in regional and global scales, and 3- the prediction of dust storms using DMs and MLAs.

1.1.1 Review of studies related to long-term spatio-temporal characterizations of dust storms

As expected, the long-term study of dust storms requires having access to long-recorded dust measurements. Furman (2003) tried to characterize dust events in the Middle East, using meteorological visibility data. The results indicated that the stations in the southwest of Iran, the north of Saudi Arabia, and Persian Gulf countries have recorded most dust events in the summertime during 1973 to 1993. Using data from synoptic stations, Azizi et al. (2012) investigated dust events in the southwest of Iran and concluded that they have increased within two periods of 1982 and 1990, and 2005 and 2008 in warm months. Because of data limitations such as data gaps, human errors in recording data, and more importantly poor distribution of weather stations especially in desert areas, ground-based measurements are mostly used for verification. Meanwhile, remote sensing tools and techniques potentially provide an unprecedented capability to capture the spatio–temporal distribution of dust storms. Many algorithms have been developed to detect dust particles from other atmospheric phenomena and ground surface features. Due to the strong absorption of Ultraviolet (UV) radiance by dust and, conversely, low ground surface reflectivity in this spectral region, an Aerosol Index (AI) has first been defined by Torres et al. (1998) for Total Ozone Mapping Spectrometer (TOMS) and Ozone Monitoring Instrument (OMI) UV radiances. TOMS-OMI AI has provided the longest global measurement of aerosols from 1979 to the present. Using this dataset, Prospero et al. (2002) have determined topographic depressions, like Mesopotamia, as the main source of dust storms. Even though researchers can benefit from the appropriate time coverage of the AI database, it cannot be used in recognizing local sources due to its unfavorable spatial resolution (1.0 ° x 1.0 °). Failing to detect dust particles in the lower atmospheric layers, being unable to discriminate dust particles from other aerosols, being contaminated by cloud covers and having sensitivity to aerosol layer height are known as other weaknesses of AI (Goudie and Middleton, 2006, Washington et al., 2003). The Moderate Resolution Imaging Spectroradiometer (MODIS) instrument, which started operating on the Terra and Aqua platforms from 1999 and 2002, respectively, could resolve most of the aforementioned deficiencies by having 36 spectral bands and high spatial resolution of 250 -

1000 meters. Numerous dust studies have been conducted based on MODIS data (Bullard et al., 2008, Hao and Qu, 2007, Qu et al., 2006, Thorsteinsson et al., 2011, Zhang and Reid, 2010). Hsu et al. (2004) implemented Deep Blue (DB) Aerosol Optical Depth (AOD) algorithm on MODIS images which is not only insensitive to dust layer height but also able to detect dust cloud over a bright surface, e.g., desert areas, at a high resolution of 10 km. Using MODIS DB AOD, Ginoux et al. (2012) have tried to distinguish dust particles from other types of aerosols, examine the global dust frequency, and identify dust sources. Results show that dust activities in the east of Iran have been profoundly influenced by annual water stream fluctuations, whereas newly intensified dust plumes of Iraq mostly form in desert areas, called natural dust sources. Besides MODIS, DB AOD data at 550 nm can also be acquired from measurements of Sea-viewing Wide Field-of-view Sensor (SeaWiFS). These data are accessible in two resolutions of 0.5 ° and 1° from 1998 to 2010. Hsu et al. (2012) have used this dataset to identify distribution and trends of aerosols in global and regional scales. Results show strong relationships between Saharan dust export as well as biomass-burning activity in the tropics with climate indices such as El Niño Southern Oscillation (ENSO).

In spite of recent improvements of remote sensing techniques in the long-term retrieval of dust-related information, the literature disclosed that existing research focusing on West Asia have used satellite data only for case studies (Abdi Vishkaee et al., 2012, Ashrafi et al., 2014, Boloorani et al., 2014, Samadi et al., 2014). In fact, the comprehensive characterization of dust storms in the region requires the combined application of the discussed datasets over a long period.

1.1.2 Review of studies related to the specification of the dust source function

Dust storms mostly form in arid and semi-arid areas where dry soil, sparse vegetation, high-speed winds and erodible sediments favor dust emission. However, a quantitative calculation of dust emission has always been a challenge (Bullard et al., 2011, Cao et al., 2015, Koven and Fung, 2008, Lee et al., 2009, Walker et al., 2009). Ginoux et al. (2001) prepared a topography-based global dust source function (SF) (Equation 1), which will be referred to as "Ginoux source function (GSF)" in this research.

Equation 1: $$S = (\frac{Z_{max} - Zi}{Z_{max} - Z_{min}})^5$$

S is the probability value assigned to pixel i to have accumulated sediments at altitude Zi, where Zi is normalized in proportion to maximum Z_{max} and minimum Z_{min} altitudes over a surrounding area of 10 ° x 10 °. Kumar et al. (2014) noted that the calculation of S requires dense observations of alluvium within the field. Due to the lack of data, S is indirectly assessed based on topographic features. GSF has been first implemented in the Goddard Chemistry Aerosol Radiation and Transport (GOCART) aerosol model, and has been applied to bare soil surfaces (Cavazos-Guerra and Todd, 2012). Bare surfaces were designated based on land cover data from the advanced very high-resolution radiometer (AVHRR) (DeFries and Townshend, 1994). Kim et al. (2013) argued that a static land cover does not reflect annual and seasonal variations of soil bareness. Therefore, they used 15-day normalized difference vegetation index (NDVI) from AVHRR and prepared a dynamic bareness map (NDVI < 0.15) and, consequently, a dynamic SF. Results show significant improvements in GOCART simulations over regions with seasonally changing soil bareness. However, further examinations indicated that the progress is rather small in a global perspective. It is attributed to the small contribution (12 %) of these regions to global dust emission. There are only small seasonal changes of soil bareness over West Asia and thus this modification does not cause significant changes in values of GSF in the region. Ginoux et al. (2012) proposed a new algorithm for SF determination in which elevation quantities are replaced with the MODIS DB AOD. Considering physical and optical properties of aerosols, authors extracted dust optical depth (DOD) from 2003 to 2009. Frequency of Occurrence (FoO) of DOD > 0.2 was used as a criterion for the determination of dust sources. According to findings of several studies (Boloorani et al., 2013, Cao et al., 2015, Moridnejad et al., 2015b), this new SF erroneously allocate high values of erodibility to a vast boundary region between Iraq and Saudi Arabia. Parajuli et al. (2014) have prepared the most recent global SF by normalizing the Spearman correlation coefficient (SCC) between monthly wind speed at 10 m and DB AOD, both with the resolution of 1 degree. Considering that wind speed and dust concentration are very dynamic

and resolution dependent, the analysis of rough spatial resolution data on a monthly basis does not seem robust enough to represent the instantaneous conditions along with dust events. Moreover, using correlation coefficient for dust source determination has led to unacceptable results over non-erodible areas such as western Iran. That is, the region of the Zagros Mountains which cannot have any contribution to dust emission (Gerivani et al., 2011), but it is attributed with erodibility values comparable with desert areas in the east of Saudi Arabia. In other words, this method leaves some values everywhere even if it is made of non-erodible lands.

The review of aforementioned studies shows that GSF, as the mostly used source function in dust forecast, needs to be updated since it is proposed when we did not have access to such long-term, free available satellite observations of dust activity as we have today. Considering the fact that other discussed studies failed to provide a realistic picture of dust sources in West Asia, it is necessary to use the knowledge about the long-term spatial distribution of dust storms for the preparation of a more accurate dust source function for the region in the second step.

1.1.3 Review of studies related to the forecast of dust storms

Dust storms are classically forecasted by deterministic dust models (DMs) which contain concentrations of at least one aerosol species as prognostic variables (Basart et al., 2012, Kumar et al., 2014, Liu et al., 2007, Marticorena and Bergametti, 1995). For short-range operational forecasts where there is nearly complete theoretical knowledge about the nature of the relationships between prognostic variables and boundary conditions, they are quite useful. However, they still have difficulties reproducing dust-related observables such as DB AOD on a monthly time scale because of limitations both in model formulation and observation operators. For predicting monthly means of AOD based on predictors available for the same months, the relationships between response and explanatory variables are less well known. However, they have been monitored through a significant number of observations. For such situations MLAs have shown a promising performance in solving engineering problems for more than three decades (Abbasi et al., 2014, Carbonell et al., 1983, Cortes and Vapnik, 1995, Hempel et al., 2012, Kotsiantis et al., 2007,

LeCun et al., 2015). MLAs are already frequently used for the prediction of air quality of urban areas (Taheri Shahraiyni and Sodoudi, 2016) and have also been applied to the adjustment of satellite AOD (Albayrak et al., 2013, Hyer et al., 2011) to have a better fit to ground-based observations. However, to the best of our knowledge, there are only a few scientific attempts to predict AOD over a whole West Asia through MLAs. Using Multiple Linear Regression (MLR), Klingmüller et al. (2016) modeled AOD, as the representative of dust concentration, in a coarse resolution of 2 degrees. Yu et al. (2015) used a similar technique for the seasonal prediction of dust storms in Saudi Arabia. The temporal correlation of 0.7 and 0.74 are achieved for summer and spring, respectively. Kaboodvandpour et al. (2015) have compared the performance of MLR in dust prediction with Artificial Neural Networks (ANN), and Adaptive Neuro-Fuzzy Inference System (ANFIS). They have chosen $PM_{10} > 200$ μg m-3 at Sanandaj station (dust receptor in Iran) as the indicator of dust occurrence (response variable). Results show that ANN and ANFIS have yielded the highest agreement (the highest $R^2 = 0.86$) and the highest consistency (the lowest Root Mean Squared Error (RMSE) = 0.07) with observations, respectively, whereas MLR has performed poorly ($R^2 = 0.416$ and RMSE = 0.0965).

To sum up, the literature left significant gaps in the high-resolution prediction of dust quantity through MLAs over whole study area and disregarded inter and cross-comparison of MLAs and DMs over a long-term period.

1.2 Research questions and hypotheses

Against the background of long-term characteristics of dust storms, dust source specification, and dust forecast, this study pursues three major aims including 1- the improvement of the knowledge about the long-term spatio-temporal distribution of West Asian dust storms using remotely sensed datasets, 2- The preparation of a local SF providing a more realistic distribution of dust sources in the study area, and 3- the development of a local dust model which has higher spatial and temporal resolutions than those described in literature. To fulfill study purposes, three major research questions and corresponding hypotheses should be addressed:

1. **What are the spatio-temporal characteristics of dust activity in West Asia during recent decades?**

The possibility of access to long records of dust quantity, the recent improvements in dust retrieval algorithms, and the significant advancement of the computational power have provided an unprecedented opportunity to study dust storms in finer spatial and temporal resolution than literature at a climatology time scale. This leads to the first hypothesis:

Hypothesis 1: the combination of remote sensing products such as TOMS-OMI AI and MODIS DB AOD help to identify the long-term characterizations of dust storms in West Asia. Research findings will indicate a significant increase in dust occurrence during the last decade. Considering the recent upsurge of dust storms, numerous dust source points are newly formed in the study area.

2. **Does a remote sensing-based SF provide a realistic distribution of dust sources in the study area? Does it outperform topography-based counterpart?**

The accurate determination of dust sources is not only critical for finding hot spots where dust mitigation programs are mainly planned for, but it provides more accurate dust emission susceptibility needed for dust forecast.

Hypothesis 2: Existing source functions, specifically GSF, do not provide a realistic distribution of dust sources in West Asia. Instead, the potential of dust emission can be quantified through the analysis of dust frequency detected by remotely sensed observations. The implementation of more realistic SF can improve the prediction accuracy of dust models.

3. **What is the best approach to be adopted for dust prediction on the monthly time scale in the study area?**

While DMs are mainly used for dust prediction, the applicability of MLAs is not fully examined yet. Particularly the dust prediction on monthly time scales, which contains many uncertainties that are not so well represented in DMs, Machine Learning Algorithms seem viable and cost-effective alternatives. In addition, there is a lack of comparative studies evaluating the performance of DMs and MLAs.

Hypothesis 3: The promising performance of MLAs in engineering problems can be also achieved in dust prediction. Considering the fact that,

here, MLAs are not elaborated and their standard settings are applied (e.g. Gaussian kernel for SVM or linear regression as the output-layer function of ANN) MLAs do not outperform DMs at this stage.

2 Materials and methods

This section briefly presents the study area and introduces the data and methods used to test the hypotheses. Long-term satellite time series with different spatial resolutions are combined with ground-based observations to characterize the spatio-temporal distribution of dust storms (research question 1). Remotely sensed datasets and the Weather Research and Forecasting model coupled with Chemistry (WRF-chem) are used to specify a new SF for the study area (research question 2). Seven state of the art DMs (2 models) and MLAs (5 models) are compared over West Asia for a sizeable period of eight years to determine the most efficient local dust model(s) (research question 3). Data and methods are explained in detail in part II in the corresponding manuscripts.

2.1 Study Area

The present study is conducted in West Asia where has numerous dust source points (Fig. 1). They are mainly located in Tigris-Euphrates alluvial plains in Iraq and Kuwait, the low-lying flatlands along the Persian Gulf and the Ad Dahna and the Rubal Khali deserts, the Oman coastal area, the Great Salt Desert in the basin to the south of Alborz mountains, Seistan Basin and Registan bordering Iran, Afghanistan and Pakistan, and Makran coastal area (Shao et al., 2011b). Because of the direction of prevailing winds (west to east), this study focuses on dust frequency over source area of Iraq, Syria and Saudi Arabia (western half of the study area).

2.2 Research data

The research described here require the application of datasets from different sources. The following data are not discussed with the regard to their precedence of use in the study but to sources they are acquired from including 1- ground-based observations 2- satellite imagery 3- model forecast and reanalysis.

2.2.1 Ground-based observations

Three datasets including present weather codes (the first and second manuscripts), ground-based AOD at 0.55um (used in all three manuscripts), and monthly precipitation (the third manuscript) are acquired from/based on ground-based observations. It is also worth mentioning that the Standardised Precipitation-Evapotranspiration Index (SPEI) used in the third manuscript is calculated mainly based on ground-based records of precipitation, acquired from Climatic Research Unit (CRU). However, because this index is only used for the preliminary examinations (not for building the final dust models), it is not described here. Further information about this index can be found on http://spei.csic.es/index.html.

- Present weather codes from manned synoptic stations:

  Visibility is known as the most relevant information of weather stations to dust quantity. It is defined as a measure of the distance at which a landmark at, say, 1 km, 2 km, and 10 km can be clearly discerned. In the most stations of the study area, meteorological visibility is estimated by the human observer which degrade the quality of reports. As such, author decided not to use values of visibility but their simultaneous present weather codes which represent certain atmospheric phenomena. Weather codes are read out via given descriptions for each. In this case, numbers between 6 and 9 and 30 and 35 are assigned to different intensity and occurrence time of dust and sandstorms. The code 98 is also representative of the occurrence of dust-laden thunderstorms (Takemi and Seino, 2005). Here the occurrence of any one of aforementioned codes is taken as the indicator of dust outbreak. Distribution of weather stations whose visibility data are used is presented in figures 7 and 3 of first and second manuscripts, respectively.

- Ground-based AOD from AERONET stations:

  AERONET, an acronym for AErosol RObotic NETwork, is a ground-based standardized automatic sun/sky-photometer network (Eck et al., 1999, Holben et al., 1998). AERONET collaboration aims to provide properties of aerosols as well as water vapor content. Sun–photometers (with a field of view of 1.2 degree) retrieve aerosol optical depth at all of the following wavelengths: 0.34, 0.38, 0.44, 0.50, 0.67, 0.87, 1.02, and 1.64um. Here interpolated AOD at 0.55um with a quality level of 2 (cloud–screened and quality-assured) is used.

The uncertainty of the AERONET AOD is spectrally dependent, with higher errors in the UV (<0.44um), and is typically between ±0.010 and ±0.02 under cloud-free conditions (García et al., 2008, Tan et al., 2015). In spite of the significant accuracy of AERONET AOD, the sparse distribution of AERNOET stations (Fig. 7, first manuscript) and, in some cases, short monitoring period limit this product to used only for the validation of satellite data (Bibi et al., 2015) and verification of model forecasts (Ginoux et al., 2001).

- Monthly precipitation from GPCC:

  The Global Precipitation Climatology Centre (GPCC) provides gridded gauge-analysis monthly precipitation for a period between 1901 and 2013 (Rudolf et al., 1994, Rudolf and Schneider, 2005). The GPCC monthly precipitation is collected from quality-controlled data of 75,000 stations over land, with monitoring durations of 10 years or longer. This product is updated on monthly basis using global data acquired via the Global Telecommunication System of the World Weather Watch (GTS) of the World Meteorological Organization (WMO). GPCC provides the monthly totals on a regular grid with a spatial resolution of 0.5 (used in this study), 1.0, and 2.5 degrees latitude by longitude (Schneider et al., 2011). "Full Data Reanalysis Version 7" used here is known as the most accurate dataset of GPCC. However, systematic measuring error and stochastic sampling error may decrease the validity of the data. For example, the latter can cause the relative errors between +/- 7% and 40% of the true area-mean (Rudolf et al., 1994).

2.2.2 Satellite imagery

In this study, three dust-related satellite products including Aerosol Index (AI, the first manuscript), standard AOD (the second manuscript), and DB AOD (all manuscripts) are utilized to explain the long-term behavior, main sources, and formation process of dust storms in West Asia. In addition, remotely sensed soil moisture and vegetation cover datasets are used for dust modeling in the third manuscript.

- AI from TOMS and OMI:

  As written by Nabavi et al. (2016), TOMS-OMI AI is known as the longest aerosol records from 1979 to present. TOMS installed on Nimbus 7 recorded data from 1979 to 1993 with a spatial resolution of 1 × 1.25 degrees. After a 4-

year cessation, it continued data gathering on the Earth Probe platform until the end of its operation in 2005. With one-year data overlap, OMI has provided AI in the resolution of 0.25 degrees from 2005 to present. In this study, TOMS-like OMI AI, named OMTO3d_V003, in 1-degree resolution, was used to have a more consistent dataset. The accuracy and precision of the OMTO3d_V003 are similar to the legacy TOMS data, except over cloudy areas where OMTO3d_V003 data is more accurate than that of the TOMS (Ahmad et al., 2004, Vasilkov et al., 2008). AI positive values are representative of mineral dust, smoke and volcanic aerosols (Ahmad et al., 2006). While the TOMS-OMI AI seems ideal for climatological studies, Mahowald and Dufresne (2004) have pointed out that AI is sensitive to dust layer height. That is, higher dust clouds lead to higher, exaggerated, AI values over desert areas and during warm periods of the year whereas dust quantity (AI) is underestimated over cooler periods and areas.

- AOD from MISR and CALIPSO

  Aerosol Optical Depth (AOD), which is also referred to as aerosol optical thickness (AOT), is known as the measure of aerosol quantity including dust. It represents the amount of light scattered or absorbed by aerosols in a column through the atmosphere; vertically-integrated aerosol extinction coefficient (Li et al., 2016). AOD, commonly reported at 550 nm, < 0.1 is the indicator of a crystal clear sky whereas high values of AOD (> 3) indicate the presence of very thick aerosols clouds.

  Multi-angle Imaging SpectroRadiometer (MISR) is one of operating NASA's Earth Observing System (EOS) instruments which observes the Earth through four spectral bands, 0.446, 0.558, 0.672, and 0.866um at nine discrete view angles. MISR's 36 data channels (4 spectral bands x 9 view angles) allow retrieving unique information about aerosols (i.e. different aerosol particle types) comparing to other EOS instruments (Kahn et al., 2010, Kahn et al., 2005). The repeat coverage of the common swath (at least 360 km) of all nine cameras is 9 days at the equator, and 2 days at poles. Although the multi-angle view of MISR, on Terra platform, could provide valuable information for the retrieval of dust particles over bright surfaces, its lower sampling is known as a drawback to measuring the short-scale variability of dust events (Li et al., 2015).

Hence, daily MISR AOD 550nm (MIL3DAE v4), with a resolution of 0.5° by 0.5°, is used only for the validation of model forecasts (second manuscript).

In this study, the need to evaluate model simulations of the vertical profile of dust is address by the use of aerosol extinction coefficient from Cloud-Aerosol LIDAR and Infrared Pathfinder Satellite Observations (CALIPSO). CALIPSO payload is launched in April 2006. It is equipped with three-channel (8.65, 10.6 and 12.05 microns) Infrared Imaging Radiometer (IIR), visible channel Wide Field Camera (WFC), and polarization-sensitive, two-wavelength lidar (CALIOP). CALIOP provides profile information of aerosols during daytime and nighttime at two wavelengths; 532 and 1064 nm (Thorsen et al., 2011). The CALIOP measurements are generally degraded during daytime due to sunlight contamination (Adams et al., 2012, Sun et al., 2016). Therefore, it is decided to use only nighttime profiles of extinction coefficients (at 532nm). This product is accessible at vertical and horizontal resolutions of 60 m and 5 km, respectively, and with a revisit time of 16 days from 2006 to 2016 (Adams et al., 2012, Ma et al., 2013).

- DB AOD from MODIS and SeaWiFS

  Considering the fact that retrieving dust particles over bright surfaces has been always challenging problem ever since the applications of satellite remote sensing (Liou and Chou, 2008), Hsu et al. (2004) implemented DB AOD algorithm on MODIS images, at a high resolution of 10 km (Sayer et al., 2014). This algorithm makes use of the 412 nm band, which sometimes is referred to as “deep blue” band, for the clear discrimination of aerosols signals (bright at deep blue) and the surface signals (dark at deep blue). MODIS, the first satellite imagery freely available to the public, is a key instrument onboard EOS Terra (launched December 1999) and Aqua (launched May 2002) satellites. The orbit of Terra and Aqua is timed so that the former, formally called EOS AM-1, goes from north to south across the equator in the morning and the latter, formally called EOS PM-1, passes south to north over the equator in the afternoon. This would result in the coverage of the entire Earth's surface every 1 to 2 days. The spatial resolution of MODIS (pixel size at nadir) is 250 m for channel 1 and 2 (0.6 µm - 0.9 µm), 500m for channel 3 to 7 (0.4 µm - 2.1 µm), and 1000 m for channel 8 to 36 (0.4 µm - 14.4 µm).

Sea-Viewing Wide Field-of-View Sensor (SeaWiFS), onboard OrbView-2, also provide needed measurements for the calculation of DB AOD. SeaWiFS, launched on August 1, 1997, provides eight spectral bands in the visible/near-infrared (VNIR) regions. SeaWiFS imagery is stored at an original spatial resolution of 1 km and its daily DB AOD is publically accessible in two resolutions of 0.5 ° (used here) and 1 ° from 1998 to 2010.

It has been shown that MODIS and SeaWiFS DB AOD have an uncertainty (one-standard-deviation confidence interval) of ±(0.03+20 %) and ±(0.05+20 %), respectively (Sayer et al., 2012, Sayer et al., 2013).

- NDVI from AVHRR

  In the third manuscript, the normalized difference vegetation index (NDVI) dataset, produced under the framework of the the Global Inventory Modeling and Mapping Studies (GIMMS) project, called NDVI3g (Tucker et al., 2005), is used to consider vegetation cover changes in the study area. Several corrections have been implemented to reduce deleterious effects of calibration loss, orbit drift, and volcanic eruption on NDVI retrieval (Chang et al., 2016, Tucker et al., 2005). NDVI3g has been derived from 15-day maximum NDVI values of AVHRR sensor mounted on NOAA 7 to 18 satellites. It has spatial and temporal resolutions of 8km and bimonthly, respectively, and accessible dataset covers the time period from July 1981 to December 2015 (Pinzon and Tucker, 2014).

- Soil moisture from ESA-CCI program

  The Climate Change Initiative (CCI) soil moisture is part of the European Space Agency (ESA) Climate Initiative program for providing Essential Climate Variables (ECV) (Liu et al., 2012, Liu et al., 2011, Wagner et al., 2012). It aims to address the needs of climate research community to long-term consistent soil moisture time series (Haas et al., 2013). This program, initiated in 2010, has provided daily surface soil moisture based on active and passive microwave sensors including C-band scatterometer data (ERS-1/2 scatterometer, METOP Advanced Scatterometer) and multi-frequency radiometer data (SMMR, SSM/I, TMI, AMSR-E, Windsat, AMSR2) during 1979 to 2014. In this study, the COMBINED dataset (CCI SM v02.2) which has a grid resolution of 0.25 degree is used.

2.2.3 Model forecast and reanalysis

Three quite different state of the art dust modeling systems including WRF-chem, Monitoring Atmospheric Composition and Climate (MACC), and Dust Regional Atmospheric Model (DREAM) are used to get fields of daily modelled AOD and dust optical depth (DOD) for summertime (Jun, July, and August) of five years between 2008 and 2012 (the second manuscript) and monthly mean AOD for April to September between 2003 and 2013 (the third manuscript).

Finally, ECMWF reanalysis is discussed as the main data source for the environmental drivers of dust formation (MLA inputs).

- AOD from WRF-chem

  WRF-chem is a fully coupled online community model (Fast et al., 2006, Grell et al., 2005, Skamarock et al., 2008) designed as Euler nonhydrostatic model to serve both operational forecasting and atmospheric research needs (Bian et al., 2011). The WRF-chem modeling system is commonly used to analyze the full interaction of dust particles and other atmospheric phenomena like cloud formation (Smoydzin et al., 2012, Ward and Cotton, 2011) or to investigate dust radiative forcing (Alizadeh Choobari et al., 2013). There is a variety of schemes available, including the Goddard Chemistry Aerosol Radiation and Transport (GOCART) (Ginoux et al., 2001), the Air Force Weather Agency (AFWA) (Su and Fung, 2015) and the University of Cologne (UoC) (Shao et al., 2011a), to parameterize mineral dust cycle. In this study, WRF-chem 3.6.1 is initiated using ERA-Interim analyses as lateral boundary conditions. Newtonian nudging toward ERA-Interim is used to keep the forecasts close to the observed atmospheric state. Soil moisture is provided from National Centers for Environmental Prediction (NCEP) Final (FNL) Operational Global Analysis data and precipitation is a standard forecast product. Total column dust concentration is the primary forecast variable which is converted into AOD at 550nm using a radiative transfer code (a so-called observation operator, (Chin et al., 2002)). For detailed descriptions of WRF-chem configuration please refer to Nabavi et al. (2017b).

- AOD and DOD from MACC

  The European Center for Medium-range Weather Forecasting (ECMWF) has provided daily aerosol forecasts including dust as the main outcome of the MACC (2003-2012) project and its successor the Copernicus Atmospheric

Monitoring Service (CAMS) (July 2012 to present). The MACC data assimilation system was constructed by extending the basic meteorological forecast system, called the Integrated Forecasting System (IFS) of ECMWF, to monitor and forecast reactive gases and five aerosol species, including mineral dust (Inness et al., 2013). The modeling part of aerosol modules of MACC (and CAMS) reanalysis are initially implemented based on Morcrette et al. (2009). Benedetti et al. (2009) complemented it with the assimilation of satellite dust-sensitive observations, namely MODIS AOD (Cuevas et al., 2015). That is, the MACC dust product is thus not a forecast but a reanalysis which certainly strengthens this product. However, MACCs primary focus is on atmospheric chemical species, not so much mineral dust. Therefore, the parameterizations for dust have been tuned relatively little.

- DOD from DREAM

  DREAM is a dust modeling system initially developed in the World Laboratory Centre, Erice, Italy between 1991and 1993. Since then, it has been continuously improved and transferred to some European dust-related research centers. Currently, it is run at the Barcelona Supercomputing Center (BSC). It focuses mainly on North Africa but also covers West Asia (Basart et al., 2012). Author has not run DREAM himself but used products from BSC-DREAM8b v2.0 version, simply called DREAM. The forecast model is initialized every 24 hours with NCEP/FNL Operational Global Analysis data and the same analysis data are used as lateral boundary conditions during the forecast runs. It provides dust optical depth at 550 nm (used in the second manuscript), dust surface concentration, and total column dust concentration as prognostic variables which can be downloaded from www.bsc.es.

- MLA features from ERA-Interim

  At the time of writing this thesis, ERA 5 reanalysis, available from 2010 to 2016, is the latest reanalysis from ECMWF. Its predecessor ERA-Interim reanalysis, used in this study, is accessible from 1979 to present (Dee et al., 2011) at a 3-hourly time resolution. According to documentation, ERA-Interim uses 2006 release of the IFS (Cy31r2) as data assimilation system which has a 4-dimensional variational analysis (4D-Var) with a 12-hour analysis window and spatial resolution of 80 km (T255 spectral) on 60 vertical levels from the surface up to 0.1 hPa (https://www.ecmwf.int/en/research/climate-

reanalysis/era-interim). Four ERA-Interim variables including 10m wind, vertical velocity, soil temperature, and albedo are used to provide some of MLA inputs (the third manuscript).

2.3 Research methods

Like research data, methods split into three sections allotted to the discussion of approaches used for the long-term study of dust storms, the specification of a local dust source function, and the preparation of a local dust model. In fact, this section summarizes methods used for the fulfillment of three steps of the study.

2.3.1 Long-term spatio-temporal characterization of dust storms

As discussed above, TOMS-OMI AI is favorable for the long-term characterization of dust storms. However, its high sensitivity to aerosol height (Mahowald and Dufresne, 2004) causes overestimation of aerosol concentration over desert areas and warm periods of the year. In addition, replacing TOMS with OMI caused an artificial decrease in AI over West Asia which can be erroneously interpreted as the reduction of dust frequency.

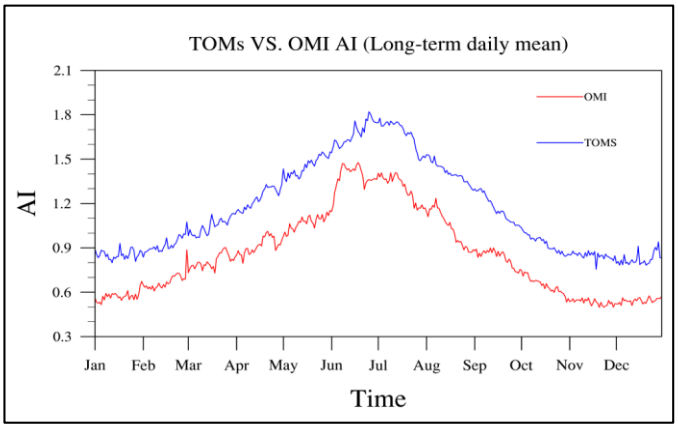

Figure 2 Area average of long-term daily mean AI over West Asia (20N to 40N and 35E to 65E). The blue curve shows area-averaged TOMS AI between 1980 and 2001 and red curve represents OMI AI between 2005 and 2014.

In order to tackle these problems and some other issues such as calibration drift of Earth Probe TOMS between 2002 and 2004 (Kiss et al., 2007) and miscalculation of AI over cloudy pixels, following measures are taken:

1. Besides the data gap between 1993 and 1996, AI recorded by TOMS during 2002 to 2004 are excluded from further examinations.

2. Because of the lower accuracy of TOMS AI over cloudy pixels, the long-term study of AI is limited to warm months (April to September) when subtropical high pressure is the dominant atmospheric pattern over West Asia resulting in mostly cloud-free conditions throughout the region.

3. Following Mahowald and Dufresne (2004), AI values or a Fixed Threshold (FT) were not used. Instead, AI has been binarized through preparing a varying threshold (VT) for the warm months to deal with the sensitivity of AI data to aerosol height. Here VT was defined as the multi-year average of AI simultaneous with SeaWiFS DB AOD between 0.5 and 0.55 during the study period.

4. Regarding the discontinuity of AI measured by TOMS and OMI, VT is separately prepared for these two instruments (Fig. 3).

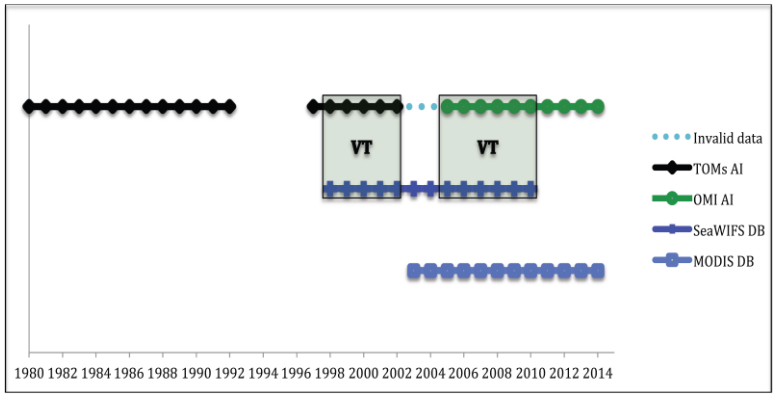

Figure 3 homogenization scheme of AI.

Having determined VT, the rough location of dust sources is determined by using the FoO of dust storms defined as the number of days where AI data exceed VT. Permanent dusty areas are empirically defined as where have a FoO > 800 in both periods 1980 to 1997 and 1998 to 2014. Emerging areas have FoO < 500 in 1980 to 1997 and FoO > 500 in 1998 to 2014 in most pixels. Extinct areas (practically non-existent) have FoO > 800 in 1980 to 1997 and FoO < 500 in 1998 to 2014. Considering the fact that this algorithm provides a binary mask of dust sources in a large scale, the magnitude of dust emission is locally quantified by the use of MODIS DB AOD. Hence, total FoO of MODIS DB AOD > 0.85 during warm months is considered as the magnitude of dust sources (Moridnejad et al., 2015a). This approach has paved the path to the specification a new dust source function described in the following section.

2.3.2 Specification of dust source function for West Asia

The prior information regarding the distribution and severity of dust sources in large (using AI) and local (using DB AOD) scales are the basis of newly proposed source function for the study area, called West Asia Source Function (WASF). In other words, WASF (Figure 4-A) is mainly constructed on the knowledge grasped from the first step of the study (Nabavi et al., 2016). The only modification is that FoO of DB AOD > 0.7 was used for the quantification of dust sources, instead of DB AOD > 0.85, to detect all active source points in the region. Comparing to GSF, WASF results in a general reduction in the erodibility in the region and consequently in dust flux. This inevitably reduces the concentration of simulated dust emission and resulting AODs. However, here, the priority is to provide a more accurate distribution of dust sources in West Asia. If so, this underestimation, a systematic bias, can be fixed through manipulation of tuning parameters.

In order to compare the performance of WASF and GSF (Fig. 4-B), they are implemented in three dust schemes of WRF-chem.

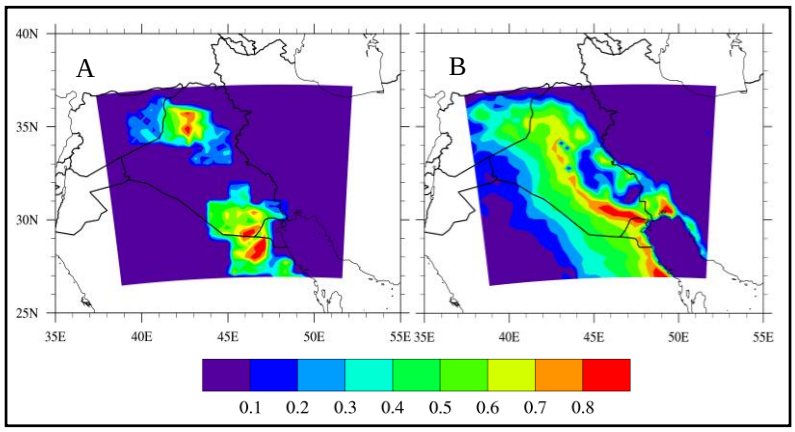

Figure 4 A: WASF designated based on FoO of DB AOD > 0.7 bounded by emerging and permanent dust source masks. B: Ginoux source function (GSF) acquired from WRF terrestrial inputs.

WRF-chem is executed for the summertime of 2008 to 2012 on a domain which is centered on 32 ° N and 45 ° E extending from about 26.5 ° N to 36.5 ° N (40 grid points) and from about 38 ° E to 52 ° E (45 grid points) with 40 levels in the vertical on a Lambert projection. In addition, DREAM and MACC DOD are also acquired for the same period to be compared with modified (with WASF) and control (with GSF) runs.

2.3.3 Developing local dust model

In order to determine a superior dust modeling system for West Asia, two different approaches, namely MLAs and numerical models, are compared (Nabavi et al., 2017a). Here, DB AOD is taken as response variable to be predicted through Five MLAs, including Random Forest (RF) Breiman (2001), Multivariate Adaptive Regression Splines (MARS) (Zhang and Goh, 2016), Support Vector Machines (SVMs) (Vapnik, 1995), Artificial Neural Network (ANN) (Konate et al., 2015), and Multivariable Linear Model (MLR) and two DMs, including WRF-chem and MACC. The study period is six months from April to September of 2003 to 2013. The study area is within the same domain as the previous step. While the descriptions of DMs are presented in the subsection 2.2.2, the general process of MLA setup, training (2003-2010) and test (2011-2013) parts, is shown in Figure 5.

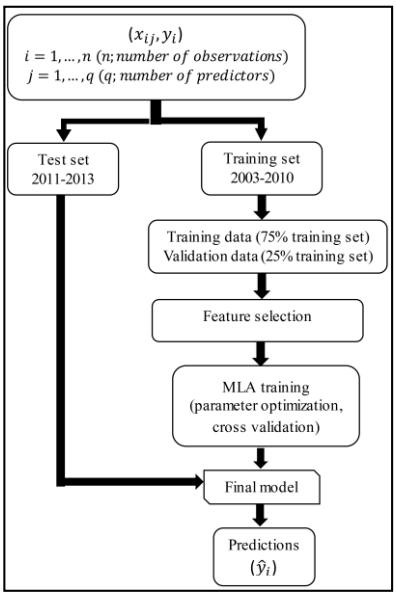

Figure 5 the flow chart of MLA prediction.

An initial judgment regarding the governing factors of dust formation is known to be critical for developing MLAs. Following the literature and authors' experiences, nine environmental parameters, including wind erosivity, vertical velocity (omega), soil moisture, soil temperature, albedo, precipitation, vegetation cover, drought intensity, and susceptibility of dust emission, are chosen as the potential parameters of dust prediction. Since the empirical selection of features may cause overfitting, here three types of FSC, including filter, wrapper, and embedded-type methods, are used to discriminate the most

informative features from the others. Figure 6 shows the basic differences between three FSC approaches used in this study.

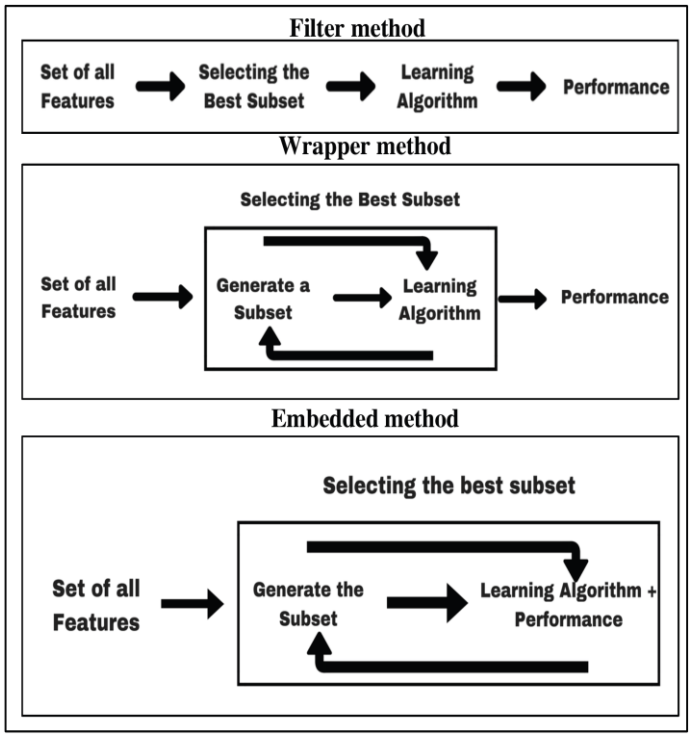

Figure 6 flow chart of three types of FSC (Hamon, 2013).

The feature pruning process resulted in the selection of six explanatory datasets, including Albedo, Dust Uplift Potential (DUP), NDVI, soil temperature, precipitation, and SF, to be used for MLA setup. However, considering the fact that none of these features could represent the apportionment of advecting dust to the total amount of AOD, the monthly area average of pruned features, except SF, calculated over main dust hot spot in the northwest of Iraq, is fed into the model as the complementary inputs of MLAs for the rest of region. Conclusively, after pruning and adding corresponding area-averaged features, 11 predictors are selected to train MLAs during 2003 and 2010.

2.4 Software

This research is mainly conducted by using NCAR Command Language (NCL) and R. NCL is used for the analysis and visualization of remote sensing data. Most of the verification analysis and MLA set up are done using packages implemented in R. ArcMap 10.4.1 is also used to visualize the distribution of ground-based stations.

2.5 List of manuscripts

The main purposes of the study are separately addressed within three peer-reviewed manuscripts:

Manuscript 1 *Chapter: 3*

Authors: **Nabavi, S. O.**; Haimberger, L.; Samimi, C.

Title: Climatology of dust distribution over West Asia from homogenized remote sensing data

Journal: *Aeolian Research 21 (2016) 93–107.*

Own contribution**:** data acquisition and analysis, figures, concept, writing, and discussion (70 %)

Manuscript 2 *Chapter: 4*

Authors: **Nabavi, S. O.**; Haimberger, L.; Samimi, C.

Title: Sensitivity of WRF-chem predictions to dust source function specification in West Asia

Journal: *Aeolian Research 24 (2017) 115–131.*

Own contribution**:** data acquisition and analysis, figures, concept, writing, discussion, and corresponding author (80 %)

Manuscript 3 *Chapter: 5*

Authors: **Nabavi, S. O.**; Haimberger, L.; Abbasi, R.; Samimi, C.

Title: Prediction of Aerosol Optical Depth in West Asia using Dust Models and Machine Learning Algorithms

Journal: *Atmospheric environment (under review).*

Own contribution**:** data acquisition and analysis, figures, concept, writing, discussion, and corresponding author (70 %)

PART II: PUBLICATIONS

3 Climatology of dust distribution over West Asia from homogenized remote sensing data

Seyed Omid Nabavi[1], Leopold Haimberger[1], Cyrus Samimi[2,3]

[1] Department of Meteorology and Geophysics, University of Vienna, Faculty of Earth Sciences, Geography and Astronomy, UZA II Althanstrasse 14, A-1010 Vienna, Austria

[2] Faculty of Biology, Chemistry and Earth Sciences, University of Bayreuth, Universitätsstr. 30, 95447 Bayreuth, Germany

[3] Bayreuth Center of Ecology and Environmental Research, BayCEER, Dr. Hans-Frisch-Straße 1-3, 95448 Bayreuth, Germany

Aeolian Research 21 (2016) 93–107

Hypothesis 1 is dealt with in this chapter, providing long-term distribution of dust storms in West Asia. It investigates possible changes in the spatio-temporal extent of dust events during last decades. This chapter discusses instrumental constraints on the use of TOMS-OMI AI in the long-term dust studies. It also shows the potentials of MODIS DB AOD for the determination of source points of dust plumes and dust transportation paths. The research concludes that northwest of Iraq is the main source of newly intensified dust storms which affect northwest and southwest of Iran in spring and summer, respectively.

- Conception of research approach: **Nabavi, S. O.** (major); Haimberger, L. (minor); Samimi, C. (minor)
- Development of research methods: **Nabavi, S. O.** (major); Haimberger, L. (major); Samimi, C. (minor)
- Data collection and data preparation: **Nabavi, S. O.** (major); Haimberger, L. (minor); Samimi, C. (minor)
- Execution of research: **Nabavi, S. O.** (major); Haimberger, L. (minor); Samimi, C. (minor)
- Analysis/Interpretation of data or preliminary results: **Nabavi, S. O.** (major); Haimberger, L. (major); Samimi, C. (major)
- Writing or substantive rewriting of the manuscript: **Nabavi, S. O.** (major); Haimberger, L. (major); Samimi, C. (minor)
- Role of **Nabavi, S. O.**: leading contribution (70 %)

Aeolian Research 21 (2016) 93–107

Contents lists available at ScienceDirect

Aeolian Research

journal homepage: www.elsevier.com/locate/aeolia

Climatology of dust distribution over West Asia from homogenized remote sensing data

Seyed Omid Nabavi [a,*], Leopold Haimberger [a,1], Cyrus Samimi [b,c,2]

[a] Department of Meteorology and Geophysics, University of Vienna, Faculty of Earth Sciences, Geography and Astronomy, UZA II Althanstrasse 14, A-1010 Vienna, Austria
[b] Faculty of Biology, Chemistry and Earth Sciences, University of Bayreuth, Universitätsstr. 30, 95447 Bayreuth, Germany
[c] Bayreuth Center of Ecology and Environmental Research, BayCEER, Dr. Hans-Frisch-Straße 1-3, 95448 Bayreuth, Germany

ARTICLE INFO

Article history:
Received 28 October 2015
Revised 30 March 2016
Accepted 4 April 2016
Available online 13 April 2016

Keywords:
Dust storms
TOMS-OMI Aerosol Index
MODIS
SeaWIFS
West Asia

ABSTRACT

In the past decade, West Asia has witnessed more frequent and intensified dust storms affecting Iran and Persian Gulf countries. Employing a varying threshold that takes into account systematic differences between TOMS and OMI data, TOMS-OMI Aerosol Index data are used to identify long-term changes in the horizontal distribution of dust storms in West Asia from 1980 to present. The northwest of Iraq and east of Syria are identified as emerging dusty areas, whereas east of Saudi Arabia and southeast of Iraq are identified as permanent dusty areas, including both dust sources and affected areas. Whereas the frequency of dust events increased slightly in the permanent dusty areas, it increased markedly in the emerging dusty areas. As expected, the frequency of dust events is highest in June and July.

The dust source areas are identified as the Iraq-Saudi Arabia boundary region and (recently) the northwest of Iraq, using MODIS deep blue aerosol optical depth data. Subsequently, a lagged correlation was implemented between identified dust sources and whole West Asia to determine the main paths and receptors of intense dust storms. Accordingly, southwest of Iran and Persian Gulf countries were determined as main receptors of summertime dust storms in West Asia. During spring, dust storms mostly hit the northern half of the region and reach to the Caspian Sea. Analyzing atmospheric patterns, Shamal and Frontal patterns were found as dominant atmospheric circulations simultaneous with summertime and springtime dust storms, respectively.

1. Introduction

Dust storms are known as a natural hazard that affects various parts of the world. According to the definition of World Meteorological Organization (WMO), dust storms are the result of strong atmospheric turbulence near the surface that lifts large amounts of dust into the atmosphere, which decrease the horizontal visibility to less than 1000 m (Goudie and Middleton, 2006). Reduction in visibility range leads to vehicle accidents. Reduction of soil productiveness, damages to agricultural products, remote communication disturbances, mechanical systems disorders (Jish Prakash et al., 2014), higher risk of respiratory diseases (Lyles et al., 2012; Ebrahimi et al., 2014) are also consequences of dust storms. In a general perspective, primary origins of dust storms are located in the world's arid regions in East Asia, Middle East, Europe, Latin America, North America, Australia, east and south of Africa, and Sahara. The Middle East has various dust source areas such as the Arabian Peninsula, Israel, Syria, Egypt, Iraq and Iran (Shao et al., 2011). In the past years, dust events have been more frequent and intensified in West Asia (Azizi et al., 2012).

1.1. Remotely sensed dust data

In order to mitigate dust disastrous effects, monitoring its sources, transport paths and affected areas is crucial (Ciren and Kondragunta, 2014). Unfortunately almost all Middle East countries have incomplete ground-based observation datasets which are largely limited to urban areas. Meanwhile, remote sensing tools and techniques potentially provide an unprecedented capability to monitor the spatial–temporal distribution of dust events. Many algorithms have been developed to detect dust events from other atmospheric phenomena and ground surface features. Ackerman (1989) proposed brightness temperature difference (BTD) between

* Corresponding author. Tel.: +43 1 4277 537 01; fax: +43 1 4277 95 37.
E-mail addresses: seyed.omid.nabavi@univie.ac.at (S.O. Nabavi), leopold.haimberger@univie.ac.at (L. Haimberger), cyrus.samimi@uni-bayreuth.de (C. Samimi).
[1] Tel.: +43 1 4277 537 01; fax: +43 1 4277 95 37.
[2] Tel.: +49 921 552237.

http://dx.doi.org/10.1016/j.aeolia.2016.04.002
1875-9637/

near-infrared channels at 3.7 and 11 μm and, later (1997), a tri-spectral (8, 11 and 12 μm) technique to differentiate dust particles from water/ice clouds. However, Ciren and Kondragunta (2014) have mentioned that the magnitude of the brightness temperature difference is sensitive to the dust layer height and the dust composition and surface emissivity. Therefore, the accuracy of dust detection can vary both spatially and temporally. Due to the strong absorption of Ultra Violet (UV) radiance by dust and low ground surface reflectivity in the UV spectral region, an Aerosol Index (AI) has first been defined by Torres et al. (1998) for Total Ozone Mapping Spectrometer (TOMS) and Ozone Monitoring Instrument (OMI) UV radiances. AI is mathematically defined as:

$$\mathrm{AI} = \log_{10}(I_{360}/I_{331})_{\mathrm{measured}} - \log_{10}(I_{360}/I_{331})_{\mathrm{calculated}} \quad (1)$$

The "*I*" denotes radiance measured by TOMS and OMI at 360 nm and 331 nm wavelengths, respectively. Since $I_{360\ \mathrm{calculated}}$ is calculated using reflectivity derived from the 331 nm radiance values, the Aerosol Index definition essentially simplifies to:

$$\mathrm{AI} = \log_{10}(I_{360\mathrm{measured}}/I_{360\mathrm{calculated}}) \quad (2)$$

The AI can identify absorbing, smoke and desert, and non-absorbing, ice and water, aerosols. AI positive values are representative of mineral dust, smoke and volcanic aerosols (Ahmad et al., 2006). Using TOMS AI, Prospero et al. (2002) depicted globally major dust sources which are in topographic depressions of former paleolakes. While the TOMS AI seems ideal for climatological studies since it is available back to 1979, it also has its weaknesses. Mahowald and Dufresne (2004) have pointed out that AI is sensitive to dust layer height. Assuming a constant dust concentration, this means higher dust clouds lead to higher, exaggerated, AI values over desert areas and during warm periods of the year whereas dust is underestimated with AI during cooler periods and areas. Therefore, they have recommended using a spatiotemporally Varying Threshold (VT) for the detection of dust events, instead of direct use of AI or determining a Fixed Threshold (FT).

Although this can partly deal with dust height-induced biases, an AI binary mask is not able to show the severity of dust storms. Moreover, TOMS AI is prepared in the resolution of ≈1° which is too rough to identify local scale dust activity. This deficiency can be addressed by the use of high-resolution Moderate Resolution images of Imaging Spectroradiometer (MODIS). Hsu et al. (2004) developed a Deep Blue (DB) Aerosol Optical Depth (AOD) algorithm for MODIS images available from 2003 to 2014. This algorithm is not only insensitive to dust height but also able to detect dust over a bright surface, e.g., desert areas, at a high resolution of 10 km. Ginoux et al. (2012) have used this algorithm to identify anthropogenic and natural sources from MODIS aerosol products. Results show that the main sources of dust storms in West Asia are vast desert areas located in the northeast of Saudi Arabia, Iraq, Iran, Syria and the regions between the Caspian Sea and Aral Lake.

Besides MODIS, DB AOD data at 550 nm can also be prepared from measurements of Sea-viewing Wide Field-of-view Sensor (SeaWIFS). These data are accessible in two resolutions of 0.5° and 1° from 1998 to 2010. Hsu et al. (2012) have used this dataset to identify distribution and trends of aerosols in global and regional scales. Results show strong relationships between Saharan dust export as well as biomass-burning activity in the tropics with climate indices such as El Niño Southern Oscillation (ENSO).

1.2. Dust storms in West Asia

The significant increase of dust storms in West Asia (Azizi et al., 2012) has fostered studies based on various research approaches (Goudie and Middleton, 2000; Furman, 2003; Taghavi and Asadi, 2007; Aurelius et al., 2007; Al Sarraf, 2010; Gerivani et al., 2011; Hamidi et al., 2013; Rezazadeh et al., 2013; Cao et al., 2015; Moridnejad et al., 2015b; Rashki et al., 2015). Some of those studies have used the discussed remote sensing techniques and algorithms for the analysis of dust storms in the region (Esmaili et al., 2006; Azizi et al., 2012; Karimi et al., 2012; Boloorani et al., 2014; Moridnejad et al., 2015a). Although these studies have yielded valuable results, they left some issues to be addressed. Esmaili et al. (2006) have used TOMS AI and meteorological data to identify major dust sources of Iran. They took only the appearance of persistent spatial–temporal patterns of AI as the indicator of Iran's dust sources before 2004. Azizi et al. (2012) and (Boloorani et al., 2014) both have applied a BTD algorithm on MODIS images during some dust cases between 2000 and 2008. They have concluded that most dust storms entering Iran form in Iraq and Syria. Karimi et al. (2012) compared different dust detection algorithms to be applied on MODIS images for the identification of dust sources in the Middle East. Since at that time MODIS DB AOD was only prepared in the resolution of 1°, they disregarded it in their local investigations and tried to propose a new dust detection algorithm called Middle East Dust Index (MEDI). However, later they used 0.1-degree resolution MODIS DB AOD to find dust intensity in local sources identified by MEDI (Moridnejad et al., 2015a).

In the present paper we try to improve the knowledge about the long-term spatiotemporal distribution of West Asian dust storms in three ways: (a) the horizontal extent of dusty areas and its changes are investigated by using a refined threshold of TOMS-OMI AI from 1980 to present, except 1993–1996 and 2002–2004, (b) the MODIS DB AOD is examined from 2003–2014 to determine dust sources by the analysis of dust storm intensity within already identified dusty areas, and (c) The main paths and receptors of dust storms are identified by applying the spatiotemporal lag-correlation method to MODIS DB AOD data. Furthermore, dominant atmospheric patterns which govern the mechanisms of dust relocation are studied. The rest of this paper is organized as follows: methods and data are presented in the next section. The research findings are presented and discussed in Section 3. Section 4 is allotted to conclusions and future work.

2. Data and methods

TOMS-OMI AI is known as the longest aerosol records from 1979 to present. TOMS installed on Nimbus 7 recorded data from 1979 to 1993 with a spatial resolution of 1 × 1.25°. After a 4-year cessation, it continued data gathering on the Earth Probe platform until the end of its operation in 2005. With one-year data overlap, OMI has provided AI in the resolution of 0.25° from 2005 to present. In this study, TOMS-like OMI AI, named OMTO3d_V003, in 1-degree resolution, was used to have a more consistent dataset. The accuracy and precision of the OMTO3d_V003 are similar to the legacy TOMS data, except over cloudy areas where OMTO3d_V003 data is more accurate than that of the TOMS (Ahmad et al., 2004; Vasilkov et al., 2008).

However, the examination of these two datasets shows some uncertainties. As documented in Kiss et al. (2007), the Earth Probe TOMS records are affected by calibration drift issues. The problem (a wavelength dependent calibration drift from changes in the optical properties of the front scan mirror) became worse in 2005 so that the TOMS AI data in the period 2002–2005 are unreliable and cannot be used, especially for any kind of trend analyses.

In addition, area average of long-term daily mean AI over West Asia shows that OMI has steadily recorded lower AI compared to TOMS (Fig. 1). The offset could have climatological reasons but also artificial reasons caused by different instrument characteristics. In fact, it is shown below that the change of instruments caused an artificial decrease in AI which can cause misinterpretation of dust activity in recent years. Such data inhomogeneities are serious

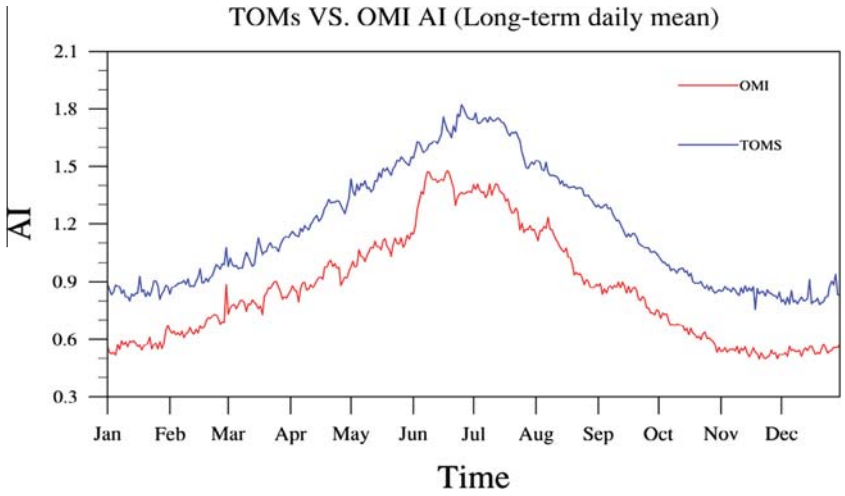

Fig. 1. Area average of long-term daily mean AI over West Asia (20N–40N and 35E–65E). Blue curve shows area-averaged TOMS AI between 1980 and 2001 and red curve represents OMI AI between 2005 and 2014. (For interpretation of the references to colour in this figure legend, the reader is referred to the web version of this article.)

issues in climate science since they can completely mask or even reverse an existing climate change signal. For atmospheric temperature, data homogenization has become a standard procedure before interpreting any data (Mears et al., 2003; Haimberger, 2007; Venema et al., 2012; Haimberger et al., 2012). More and more satellite data are reprocessed in order to reduce the effect of calibration drifts and -offsets between various instruments. In our particular case, we have to offset the different calibration of TOMS and OMI. The lack of temporal overlap period between reliable TOMS data and OMI data makes it particularly challenging to create homogeneous climatological time series derived from AI.

Another, aforementioned, problem is AI sensitivity to dust layer height which caused AI overestimation (underestimation) in warm (cold) periods or areas. As shown in Fig. 2, highlands in western Saudi Arabia host a constant high boundary layer (Dee et al., 2011). This has a profound effect on aerosol height and yields significant biases in the intensity of recorded AI in the region (discussed later). The effect of aerosol height on AI is so obvious that Ginoux and Torres (2003) have taken planetary boundary layer height (h_{PBL}) as one of the main inputs for the simulation of AI.

In order to tackle all above-mentioned issues, following measures are taken:

1. Besides the data gap between 1993 and 1996, AI recorded by TOMS during 2002–2004 are excluded from further examinations.
2. Because of higher accuracy of OMI AI over cloudy pixels, long-term study of AI is limited to warm months (April–September) when subtropical high pressure is dominant atmospheric pattern over West Asia resulting in mostly cloud free conditions throughout the region.
3. Following Mahowald and Dufresne (2004) we do not use directly AI or FT. Instead we have prepared a VT for the warm months to deal with the sensitivity of AI data to aerosol height. Here VT was defined as the multi-year average of AI simultaneous with SeaWifs DB AOD between 0.5 and 0.55 during warm months. It is worth mentioning that choosing this range is based on subjective examinations of SeaWIFS DB AOD during 65 dust storms between 1998 and 2010 and conducted researches by Mahowald and Dufresne (2004) and Moridnejad et al. (2015a). In fact, DB AOD 0.5–0.55 is used to make sure that intense dust cases are excluded from the preparation of VT so that it is only determined by varying boundary layer height and a roughly constant dust concentration.

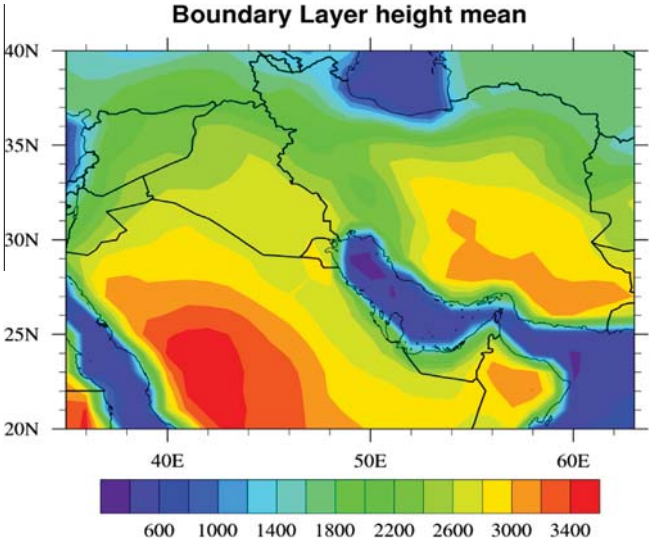

Fig. 2. Long term mean of boundary layer height (m) during the warm season (April–September) 1980–2014 at 12Z from ERA-Interim reanalyses (Dee et al., 2011).

4. Regarding the different distribution of AI measured by TOMS and OMI, VT is separately prepared for these two instruments. To do so, SeaWifs DB AOD between 1998–2001 and 2005–2010 is respectively used for calculating VT of TOMS and OMI. Fig. 3 illustrates the homogenization strategy used for the preparation of AI-based VT.
5. In order to examine efficiency of SeaWIFS DB as an indicator of dust occurrence, it is checked against four AErosol RObotic NETwork (AERONET) stations located in Saudi Arabia and Persian Gulf countries (see Figs. 4 and 7).

Considering different spatial resolution and instrumental characteristics of surface stations compared to satellite data, the agreement of SeaWIFS DB AOD with these stations is acceptable. While the lowest correlation (Null.65) belongs to Dhadnah, it increases orderly in Kuwait (0.68), Solar Village (0.7), and Mezaria (0.81) (Fig. 4A–D). This agreement ensures to a great extent that SeaWIFS DB AOD can detect the outbreak of dust storms and exclude severe dust cases by using threshold 0.5 < AOD < 0.55. Fig. 5 shows separate VTs for TOMS (Fig. 5A) and OMI (Fig. 5B). Over some regions

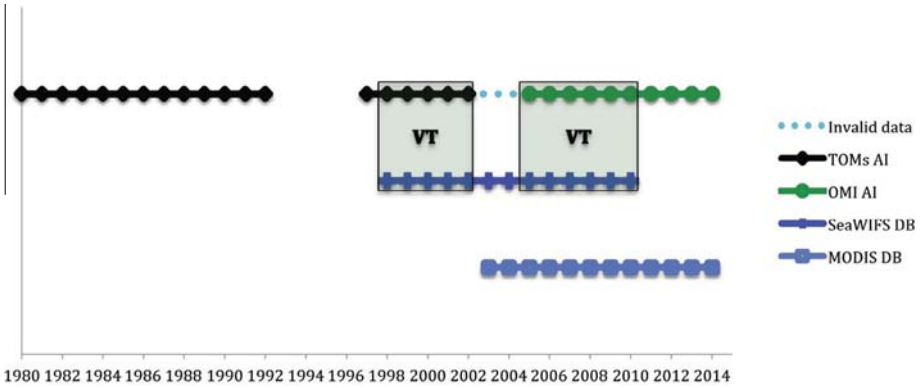

Fig. 3. Timeline of availability of different satellite data used in this study. Systematic differences between TOMS and OMI AI are offset by different varying thresholds used for calculation of FoO from AI. Note SeaWIFS is only data set with significant overlap with both TOMS and OMI. Rectangles indicate time intervals used for calculating the VTs.

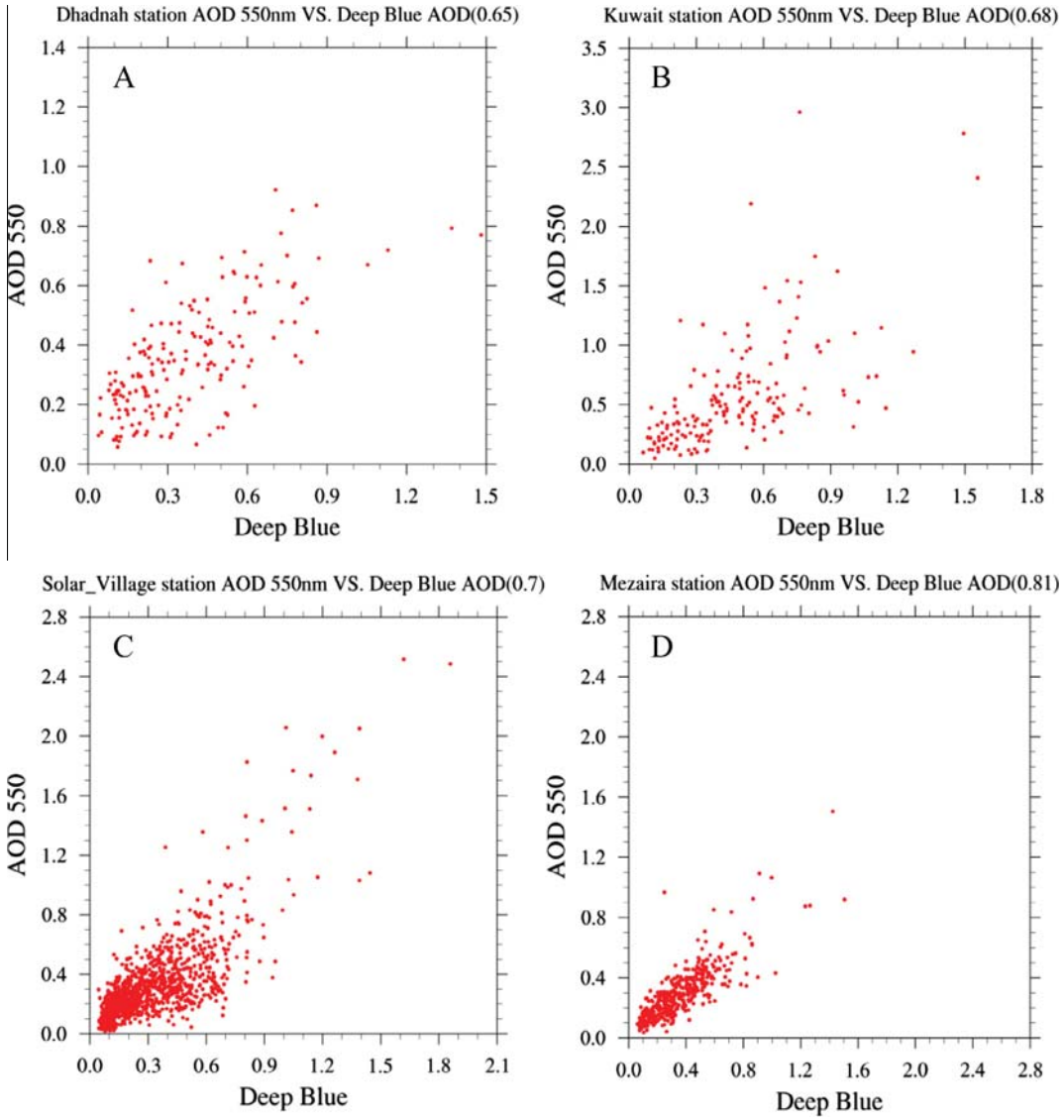

Fig. 4. Scatter plots between SeaWIFS DB AOD 550 nm and AERONET stations AOD 550 nm for stations A) Dhandah (25.5 N and 56.31E), B) Kuwait University (29.31 N and 47.96E), C) Solar Village (24.9 N and 46.38E), and D) Mezaria (23 N and 53.76E), see also Fig. 7. Values in parantheses are Spearman correlation coefficients.

the AOD has never been between the thresholds and therefore there is not complete data coverage in these figures. As discussed earlier, AI is not only function of aerosol concentration, but also it is affected by boundary layer (aerosol) height. Assuming a constant dust concentration by the use of AOD between 0.5 and 0.55, high VT in the west of Saudi Arabia, especially in TOMS VT,

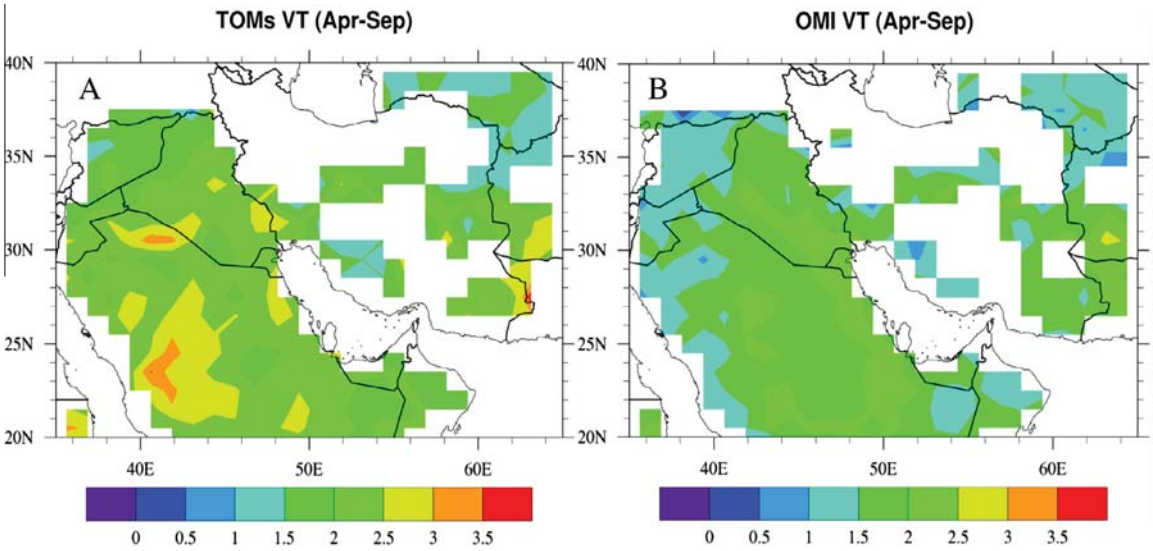

Fig. 5. VT for TOMS AI (A) calculated using SeaWIFS DB AOD for the period 1998–2001 and OMI AI (B) calculating using SeaWIFS DB AOD for period 2005–2008. White areas indicate no data (AOD (almost) never between 0.5 and 0.55).

is because of high boundary layer in the region (Fig. 2). As expected, OMI VT is generally lower than TOMS VT throughout the study region which offsets higher AI recorded by TOMS.

Frequency of Occurrence (FoO) of dust defined as the number of days where AI data exceed a previously defined VT, is used here to measure dust activity changes over time. Therefore the consistency of VTs over TOMS and OMI periods is critical. The VT consistency is tested by the ratio of the multi-year monthly sum of Frequency of Occurrence (FoO) of dust storms detected by VT throughout West Asia to corresponding cases determined by SeaWIFS DB AOD > 0.5. This ratio is separately made for TOMS and OMI by the comparison AI and DB in two periods 1998–2001 and 2005–2008, respectively. To make a comparison, the same process is done for FT, AI > 1 Prospero et al. (2002), shown in Fig. 6.

Although TOMS and OMI VT are a yielding higher number of dust cases compared to DB (between 4 and 6 times), they resulted in an approximately same ratio in both periods. This consistent ratio is a necessary condition that determined changes by AI are caused by real changes in dust frequency and are not significantly affected by the use of different instruments. The higher ratio of FoO for OMI VT compared to TOMS VT in August and September means that there might be a slight underestimation of TOMS VT FoO in these months. We also note that this homogenization procedure depends on the homogeneity of SeaWIFS data. So far we have not found any indications that the SeaWIFS data are inhomogeneous.

In contrast, FT FoO ratios are obviously different during TOMS and OMI periods. This is because of temporal discontinuity of AI due to instrumentation changes. While the ratio of TOMS FT FoO to DB FoO varies profoundly from 10 to 30, it is much lower and more stable in OMI period. This leads to an artificial decrease in the number of detected dust cases by OMI FT in recent years which will be discussed later.

In addition to the examination above, the performance of FT and VT is also evaluated by using a contingency table in the next section. In this method, the variable "*a*" represents true positives, the number of dust events detected by DB AOD (AOD > 0.5), FT (AI > 1) and VT; the variable "*b*" represents false positives, the number of times where DB indicates "no dust," but FT and VT indicate "dust"; the variable "*c*" represents false negatives, the number of times where DB indicates "dust," but FT and VT indicate "no dust"; the variable "*d*" represents true negatives, the number of times where all three algorithms indicate "no dust". These four elements are components of accuracy equation:

$$\text{Accuracy}(\%) = \frac{a+d}{a+b+c+d} * 100 \quad (3)$$

Having done verification, dusty areas of West Asia were identified through annual analysis of VT FoO. As the study period was divided into two 14-year periods: 1980–1997 (with a 4-year data gap) and 1998–2014 (with a 3-year data gap). The VT FoO of 800 and 500 days per each 14 years were used, as two empirical thresholds, to separate permanent, extinct and emerging dusty areas. Permanent dusty were defined as where have a FoO > 800 in both periods 1980–1997 and 1998–2014. Emerging areas have FoO < 500 in 1980–1997 and FoO > 500 in 1998–2014 in most pixels. Extinct areas (practically nonexistent) have FoO > 800 in 1980–1997 and FoO < 500 in 1998–2014. In order to discriminate dust sources from affected regions in identified dusty areas, the intensity of dust emission is locally examined by the use of MODIS DB AOD which is accessible from 2003 to present. In this study, total FoO of MODIS DB AOD > 0.85 during warm months is considered as the indicator of dust sources (Moridnejad et al., 2015a). After determination of dust sources, main dust paths and receptors were identified by the use of lagged cross-correlation between MODIS DB AOD of dust sources and the whole region (Ke-Yi, 2010).

Besides using remotely sensed data, meteorological stations data are also used in some parts of study to validate results. These data are acquired from synoptic stations in western Iran (Fig. 7). In the following image, synoptic stations in the southwest of Iran (Khuzestan plain) are discriminated with a red background which will be discussed in the next section. Furthermore, AEORONET stations used earlier for the validation of SeaWIFS DB are shown by stars.

3. Results and discussion

In order to describe the long-term behavior of dust storms in West Asia, FT FoO and VT FoO of dust storms, during warm months, are summed up in seven 4-year time slices from 1980 to 2014 (Fig. 8). It is worth to mention that time slices between 1992–1999 and 2000–2006 have 4 and 3-year data gaps, respectively.

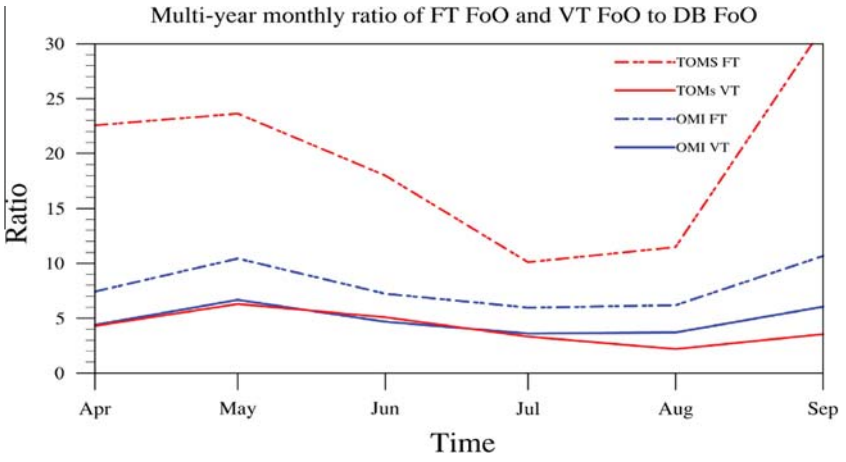

Fig. 6. Multi-year monthly ratio of FoO of dust storms determined by FT and VT to FoO detected by SeaWIFS DB AOD for the periods 1998–2001 (TOMS) and 2005–2008 (OMI).

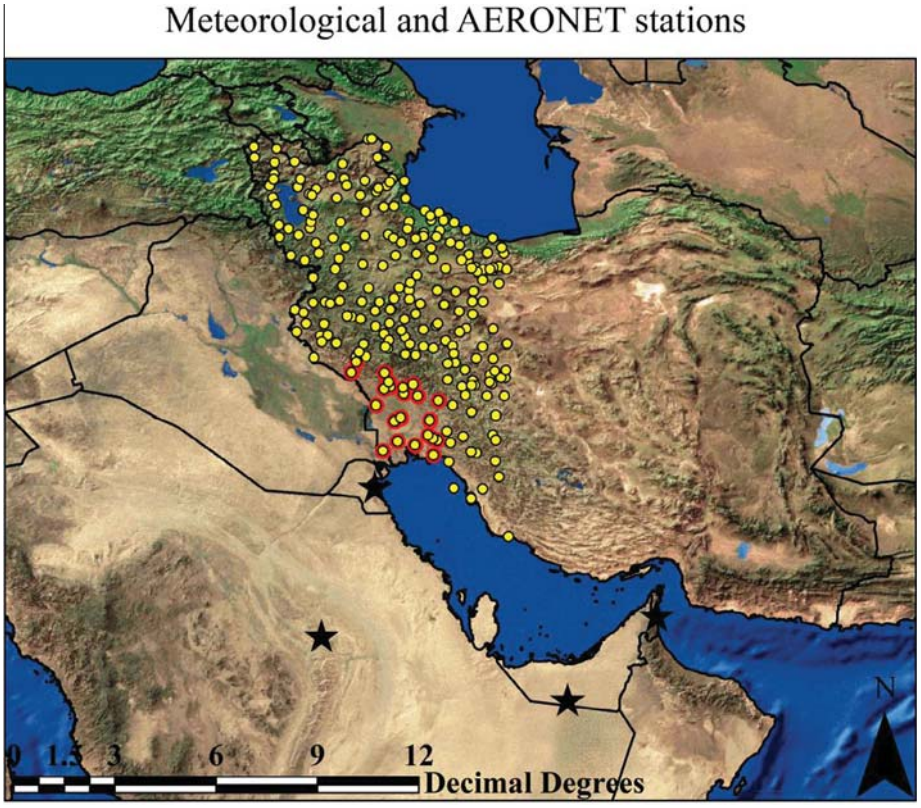

Fig. 7. Synoptic stations in the western half of Iran (yellow dots). Yellow dots with red background are stations in Khuzestan plain. Stars indicate the location of AERONET stations used for comparison with SeaWIFS DB AOD. (For interpretation of the references to color in this figure legend, the reader is referred to the web version of this article.)

Apart from the constant overestimation of FT FoO to VT FoO, the most obvious difference between them is the reverse trend of dust activity after 2006. As discussed in the last section (Fig. 6), the number of detected dust storms (FoO) by FT is much lower in OMI period which is because of the general reduction of AI recorded by this instrument (Fig. 1). For example, the Rub al Khali desert[3], in the east of Saudi Arabian Peninsula, is shown by a lower number dust cases between 2011 and 2014 comparing to 2000–2006. This is while VT yields the same or even higher number of cases in the 2011–2014 period. Another instance is northwest of Iraq where VT FoO increases between 2007 and 2010. However, corresponding FT FoO shows a decrease during the same period. In fact, the use of OMI FT caused a reduction of detected dust cases between 2007 and 2014[4]. In addition to instrumental discontinuity, the offensive effect of boundary layer height on AI is remarkably seen among FT FoO, especially during TOMS period, in the western half of Saudi Arabia and southeast of Iran. According to total difference between FT FoO and VT FoO (Fig. 9A), these overestimations occur mostly in regions where boundary layer height is correlated with AI

[3] The empty quarter.

[4] Although OMI FT is also involved in time slice of 2000–2006, because two years of that (2000 and 2001) are TOMS AI, the significant reduction is seen after this period.

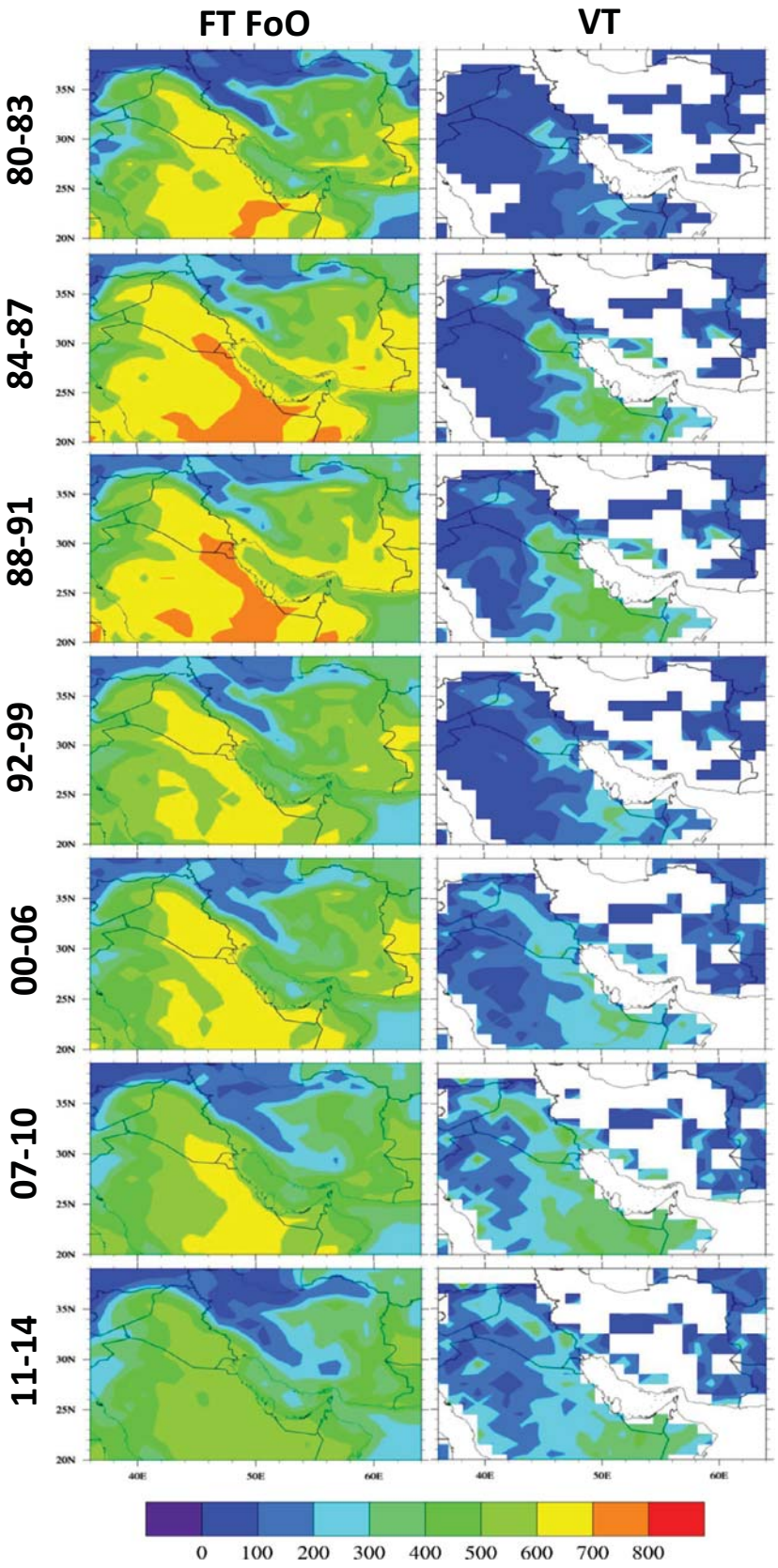

Fig. 8. 4-year FoOs in units days of dust storms in West Asia based on FT (left) and VT (right) for time different intervals (1980–1983, 1984–1987, . . .) in the period 1980–2014. Intervals 1992–1999 and 2000–2006 appear longer but contain only 4 years of valid data as well.

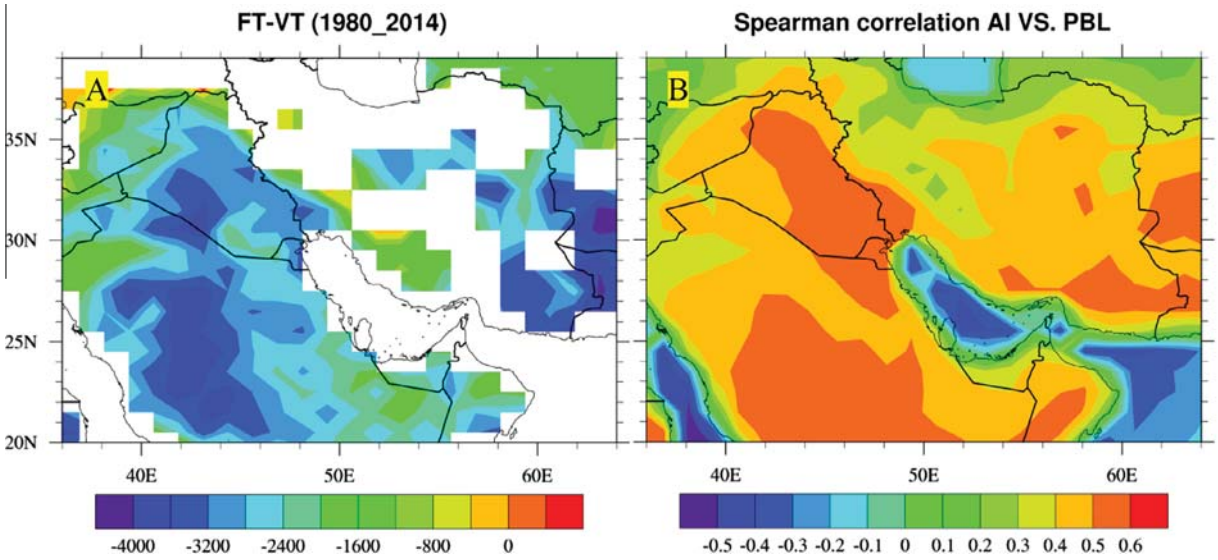

Fig. 9. Panel A: Overall difference between FT FoO and VT FoO in units days from April to September for the period 1980–2014. Panel B: Spearman correlation coefficient between AI and Planetary Boundary Layer (PBL) height during April to September from 1980 to 2014.

(Fig. 9B). In fact, positive correlations represent desert areas where high boundary layer height can be assumed as the main reason of AI overestimation.

The accuracy (Eq. (1)) of FT and VT is evaluated based on both SeaWIFS DB and MODIS DB products. Concerning that VT is prepared by using SeaWIFS DB, it is better not to use it also for the verification. However, the main barrier is that MODIS DB does not cover any part of TOMS period. So verification is first done by the use of SeaWIFS DB for both TOMS (1998–2001) and OMI periods (2004–2010) and then OMI (2005–2014) is also verified by MODIS DB. In this way, we can compare OMI verifications based on both instruments and make sure that the reliance of VT on SeaWIFS DB cannot mislead. The accuracy of TOMS (Fig. 10A) and OMI (Fig. 10B) FT against SeaWIFS DB shows a similar pattern namely the lowest accuracy in the west of Saudi Arabia, south of Iraq and southeast of Iran. These are regions where VT could bear a significant improvement for both instruments (Fig. 10D and E). Although the accuracy of OMI FT rises when MODIS DB is used (Fig. 10C), it also causes higher accuracy for OMI VT (Fig. 10F). Regarding the similar pattern of TOMS and OMI accuracy using both SeaWIFS and MODIS DB and higher accuracy of VT, it can be concluded that VT is much more reliable than FT for the detection of dust storms during the whole study period.

As explained in Section 2, we have used VT-based FoO to separate permanent (Fig. 11A), emerging (Fig. 11C) and extinct dusty areas in the region. The permanent dusty areas are mostly identified in the east of Saudi Arabia. Based on annual area-averaged VT FoO, after two main upsurges of permanent dusty areas in 1984 and 1991, the most recent peak happened in 2008 in this region (Fig. 11B). The sample average and standard deviation of the mean of permanent dust areas have changed from 73 and 8.5 during 1980–1992 to 75 and 6.8 during 1997–2014. The annual area-averaged FoO of dust storms of emerging dusty areas, covered the east of Syria, northwest of Iraq, and a small area in the Sistan Basin in eastern Iran, has strongly increased in recent years, with a peak in 2008. Similarly, dust frequency average and standard deviation of the mean of emerging areas have profoundly increased from 22 and 3.9 to 67 and 7.8, respectively (Fig. 11D). This implies more frequent and fluctuating dust events in emerging dusty areas during the past decade. It is worth mentioning that episodes of low/high dust frequency in emerging areas have coincided with permanent areas. This can be attributed to the fact that dust factors, like drought, or/and the resulting dust plumes affect most of the region during dusty periods. As an example, Trigo et al. (2010) studied a very intense drought in Fertile Crescent[5] between 2007 and 2009 found as the driest two-year case for the region since 1940.

This drought has taken place exactly when emerging and, with less frequency, permanent areas have been simultaneously activated. Fig. 12 shows that most parts of dusty areas, especially emerging ones, were under a very profound reduction of precipitation during October–May in 2007–2008 (Fig. 12A) and 2008–2009 (Fig. 12B).

Interestingly, Notaro et al. (2015) have found that the upsurge of dust storms in Saudi Arabia between 2008 and 2012 mostly originated from drought-stricken sources across the Fertile Crescent. In fact, it can be inferred that while dust intensification of emerging dusty areas is mostly because of local intense drought, permanent dusty areas are affected by local drought-driven dust cases and intensified dust storms in Iraq traveling to Arabian Peninsula. It is worth mentioning that extinct areas, i.e. to be active only in the first period, were also considered, but very few points with decreasing dust frequency were found in the recent period (not shown here). This means that dust sources of West Asia have been mostly growing in three last decades.

Fig. 13 shows the area-averaged monthly VT FoO in permanent (13-A) and emerging (13-B) dusty areas during last decades, except 1993–1997 and 2002–2004. In the permanent dusty areas, dust storms spread in all warm months with a peak in June and July during the whole study period. Conversely, the monthly distribution of dust storms in emerging areas shows two different periods of dust activity from 1980 to 2000 and after that. In the first period, there were only few dust cases mainly in July. In the second period, the number of dust cases increased markedly and the period of dust activity expanded to whole warm months. This affirms that dust frequency has increased both spatially (Fig. 11C) and temporally (Fig. 13B) in the emerging dusty areas.

[5] The Fertile Crescent is the region in the Middle East which curves, like a quarter-moon shape, from the Persian Gulf, through modern-day southern Iraq, Syria, Lebanon, Jordan, Israel and northern Egypt.

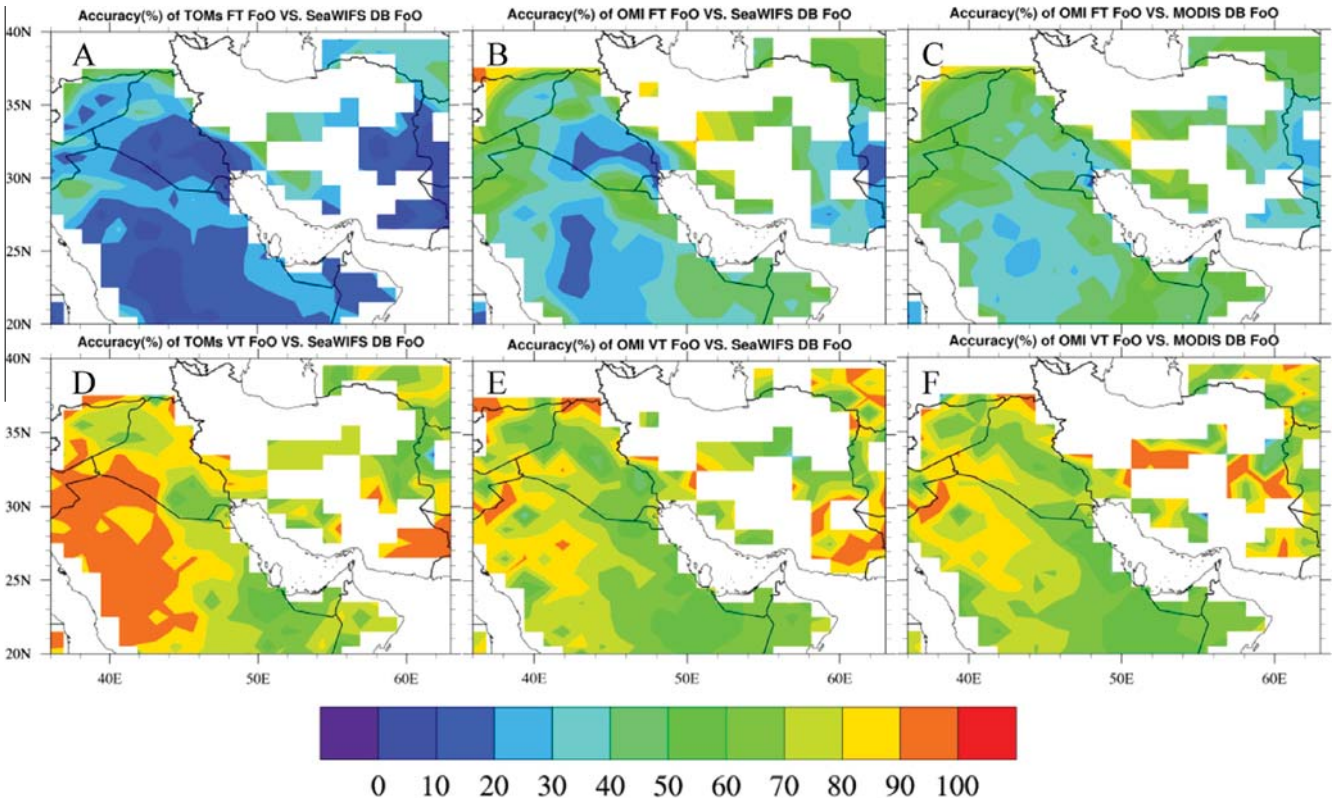

Fig. 10. Accuracy (%) of TOMS FT against SeaWIFS DB (A), OMI FT against SeaWIFS DB (B), OMI FT against MODIS DB (C), TOMS VT against SeaWIFS DB (D), OMI VT against SeaWIFS DB (E), and OMI VT against MODIS DB (F). Missing pixels in FT figures are advertently made to have an appearance like VT.

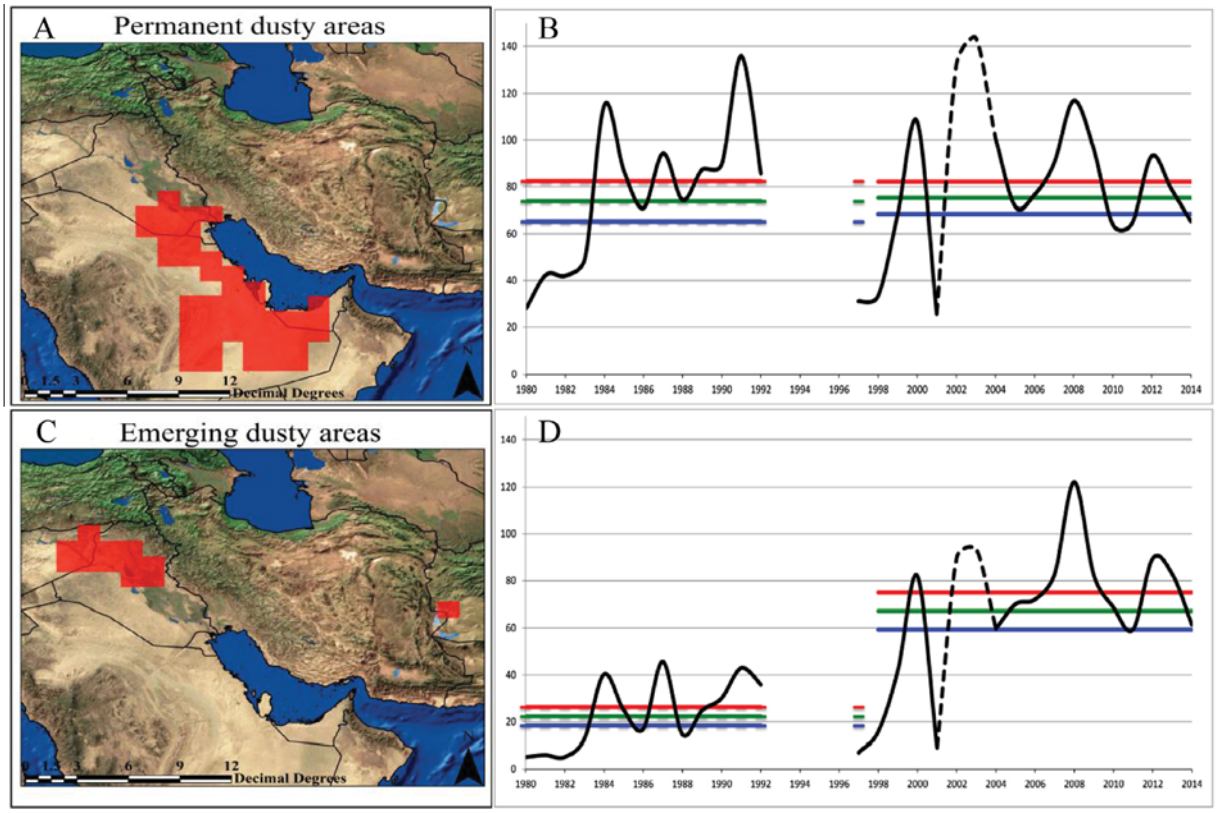

Fig. 11. Permanent (A) and emerging (B) dusty areas in West Asia from 1980–2014. C and D are respectively the area-averaged annual FoOs of VT-detected dust storms within permanent and emerging dusty areas. The blank belongs to data gaps between 1993 and 1997 and dash line is the representative of invalid data between 2002 and 2004.

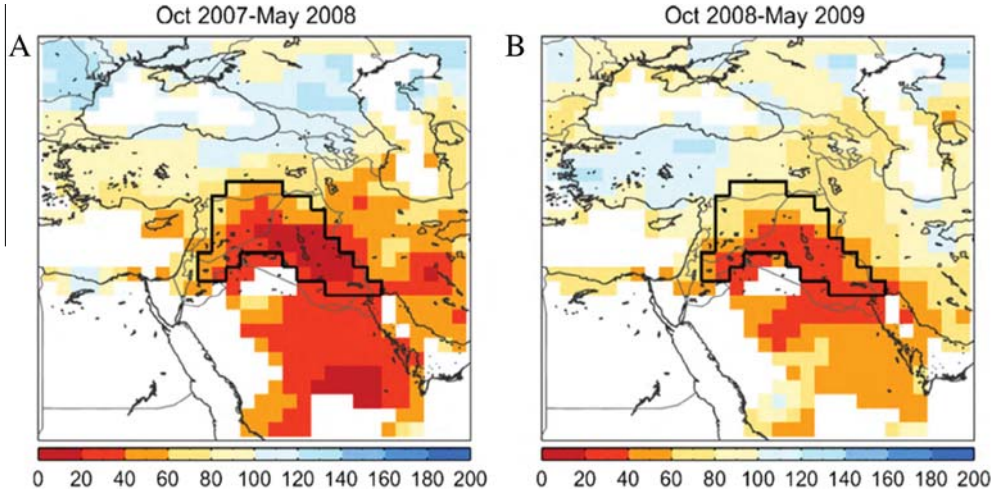

Fig. 12. Accumulated monthly precipitations (expressed in percentage relative to the 1940–2009 normal) during October to May in 2007–2008 (a) and 2008–2009 (b). Black polygon is the boundary of Fertile Crescent (Trigo et al., 2010).

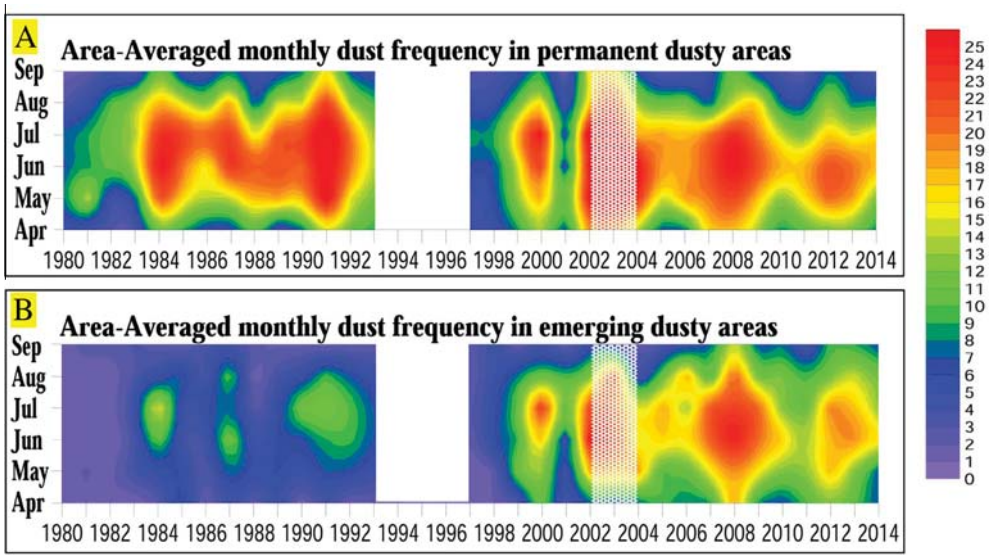

Fig. 13. Area averaged monthly VT FoO (averaged number of dusty days per month) in A) permanent and B) emerging dusty areas as indicated in Fig. 11. Data gap 1993–1997 and invalid data 2002–2004 are masked and blurred, respectively.

In order to validate these results and to check if monthly dust distribution is properly represented on dusty areas by VT, these examinations are also done for southwestern Iran. This region has been chosen since its weather data are freely available from 1980 to present and since it is frequently hit by dust storms coming from the western half of the region (discussed later). The most reliable meteorological data related to dust storms are weather codes. For this study, all meteorological dust codes, 6–9 and 30–35 (WMO, 2011), acquired from synoptic stations in Khuzestan plain are considered to have both local and regional dust storms. The comparison of VT-based time series (Fig. 14A) and ground-based observations (Fig. 14B) shows that this refined threshold managed to represent main characteristics of observational time series. For example, the dusty episodes in 1984, 1991, 2000, and 2008 are seen in both distributions. Furthermore, monthly peaks of both time series happened during June to August. Further examinations show that differences between these two time series, such as higher number of cases before 1984 or peak displacement from 2008 in VT FoO to 2009 in observations, can be attributed to the rough resolution of AI which cannot detect local dust cases recorded by meteorological stations.

As discussed earlier, a dusty area consists of both dust emitting and affected spots. To discriminate these regions, those parts of dusty areas that emit high-intensity dust storms are determined as dust sources. Intense dust cases from MODIS DB AOD (Ginoux et al., 2012; Moridnejad et al., 2015a) were defined by FoO of MODIS DB AOD exceeding 0.85.

The tally of intense dust storms covers up main sources of permanent dusty areas spread out in the southeast, east and northeast of Saudi Arabian Peninsula and southeast of Iraq (Fig. 15A). However, most dust sources have been concentrated in the northern part of permanent dusty areas. The examination of the FoO of intense dust storms within emerging dusty areas showed a hot spot in the northwest of Iraq (Fig. 15B). In fact, it can be claimed that northwest of Iraq close to the confluence of Tigris and Euphrates is the main source of recent dust storms in West Asia. In order to find main dust paths and affected areas of these two dust sources, i.e. the northeast of Saudi Arabia and southeast of

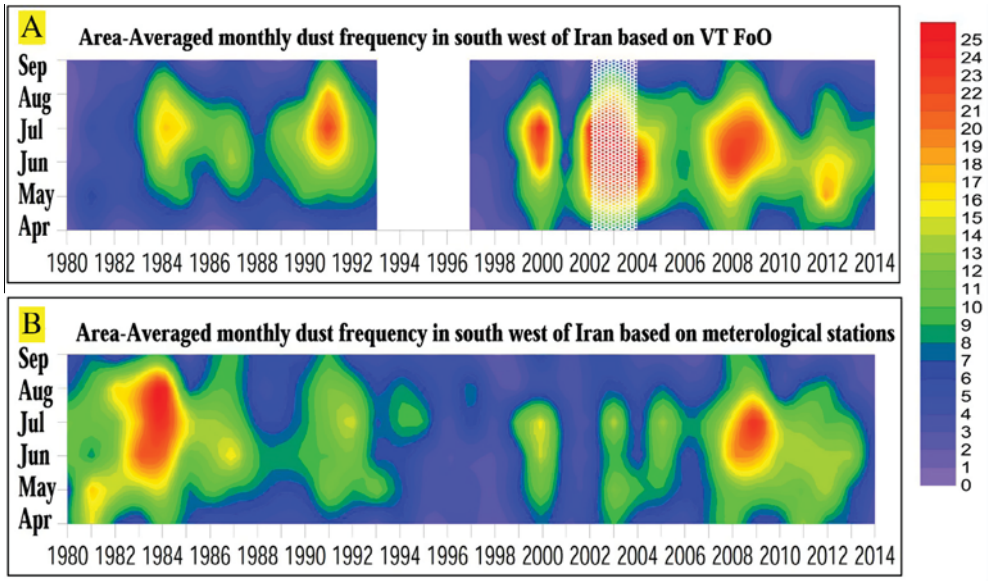

Fig. 14. (A) Area averaged monthly VT FoO (averaged number of dusty days per month) in the south west of Iran based on AI VT and (B) meteorological stations. Data gap 1993–1997 and invalid data 2002–2004 are masked and blurred in figure A, respectively.

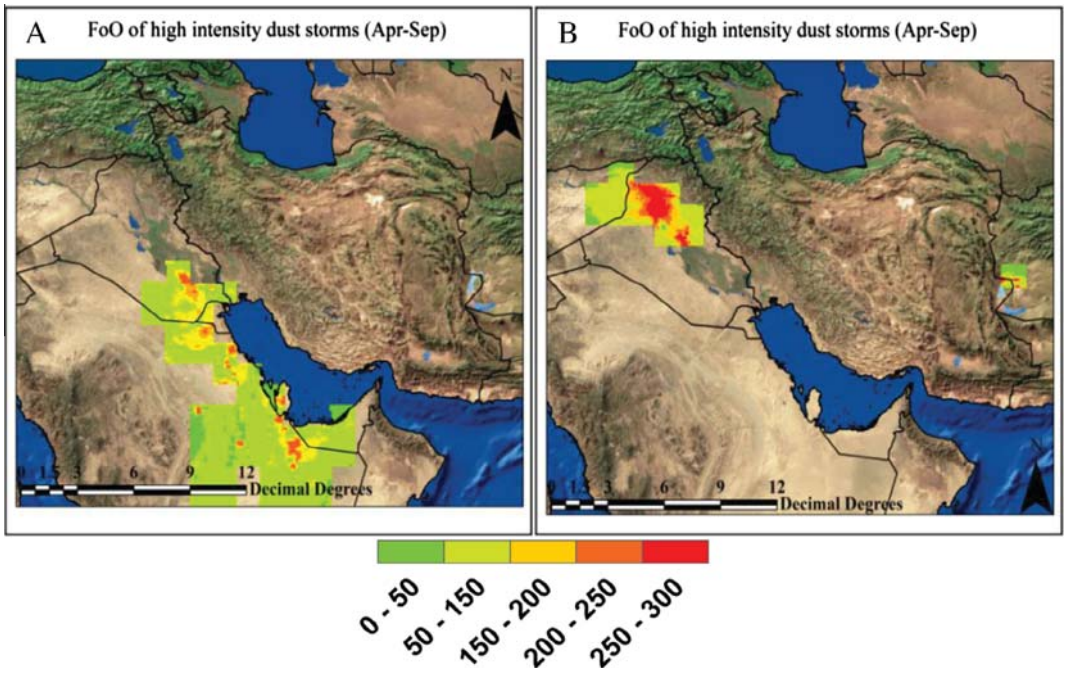

Fig. 15. FoO of high intensity dust storms (MODIS DB AOD > 0.85) in units days during April to September for the whole MODIS period 2003 to 2014 within permanent (A) and emerging (B) dusty areas.

Iraq and northwest of Iraq, a lagged correlation was computed between area-averaged MODIS DB AOD recorded in dust sources and West Asia for warm seasons (Fig. 16). The zero-lagged correlation represents the first day of dust outbreak, it shows the highest correlation with already identified dust sources and their surrounding areas, as expected. This is why zero-lagged correlation of permanent dust sources, during spring, increases getting closer to the southeast of Iraq and northern Arabian Peninsula. However, there is a high correlation tongue toward the north of Iraq and northwest Iran at lag zero (Fig. 16A). At lag 1, there are two moderate correlation clouds to the middle of Iran and south of Saudi Arabia (Fig. 16B).

The extension of a high correlation area to the north of Iraq, northwest of Iran, and south of Turkey is also visible for emerging dust sources, especially at 1-lagged correlation, during March to May (Fig. 16C and D). Since these areas are mountainous and cannot be affected by local dust sources, this pattern means that north of Iraq and northwest of Iran are two of the main receptors of dust storms formed in both dust source areas during spring. During summer, the high correlation of permanent dust sources and study areas is located from the northwest of Iraq to southeast of the east of Saudi Arabia at lag zero (Fig. 16E) and southeast Saudi Arabia and southwest of Iran at lag one (Fig. 16F). Similarly, lagged correlation of emerging dust source and West Asia show a

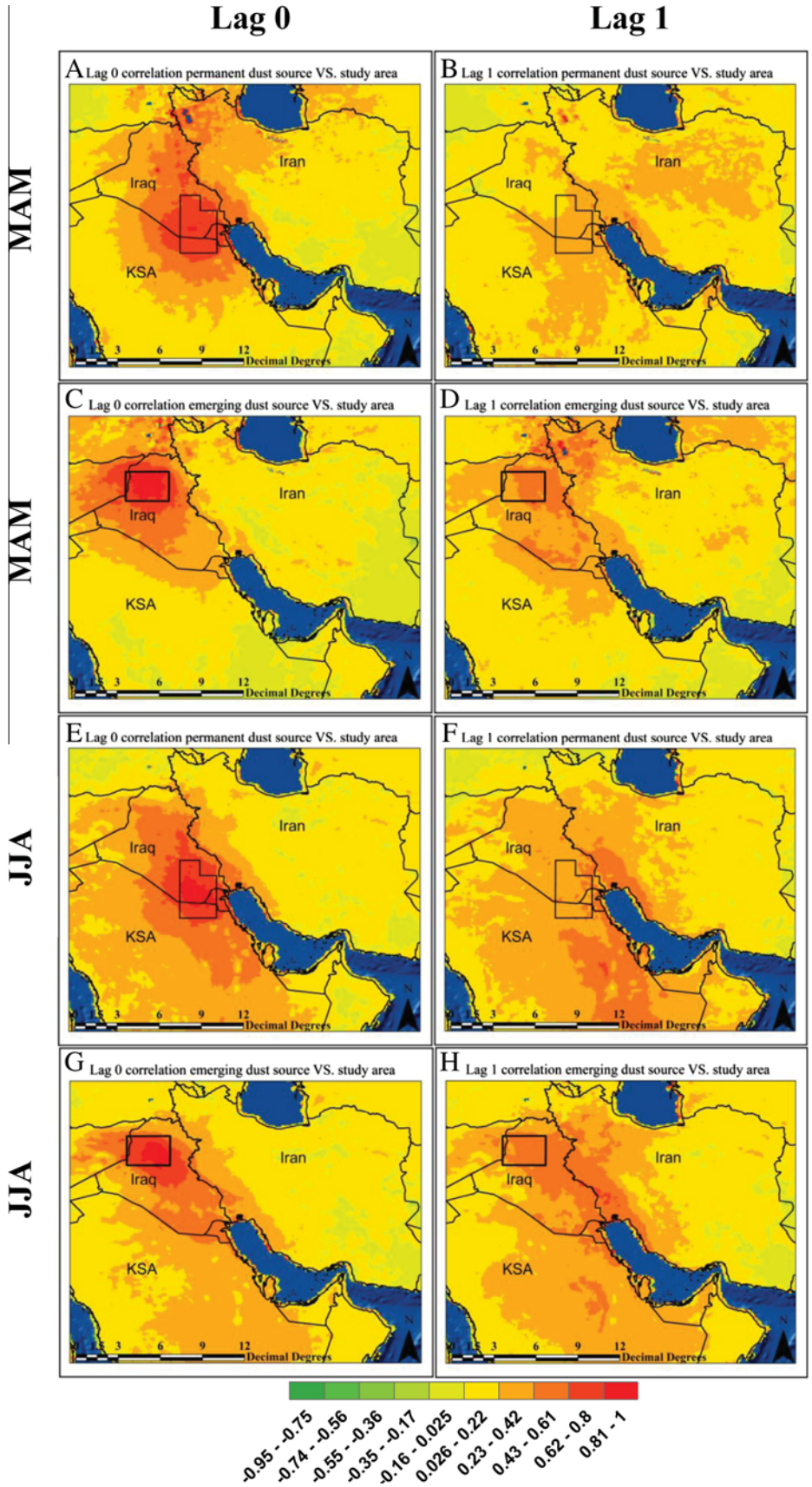

Fig. 16. Map of lagged Pearson correlation coefficients between dust sources, shown by black polygons, and study area during spring (MAM) and summer (JJA), calculated from MODIS DB AOD for period 2003–2014.

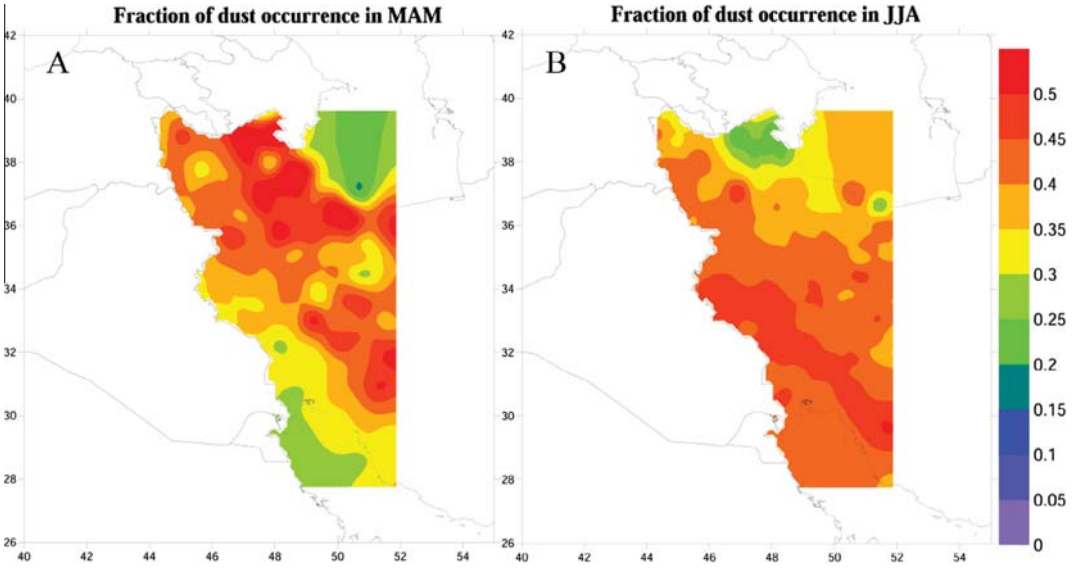

Fig. 17. The fraction of seasonal FoO of dust storms to total annual FoO of dust storms reported by synoptic stations in the West Iran (A) in Spring (B) in Summer for period 1980–2014.

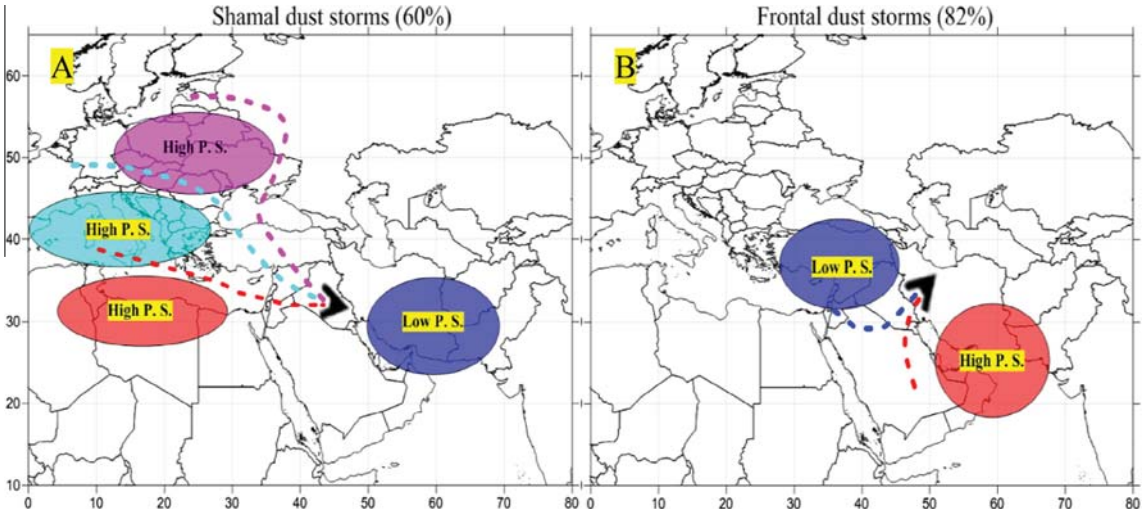

Fig. 18. Atmospheric patterns simultaneous with 60 percent of Shamal dust storms (A) and 86 percent of Frontal dust storms (B) adapted from Hamidi et al. (2013). Colored ellipses and curves are surface pressure systems and blowing winds, respectively. Shamal dust storms may be further classified depending on location of high-pressure systems (East-Central Europe, Mediterranean Sea or North of Africa). (For interpretation of the references to color in this figure legend, the reader is referred to the web version of this article.)

northwest-southeast path from northwest of Iraq to the southwest of Iran (Fig. 16G and H). Although lag-1 correlations of 0.23–0.42 cover most of the region during summertime, this grade of correlation over the Zagros Mountains can be a sign of dust transport from permanent and emerging dust sources to the west and northwest of Iran by thin dust plumes. To sum up, lagged correlation of identified permanent and emerging dust sources show two seasonal distinctive dust paths and receptors. Springtime dust (correlation) paths are both northward and reach south of Turkey and northwest Iran. During summer, dust storms take the northwest-southeast path and affect southwest of Iran, southeast of Iraq, Saudi Arabia, and other Persian Gulf countries. With the intention of verifying identified receptors, because of data accessibility, the seasonal fraction of dust events is examined in the west of Iran, by using meteorological dust codes of synoptic stations (Fig. 7).

Regarding that only dust cases formed in the warm period are studied here, fraction of dust occurrence, i.e. total seasonal FoO of dust storms/total annual FoO of dust storms, is just examined for spring and summer from 1980 to 2014.

According to lag correlation method, northwest and southwest of Iran are two of main receptors of dust storms during spring and summertime, respectively. These patterns are replicated in the 35-year climatologies of seasonal dust fraction. The north and northwest of Iran received the majority (more than 40–50 percent) of annual recorded dust events during spring (Fig. 17A). During summertime, the largest fraction of detected dust storms relocates to the southwest of Iran and it decreases to less than 40 percent in the northwest of this country (Fig. 17B). These patterns are consistent with Hamidi et al. (2013), who identify two main types of dust storms, called Shamal and Frontal dust storms, in West Asia. Analyzing atmospheric circulations of 180 dusty days, they found that Shamal is the most frequent type of dust storms in West Asia. Further examinations showed that 60% of Shamal dust storms are simultaneous with high-pressure systems, to the west of the

region, reaching from northern Europe to north of Africa and a low-pressure system centered over southern Iran. This atmospheric pattern causes strong winds (color dash lines), called Shamal Winds (Strachan, 2005), from northwest of Iraq to Persian Gulf countries (Fig. 18A). This circulation has the highest frequency in June and July when dust storms are mostly recorded in the southwest of Iran (Fig. 17B). During spring, Shamal dust storms are much less frequent but there are frequent dust storms of Frontal type, with high pressure over southern Iran and low pressure over the eastern Mediterranean Sea, Turkey and northern Iraq (Fig. 18B). This kind of circulation, which included 82% of studied Frontal cases transports dust plumes to north and northwest of Iran.

4. Conclusion and future work

This study aimed to investigate long-term activity of dust storms in West Asia, a region which experienced intensified dust storms in recent years. Preparing a Varying Threshold (VT) for Aerosol Index of TOMS and OMI, analysis of dust activity showed a temporal and spatial expansion of dust storms in the east of Syria and northwest of Iraq, called emerging dusty areas, in the last decade. Besides that, east and northeast of Saudi Arabia were found as permanent dusty area emitting large amounts of dust, at least from 1980 onward. The increase of dust storms in West Asia, especially in emerging areas, was attributed to an extreme drought in the Fertile Crescent during 2007–2012. According to monthly distribution of dust storms, June and July are the main periods of dust activity in West Asia. During recent years, dust storms of emerging dusty areas are becoming expanded to the whole warm period of the year what is commonplace in permanent dust areas from the beginning of study period. In order to discriminate dust sources from affected areas which constitute dusty areas, high-intensity dust storms are examined as an indicator of dust sources. Results show two main dust sources in the northwest of Iraq and southeast of Iraq and northern Saudi Arabia. Subsequently, the lagged correlation method revealed that there two distinct dust paths and receptors during spring and summertime in West Asia. During spring, dust storms are transported to the north of Iraq and northwest of Iran by a Frontal mechanism. During summer, Shamal atmospheric pattern makes dust plumes take northwest-southeast direction hitting southwest of Iran and Persian Gulf countries.

Considering the fact that the comprehensive understanding of dust storm is not achievable only through the study of its horizontal distribution, the future work aims to investigate the vertical structure of this phenomenon in West Asia. This can be done by using Weather Research and Forecasting model coupled with Chemistry (WRF-chem, (Grell et al., 2005)) simulations and Cloud-Aerosol Lidar and Infrared Pathfinder Satellite Observations (CALIPSO, (Ma et al., 2013; Adams et al., 2012)) products but is beyond the scope of this paper.

Acknowledgements

This work has been financially supported by EU 7th framework program ERA-CLIM (No. 265229) and the Austrian Science Funds FWF (Project P25260-N29).

References

Ackerman, S.A., 1989. Using the radiative temperature difference at 3.7 and 11 μm to tract dust outbreaks. Remote Sens. Environ. 27, 129–133.
Adams, A.M., Prospero, J.M., Zhang, C., 2012. CALIPSO-derived three-dimensional structure of aerosol over the Atlantic Basin and adjacent continents. J. Clim. 25, 6862–6879.
Ahmad, Z., Bhartia, P., Krotkov, N., 2004. Spectral properties of backscattered UV radiation in cloudy atmospheres. J. Geophys. Res. Atmos. 109.
Ahmad, S.P., Torres, O., Bhartia, P., Leptoukh, G., Kempler, S., 2006. Aerosol index from TOMS and OMI measurements. In: Proc. of the 86th AMS Annual Meeting.
Al Sarraf, H., 2010. Relationship between the land/sea breeze circulations and the air pollution dispersion over the coastal area of Kuwait.
Aurelius, L., Buttgereit, V., Cammelli, S., Zanina, M., 2007. The impact of Shamal winds on tall building design in the Gulf Region. Proceedings.
Azizi, G., Shamsipour, A., Miri, M., Safarrad, T., 2012. Synoptic and remote sensing analysis of dust events in southwestern Iran. Nat. Hazards 64, 1625–1638.
Boloorani, A.D., Nabavi, S.O., Bahrami, H.A., Mirzapour, F., Kavosi, M., Abasi, E., Azizi, R., 2014. Investigation of dust storms entering Western Iran using remotely sensed data and synoptic analysis. J. Environ. Health Sci. Eng. 12, 124.
Cao, H., Amiraslani, F., Liu, J., Zhou, N., 2015. Identification of dust storm source areas in West Asia using multiple environmental datasets. Sci. Total Environ. 502, 224–235.
Ciren, P., Kondragunta, S., 2014. Dust aerosol index (DAI) algorithm for MODIS. J. Geophys. Res.: Atmos. 119, 4770–4792.
Dee, D., Uppala, S., Simmons, A., Berrisford, P., Poli, P., Kobayashi, S., Andrae, U., Balmaseda, M., Balsamo, G., Bauer, P., 2011. The ERA-Interim reanalysis: Configuration and performance of the data assimilation system. Quartly J. R. Meteorol. Soc. 137, 553–597.
Ebrahimi, S.J., Ebrahimzadeh, L., Eslami, A., Bidarpoor, F., 2014. Effects of dust storm events on emergency admissions for cardiovascular and respiratory diseases in Sanandaj, Iran. J. Environ. Health Sci. Eng. 12, 110.
Esmaili, O., Tajrishy, M., Arasteh, P.D., 2006. Evaluation of dust sources in Iran through remote sensing and synoptical analysis. Atlantic Eur. Conf. Remote Imaging Spectrosc., 136–143
Furman, H.K.H., 2003. Dust storms in the Middle East: sources of origin and their temporal characteristics. Indoor Built Environ. 12, 419–426.
Gerivani, H., Lashkaripour, G.R., Ghafoori, M., 2011. The source of dust storm in Iran a case study based on geological information and rainfall data. Carpathian J. Earth Environ. Sci. 6.
Ginoux, P., Torres, O., 2003. Empirical TOMS index for dust aerosol: applications to model validation and source characterization. J. Geophys. Res.: Atmos. 108.
Ginoux, P., Prospero, J.M., Gill, T.E., Hsu, N.C., Zhao, M., 2012. Global-scale attribution of anthropogenic and natural dust sources and their emission rates based on MODIS Deep Blue aerosol products. Rev. Geophys. 50.
Goudie, A.S., Middleton, N.J., 2000. Dust storms in south west Asia. Acta Univ. C., 73–83, Supplement
Goudie, A., Middleton, N.J., 2006. Desert Dust in the Global System. Springer Science and Business Media.
Grell, G.A., Peckham, S.E., Schmitz, R., McKeen, S.A., Frost, G., Skamarock, W.C., Eder, B., 2005. Fully coupled "online" chemistry within the WRF model. Atmos. Environ. 39, 6957–6975.
Haimberger, L., 2007. Homogenization of radiosonde temperature time series using innovation statistics. J. Clim. 20, 1377–1403.
Haimberger, L., Tavolato, C., Sperka, S., 2012. Homogenization of the global radiosonde temperature dataset through combined comparison with reanalysis background series and neighboring stations. J. Clim. 25, 8108–8131.
Hamidi, M., Kavianpour, M.R., Shao, Y., 2013. Synoptic analysis of dust storms in the Middle East. Asia-Pac. J. Atmos. Sci. 49, 279–286.
Hsu, N.C., Tsay, S.-C., King, M.D., Herman, J.R., 2004. Aerosol properties over bright-reflecting source regions. Geoscience and Remote Sensing, IEEE Transactions on 42, 557–569.
Hsu, N., Gautam, R., Sayer, A., Bettenhausen, C., Li, C., Jeong, M., Tsay, S.-C., Holben, B., 2012. Global and regional trends of aerosol optical depth over land and ocean using SeaWiFS measurements from 1997 to 2010. Atmos. Chem. Phys. Discuss. 12, 8465–8501.
Jish Prakash, P., Stenchikov, G., Kalenderski, S., Osipov, S., Bangalath, H., 2014. The impact of dust storms on the Arabian Peninsula and the Red Sea. Atmospheric Chemistry & Physics Discussions 14, 19181–19245.
Karimi, N., Moridnejad, A., Golian, S., Vali Samani, J.M., Karimi, D., Javadi, S., 2012. Comparison of dust source identification techniques over land in the Middle East region using MODIS data. Canadian J. Remote Sens. 38, 586–599.
Ke-Yi, C., 2010. The northern path of Asian dust transport from the Gobi desert to North America. Atmos. Oceanic Sci. Lett. 3, 155–159.
Kiss, P., Janosi, I., Torres, O., 2007. Early calibration problems detected in TOMS Earth-Probe aerosol signal. Geophys. Res. Lett. 34.
Lyles, M., Fredrickson, H., Bednar, A., Fannin, H., Griffin, D., Sobecki, T., 2012. Medical geology in the Middle East: potential health risks from mineralized dust exposure. EGU Gen. Assembly Conf. Abstr., 1668
Ma, X., Bartlett, K., Harmon, K., Yu, F., 2013. Comparison of AOD between CALIPSO and MODIS: significant differences over major dust and biomass burning regions. Atmos. Meas. Tech. 6, 2391–2401.
Mahowald, N.M., Dufresne, J.L., 2004. Sensitivity of TOMS aerosol index to boundary layer height: Implications for detection of mineral aerosol sources. Geophys. Res. Lett. 31.
Mears, C.A., Schabel, M.C., Wentz, F.J., 2003. A reanalysis of the MSU channel 2 tropospheric temperature record. J. Clim. 16, 3650–3664.
Moridnejad, A., Karimi, N., Ariya, P.A., 2015a. A new inventory for middle east dust source points. Environ. Monit. Assess. 187, 1–11.
Moridnejad, A., Karimi, N., Ariya, P.A., 2015b. Newly desertified regions in Iraq and its surrounding areas: Significant novel sources of global dust particles. J. Arid Environ. 116, 1–10.
Notaro, M., Yu, Y., Kalashnikova, O.V., 2015. Regime shift in Arabian dust activity, triggered by persistent Fertile Crescent drought. J. Geophys. Res.: Atmos. 120.

Prospero, J.M., Ginoux, P., Torres, O., Nicholson, S.E., Gill, T.E., 2002. Environmental characterization of global sources of atmospheric soil dust identified with the Nimbus 7 Total Ozone Mapping Spectrometer (TOMS) absorbing aerosol product. Rev. Geophys. 40, 2-1-2-31.

Rashki, A., Kaskaoutis, D., Francois, P., Kosmopoulos, P., Legrand, M., 2015. Dust-storm dynamics over Sistan region, Iran: seasonality, transport characteristics and affected areas. Aeolian Res. 16, 35–48.

Rezazadeh, M., Irannejad, P., Shao, Y., 2013. Climatology of the Middle East dust events. Aeolian Res. 10, 103–109.

Shao, Y., Wyrwoll, K.-H., Chappell, A., Huang, J., Lin, Z., McTainsh, G.H., Mikami, M., Tanaka, T.Y., Wang, X., Yoon, S., 2011. Dust cycle: An emerging core theme in Earth system science. Aeolian Research 2, 181–204.

Strachan, J., 2005. Winds of the world. Weather 60, 331–332.

Taghavi, F., Asadi, A., 2007. The Persian Gulf 12th April 2007 dust storm: observation and model analysis.

Torres, O., Bhartia, P., Herman, J., Ahmad, Z., Gleason, J., 1998. Derivation of aerosol properties from satellite measurements of backscattered ultraviolet radiation: theoretical basis. J. Geophys. Res.: Atmos. 103, 17099–17110.

Trigo, R.M., Gouveia, C.M., Barriopedro, D., 2010. The intense 2007–2009 drought in the Fertile Crescent: Impacts and associated atmospheric circulation. Agric. For. Meteorol. 150, 1245–1257.

Vasilkov, A., Joiner, J., Spurr, R., Bhartia, P.K., Levelt, P., Stephens, G., 2008. Evaluation of the OMI cloud pressures derived from rotational Raman scattering by comparisons with other satellite data and radiative transfer simulations. Journal of Geophysical Research: Atmospheres 113.

Venema, V.K., Mestre, O., Aguilar, E., Auer, I., Guijarro, J.A., Domonkos, P., Vertacnik, G., Szentimrey, T., Stepanek, P., Zahradnicek, P., 2012. Benchmarking homogenization algorithms for monthly data. Clim. Past 8, 89–115.

WMO 2011. Manual on Codes. I.1.

4 Sensitivity of WRF-chem predictions to dust source function specification in West Asia

Seyed Omid Nabavi[1], Leopold Haimberger[1], Cyrus Samimi[2,3]

[1] Department of Meteorology and Geophysics, University of Vienna, Faculty of Earth Sciences, Geography and Astronomy, UZA II Althanstrasse 14, A-1010 Vienna, Austria

[2] Faculty of Biology, Chemistry and Earth Sciences, University of Bayreuth, Universitätsstr. 30, 95447 Bayreuth, Germany

[3] Bayreuth Center of Ecology and Environmental Research, BayCEER, Dr. Hans-Frisch-Straße 1-3, 95448 Bayreuth, Germany

Aeolian Research 21 (2016) 93–107

This chapter addresses Hypothesis 2 in which WASF is assumed as a more realistic representation of dust source distribution in the study area than GSF. A state-of-the-art dust model, WRF-chem, is used to check the effect of WASF on the accuracy of dust predictions. The beneficial impact of newly proposed source function is examined separately on the performance of three dust schemes of WRF-chem. Moreover, this study draws an inter-comparison between WRF-chem predictions and predicted DOD at 550nm by MACC and DREAM. Findings indicate that implementation of WASF could significantly improve the performance of all three dust schemes and that WRF-chem with WASF outperformed MACC and DREAM over the main dust sources.

- Conception of research approach: **Nabavi, S. O.** (major); Haimberger, L. (minor); Samimi, C. (minor)
- Development of research methods: **Nabavi, S. O.** (major); Haimberger, L. (minor); Samimi, C. (minor)
- Data collection and data preparation: **Nabavi, S. O.** (major); Haimberger, L. (minor); Samimi, C. (minor)
- Execution of research: **Nabavi, S. O.** (major); Haimberger, L. (minor); Samimi, C. (minor)
- Analysis/Interpretation of data or preliminary results: **Nabavi, S. O.** (major); Haimberger, L. (major); Samimi, C. (minor)
- Writing or substantive rewriting of the manuscript: **Nabavi, S. O.** (major); Haimberger, L. (major); Samimi, C. (minor)
- Role of **Nabavi, S. O.**: leading contribution (80 %)

Aeolian Research 24 (2017) 115–131

Contents lists available at ScienceDirect

Aeolian Research

journal homepage: www.elsevier.com/locate/aeolia

Sensitivity of WRF-chem predictions to dust source function specification in West Asia

Seyed Omid Nabavi [a,*], Leopold Haimberger [a], Cyrus Samimi [b,c]

[a] Department of Meteorology and Geophysics, Faculty of Earth Sciences, Geography and Astronomy, University of Vienna, UZA II Althanstrasse 14, A-1010 Vienna, Austria
[b] Faculty of Biology, Chemistry and Earth Sciences, University of Bayreuth, Universitätsstr. 30, 95447 Bayreuth, Germany
[c] Bayreuth Center of Ecology and Environmental Research, BayCEER, Dr. Hans-Frisch-Straße 1-3, Universitätsstr. 30, 95448 Bayreuth, Germany

ARTICLE INFO

Article history:
Received 25 August 2016
Revised 22 December 2016
Accepted 26 December 2016

Keywords:
WRF-chem
Source function
Dust storms
West Asia

ABSTRACT

Dust storms tend to form in sparsely populated areas covered by only few observations. Dust source maps, known as source functions, are used in dust models to allocate a certain potential of dust release to each place. Recent research showed that the well known Ginoux source function (GSF), currently used in Weather Research and Forecasting Model coupled with Chemistry (WRF-chem), exhibits large errors over some regions in West Asia, particularly near the IRAQ/Syrian border.

This study aims to improve the specification of this critical part of dust forecasts. A new source function based on multi-year analysis of satellite observations, called West Asia source function (WASF), is therefore proposed to raise the quality of WRF-chem predictions in the region. WASF has been implemented in three dust schemes of WRF-chem. Remotely sensed and ground-based observations have been used to verify the horizontal and vertical extent and location of simulated dust clouds. Results indicate that WRF-chem performance is significantly improved in many areas after the implementation of WASF. The modified runs (long term simulations over the summers 2008–2012, using nudging) have yielded an average increase of Spearman correlation between observed and forecast aerosol optical thickness by 12–16 percent points compared to control runs with standard source functions. They even outperform MACC and DREAM dust simulations over many dust source regions. However, the quality of the forecasts decreased with distance from sources, probably due to deficiencies in the transport and deposition characteristics of the forecast model in these areas.

1. Introduction

Most dust storms form in arid and semi-arid areas where dry soil, sparse vegetation, high-speed winds and erodible sediments favor dust emission. In the last decade, an unprecedented upsurge of dust storms in West Asia, particularly west of the Iranian plateau, has caused many problems for inhabitants. According to recent studies (Boloorani et al., 2014; Nabavi et al., 2016), the northern floodplains of Iraq are the most active dust sources in the region. However, a realistic quantitative calculation of dust emission has always been a challenge. In numerical models forecasting dust, the dust emission flux (F) is typically parameterized by time-independent dust source function (DSF), commonly denoted by S, and time-dependent factors such as wind speed (Ginoux et al., 2001). Although not time-dependent, at least on sub-decadal time scales, the specification of S is far from trivial as well (Koven and Fung, 2008; Lee et al., 2009; Walker et al., 2009; Bullard et al., 2011; Cao et al., 2015).

In the following we discuss some well-established DSFs in two main categories:

1.1. Source functions based on physical characteristics of land surface

Ginoux et al. (2001) prepared a topography-based global DSF (Eq. (1)), which will be referred to as "Ginoux source function (GSF)" in this paper.

$$S = \left(\frac{Z_{max} - Zi}{Z_{max} - Z_{min}}\right)^5 \quad (1)$$

S is the probability value assigned to pixel i to have accumulated sediments at altitude Zi, where Zi is normalized in proportion to maximum Z_{max} and minimum Z_{min} altitudes over a surrounding area of $10° \times 10°$.

* Corresponding author.
E-mail addresses: seyed.omid.nabavi@univie.ac.at (S.O. Nabavi), leopold.haimberger@univie.ac.at (L. Haimberger), cyrus.samimi@uni-bayreuth.de (C. Samimi).

http://dx.doi.org/10.1016/j.aeolia.2016.12.005
1875-9637/

Kumar et al. (2014) noted that the calculation of S requires dense observations of alluvium in the study area. Due to the lack of data, S is indirectly assessed based on topographic features. GSF has been first implemented in the Goddard Chemistry Aerosol Radiation and Transport (GOCART) aerosol model, and has been applied to bare soil surfaces (Cavazos-Guerra and Todd, 2012). Bare surfaces were designated based on land cover data from the advanced very high-resolution radiometer (AVHRR) (DeFries and Townshend, 1994). Kim et al. (2013) argued that a static land cover does not reflect annual and seasonal variations of soil bareness. So, they used 15-day normalized difference vegetation index (NDVI) data from AVHRR and prepared a dynamic bareness map (NDVI < 0.15) and, consequently, a dynamic DSF. Results showed significant improvements in GOCART simulations over regions with seasonally changing soil bareness. However, further examinations indicated that the progress is rather small in a global perspective. It is attributed to the small contribution (12%) of these regions to global dust emission. Over West Asia there is very little seasonal change of soil bareness and thus does not cause significant modifications on values of GSF. Zender et al. (2003) have proposed two other source functions, called Geomorphic and Hydrologic, and compared them with GSF. The Hydrologic erodibility function was determined based on the runoff at the local and upstream neighbor grid cells. The Geomorphic source function was defined as the total of the area of all grid cells that flow into a given grid cell. Both functions were, normalized by the maximum value of the neighboring grid cells. Using the Dust Entrainment and Deposition (DEAD) model, they have concluded that the geomorphic source function most closely represents realistic global erodibility. However, it is noted that both source functions are strongly affected by discrete values of flow direction and topography. In addition, results showed that GSF outperformed these two functions over the North African dust sources, known as the strongest dust source in the world (Shao et al., 2011b). To sum up, all above-mentioned algorithms use land surface features, i.e. geomorphology, hydrology, and vegetation characteristics of land surfaces, to indirectly identify the most probable locations of dust sources.

1.2. Source functions based on direct observation of dust particles

During the past few decades, various remote sensing algorithms have been developed to increase the accuracy of dust detection and, subsequently, improve the identification of dust sources (Ackerman, 1989, 1997; Torres et al., 1998; Hsu et al., 2004; Roskovensky and Liou, 2005; Karimi et al., 2012; Samadi et al., 2014). Prospero et al. (2002) assumed the frequency of occurrence (FoO) of Total Ozone Mapping Spectrometer (TOMS) Aerosol Index (AI) > 0.7 for designating dust sources. As a result, topographic depressions were determined as the main sources of dust emission. According to their findings, almost entire West Asia is determined as a vast dust source during July.

Although the TOMS AI has long time coverage (since 1979 to present) and seems ideal for climatological studies of dust sources, Mahowald and Dufresne (2004) have pointed out that AI is sensitive to dust layer height. This causes exaggerated AI values over desert areas and during warm periods of the year. In fact, high AI does not necessarily represent a dust source and it can be merely because of high surface temperature, boundary layer and, consequently, highly elevated aerosol particles. Therefore, they have recommended using a spatiotemporally varying threshold (VT) for the detection of dust events, instead of direct use of AI or determining a fixed threshold (FT).

Ginoux et al. (2012) proposed a new algorithm for dust source determination in which AI is replaced with the Moderate Resolution Imaging Spectroradiometer (MODIS) deep blue aerosol optical depth (DB AOD). Considering physical and optical properties of aerosols, authors extracted dust optical depth (DOD) from the already retrieved AOD from 2003 to 2009. FoO of DOD > 0.2 was used as a criterion for the determination of dust sources. This new source function, which is officially implemented in NASA Unified Weather Research and Forecasting Model (NU-WRF) (Zaitchik et al., 2013), designated a boundary region between Iraq and Saudi Arabia and northwest of Iraq as two main dust sources of West Asia. Using different approaches, several studies have also documented the latter as a hot spot in the region (Boloorani et al., 2013, 2014; Cao et al., 2015; Moridnejad et al., 2015b). In contrast, another hot spot, found in the north of Saudi Arabia, has not been reported as a major origin of dust storms. Conducting a preliminary study, we also found that Ginoux's new source function did not result in a significant progress in the accuracy of WRF-chem predictions. Hence, here, this source function is excluded from further examinations.

Parajuli et al. (2014) prepared the most recent global DSF by normalizing the Spearman correlation coefficient (SCC) between monthly wind speed at 10 m and DB AOD, both with the resolution of 1 degree. Considering that wind speed and dust concentration are very dynamic and resolution dependent, the analysis of rough spatial resolution data on a monthly basis does not seem robust enough to represent the instantaneous conditions along with dust events. Moreover, using correlation coefficient for dust source determination has led to unacceptable results over non-erodible areas such as western Iran. This is the region of the Zagros Mountains which cannot have any contribution to dust emission (Gerivani et al., 2011), but it is attributed with erodibility values comparable with desert areas in the east of Saudi Arabia. In other words, this method leaves some values everywhere even if it is made of non-erodible lands.

Given the deficiencies found in the existing literature, this study aims to provide a new DSF called West Asia source function (WASF) which is based on more detailed information of dust distribution in the region (Nabavi et al., 2016). The second aim of this study is to demonstrate the beneficial impact of WASF on forecasts with WRF-chem.

The detailed descriptions of WASF, WRF-chem dust schemes, verification data and methods are presented in the next section, results are discussed in section 3 and Section 4 is allotted to conclusions.

2. Data and methods

In this section we first describe which input data are used and how these data are processed for creating WASF. Then, we discuss WRF-chem dust schemes, in which WASF has been implemented, and the model configuration in subsections 2 and 3, respectively. The fourth part of this section presents data and methods used for the verification of WRF-chem simulations.

2.1. Data and methods used for preparing West Asia source function (WASF)

The basic data source for WASF is TOMS-Ozone Monitoring Instrument (OMI) AI in the resolution of ≈1 degrees, which is available back to 1979. Principally, the value of AI can be used to discriminate air parcels as dusty/not dusty. However, AI data are delicate to use because the AI values depend not only on dust concentration and it contains several temporal inhomogeneities. Nabavi et al. (2016) have discussed that AI sensitivity to aerosol height can lead to erroneous identification of dust sources over regions with high boundary layer, like west of Saudi Arabia. In this paper, also several strong temporal inhomogeneities introduced by the switch from TOMS to OMI in 2005 and by calibration drift

issues of TOMS-data in the period 2002–2004 have been highlighted. In order to deal with these problems, they have recommended following measures replicated here:

1. Besides the data gap between 1993 and 1996, AI recorded by TOMS during 2002–2004 were excluded from examinations.
2. Following Mahowald and Dufresne (2004), original data of AI or a fixed threshold (FT) were not used in examinations. Instead they have prepared a Varying Threshold (VT) for the warm months to deal with the sensitivity of AI data to aerosol height. VT was defined as the multi-year average of AI simultaneous with Sea-Viewing Wide Field-of-View Sensor (SeaWifs) DB AOD between 0.5 and 0.55 during warm months. Choosing this range was based on subjective examinations of SeaWIFS DB AOD during 65 dust storms between 1998 and 2010 and conducted researches by Mahowald and Dufresne (2004) and Moridnejad et al. (2015a). In fact, DB AOD 0.5–0.55 was used to make sure that intense dust cases are excluded from the preparation of VT so that it is only determined by varying boundary layer height and a roughly constant dust concentration.
3. Finally, the VT was separately prepared for TOMS and OMI instruments which helps avoiding a discontinuity in AI dataset (dust occurrence).

By the analysis of FoO of VT-based dust cases and considering the temporal length of dust activity, they grouped main dust sources of the region as permanent and emerging dust sources, located in the eastern half of Saudi Arabia and south east of Iraq and northwest of Iraq and east of Syria, respectively (Fig. 1).

Permanent dusty areas were defined as where FoO of VT-based dust cases >800 in both study periods 1980–1997 and 1998–2014. Emerging areas covers regions with FoO of VT-based cases <500 during 1980–1997 and >500 between 1998 and 2014 in most pixels. In order to use these dust source masks as source function, they need to be quantified in higher resolution. Considering that Nabavi et al. (2016) used a threshold of DB AOD > 0.8 for the detection of high-intensity dust sources, here we used DB AOD > 0.7 to include all activating source points in the region. This threshold is implemented on DB AOD with an approximate resolution of 0.1 degree during 2003 to 2014. Fig. 2A shows the quantified masks of permanent and emerging dust sources using DB-based FoO of dust cases (AOD DB > 0.7), normalized by the high percentile. Unlike GSF (Fig. 2B), regions in the west and middle of Iraq got no erodibility in WASF. In other words, WASF yields the highest erodibility values for the northwest and southeast of Iraq, eastern Syria and eastern half of Saudi Arabia. The reliance of GSF on elevation variations has caused the assignment of high values to the middle and southeast of Iraq and eastern half of Saudi Arabia located in topographic concavities.

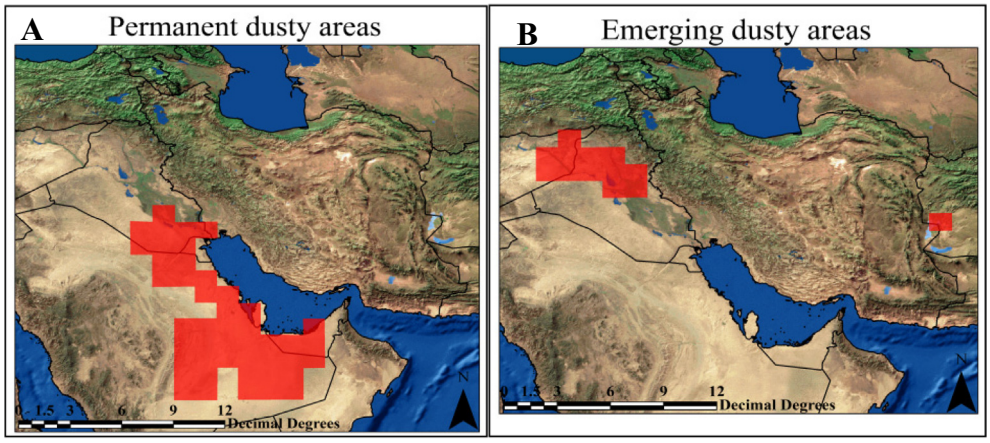

Fig. 1. Permanent (A) and emerging (B) dust sources in West Asia (Nabavi et al., 2016).

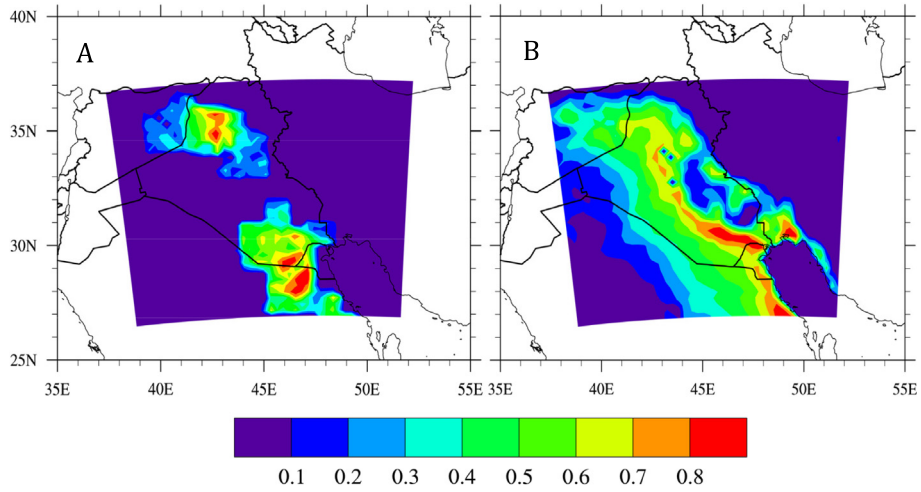

Fig. 2. A: WASF source function using DB AOD > 0.7 bounded by emerging and permanent dust source masks shown in Fig. 1. B: Ginoux source function (GSF) acquired from WRF terrestrial inputs.

Comparing to GSF, WASF results in a general reduction in the erodibility in the region and consequently in dust flux. This inevitably reduces the concentration of simulated dust emission and resulting AODs. However, here, the priority is to provide a more accurate source function for West Asia. If so, this underestimation, a systematic bias, can be fixed through manipulation of tuning parameters, for example parameter C in Eq. (2).

It is worth mentioning that WASF can be simply implemented in WRF-chem terrestrial inputs by the execution of a Linux shell script named WASF_implementation.sh. This script along with WASF_implementation.ncl, written in the NCAR Command Language (NCL) version 6.3, and WASF.nc should be placed in the WRF Preprocessing System (WPS) directory. They are all publically available at ftp://srvx1.img.univie.ac.at/pub/WASF.

2.2. WRF-chem dust schemes

In the following, three dust schemes, in which WASF has been implemented, are presented to clarify the role of source function in regulating the dust emission flux.

2.2.1. GOCART dust scheme

GOCART, as a general aerosol model, simulates major aerosol components of atmosphere such as salt, dust, sulfate and black carbon. (Chin et al., 2000; Ginoux et al., 2001). Following Gillette and Passi (1988), GOCART dust simulations require knowledge of the 10 m wind speed and of the lowest wind speed (threshold velocity) inducing wind erosion. The following expression approximates the amount of emitted dust F_p for the dust size class p:

$$F_p = CS\, s_p\, u^2(u - u_t) \quad if\ u > u_t \tag{2}$$

where C is a constant assumed to be 1 mg s^2 m^{-5}. In the present study, C is modified to the most recommended value of 2.2 (Kumar et al., 2014) to compensate partly the reduction of erodibility by WASF. s_p is the proportion of each particle size within the soil, u and u_t are the wind speed at 10 m and threshold velocity of wind erosion, respectively. S is the DSF, i.e. our subject of sensitivity examinations.

2.2.2. AFWA dust scheme

The Air Force Weather Agency (AFWA) dust scheme is based on the work of Marticorena and Bergametti (1995) and is composed of three main components including threshold friction velocity,

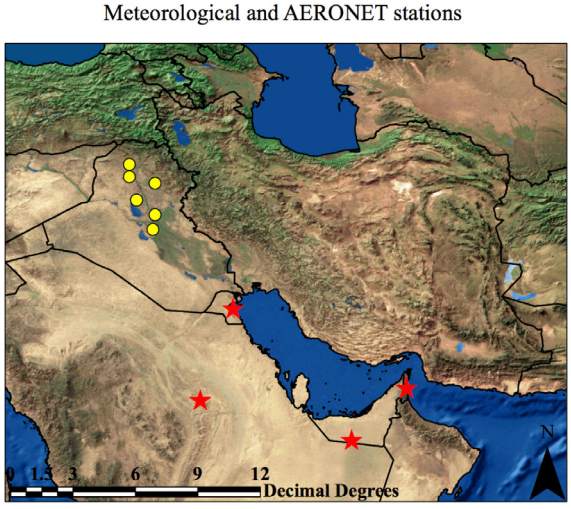

Fig. 3. Synoptic stations (Climate Data OnLine (CDO)) in the northwest of Iraq (yellow dots). Stars indicate the location of AERONET stations ((For interpretation of the references to colour in this figure legend, the reader is referred to the web version of this article.)

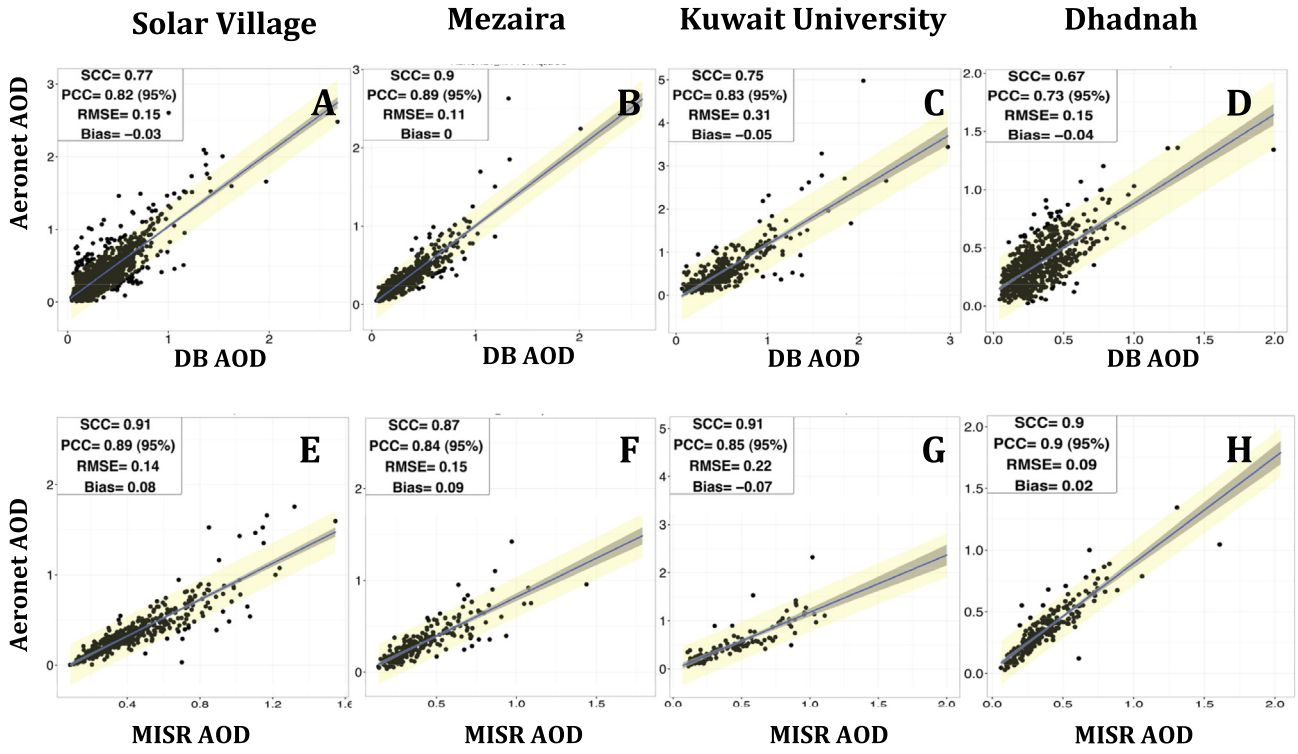

Fig. 4. Scatter plots between MODIS DB (A–D) and MISR (E–H) AODs 550 nm and AERONET stations AOD 550 nm, see also Fig. 3. Values in the boxes are Spearman Correlation Coefficients (SCC), Pearson Correlation Coefficient (PCC), Root Mean Square Error (RMSE) and bias. Gray and light yellow bands are respectively representatives of confidence intervals and prediction intervals. (For interpretation of the references to colour in this figure legend, the reader is referred to the web version of this article.)

saltation flux, and bulk vertical dust flux. To avoid redundancy, in the following, only two latter components are discussed.

A) Saltation flux: the dust flux is quantified through saltation flux (Eq. (3)).

$$H = C\frac{\rho_a}{g}u_*^3\left(1+\frac{u_{*t}}{u_*}\right)\left(1-\frac{u_{*t}^2}{u_*^2}\right), \tag{3}$$

where C is an empirical constant, ρ_a is the density of air parcel, g is the acceleration of gravity, u_* and u_{*t} are, respectively, friction velocity and threshold friction velocity.

B) Bulk vertical dust flux: the concentration of elevated dust triggered by saltation is explained by following expression (Eq. (4)).

$$F_{bulk} = H\alpha * S, \tag{4}$$

where α is the sandblasting efficiency factor chosen equal to $10^{0.314(\%clay)-6}$ (Gillete, 1979). In this dust scheme again S is the DSF to be examined.

2.2.3. Shao size-resolved dust scheme

The amount of emitted dust of size d_i is calculated as a weighted average over the particle sizes of d_1 and d_2:

$$F(d_i) = \int_{d_1}^{d_2} F(d_i;d_s)p_s(d)\delta d \tag{5}$$

where $F(d_i;d_s)$ is defined as (Shao, 2004) and p_s is:

$$p_s(d) = \gamma p_m(d) + (1-\gamma)p_f(d) \tag{6}$$

Shao et al. (2011a) simplified this statement and assumed $\gamma = 1$. Because of this simplification, $p_f(d)$, the fully disturbed soil particle size distribution, is omitted in the simplified scheme (Su and Fung, 2015). Consequently, $p_s(d) = p_m(d)$, the minimally disturbed soil particle-size distribution, and is defined as:

$$p_m(d) = \frac{1}{d}\sum_{j=1}^{J}\frac{w_j}{\sqrt{2\pi\sigma_j}}exp\left(-\frac{(\ln d - \ln D_j)^2}{2\sigma_j^2}\right) \tag{7}$$

where J is the number of modes, w_j is the weight for the j th mode of the particle size distribution, D_j and are parameters for the log-normal distribution of the j th mode (Shao, 2004). Considering Eq. (7), fine dust particles are the main contributors to dust emission in Shao simulations, discussed later. As documented in the WRF source code, the Shao dust scheme uses the DSF only to constrain the boundaries of dust sources instead of using it for scaling dust emission (as it is the case in GOCART and AFWA schemes).

2.3. Model configuration

The model domain (Fig. 2) is centered on 32° N and 45° E extending from about 26.5° N to 36.5° N (40 grid points) and from about 38° E to 52° E (45 grid points) with 40 levels in the vertical on a Lambert projection. Static geographical fields are interpolated to the model domain resolution, 10 km, by using the WRF preprocessing system (WPS). NCEP Final Analysis (FNL) 6-hourly data, with a spatial resolution of 1° × 1°, are used to provide the meteorological initials and boundary conditions. Surface processes are initialized and predicted by the use of the Noah Land Surface

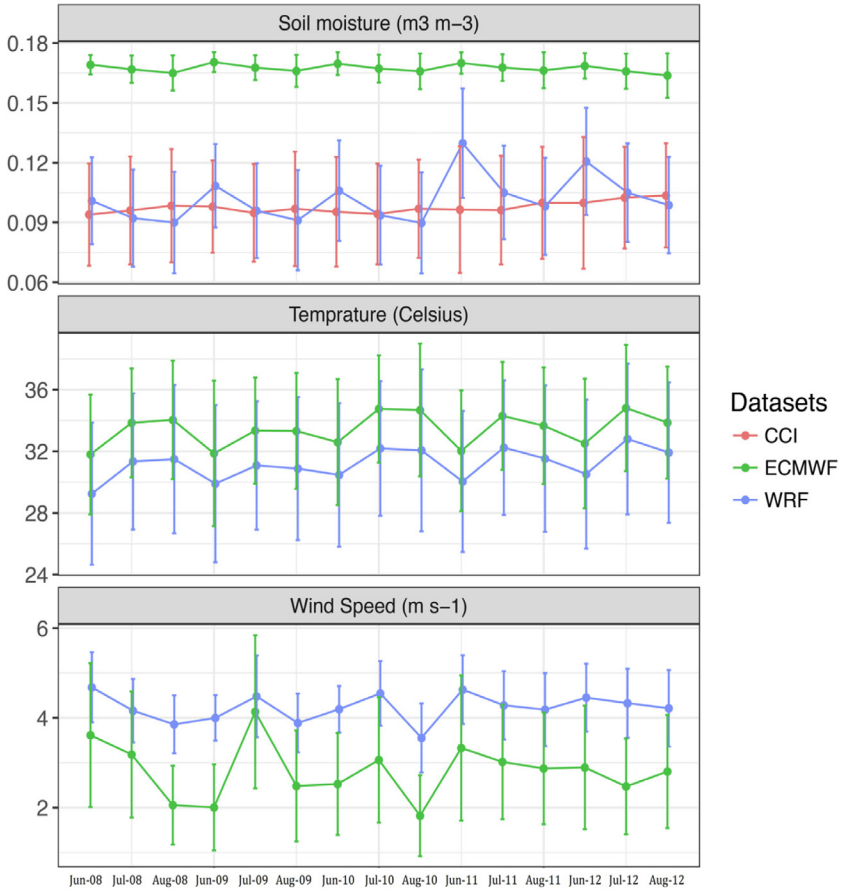

Fig. 5. Area-averaged volumetric soil moisture (m3 m-3) at 0–10 cm depth, air temperature at 2 m and wind speed at 10 m over West Asia during summer months 2008–2012. WRF-chem simulations are blue dotted lines, ECMWF simulations are green dotted lines and ESA-CCI soil moisture is red dotted line. Error bars are one standard deviation. (For interpretation of the references to colour in this figure legend, the reader is referred to the web version of this article.)

model (Chen and Dudhia, 2001) and MM5 similarity scheme (Beljaars, 1995). According to Lo et al. (2008) and Kumar et al. (2014), the horizontal winds (if_no_pbl_nudging_uv = 0), water vapor mixing ratio (if_no_pbl_nudging_q = 0), and temperature (if_no_pbl_nudging_t = 0) are nudged (grid_fdda = 1) towards the meteorological fields at all vertical levels. Nudging was necessary to have realistic meteorological forecast fields throughout the period (30 days) of the individual forecasts. It is important to note that the meteorological fields, apart from the dust parameters, have been practically equal in the control and modified runs since the dust concentration has a relatively weak feedback on the meteorological fields. The dust parameters have of course not been subject to nudging. WSM 5-class and YSU are respectively used as schemes for microphysics (mp_physics = 4) and boundary layer physics (bl_pbl_physics = 1). Longwave and shortwave radiation options are set to rrtm scheme (ra_lw_physics = 1) and Goddard short wave convective (ra_sw_physics = 2), respectively. The physical parameterization settings are those used in standard WRF-chem runs and are proven to be robust under a large variety of meteorological conditions. It is possible that one could achieve better skills with other physical parameterizations or parameters, but this has been considered beyond the scope of the study.

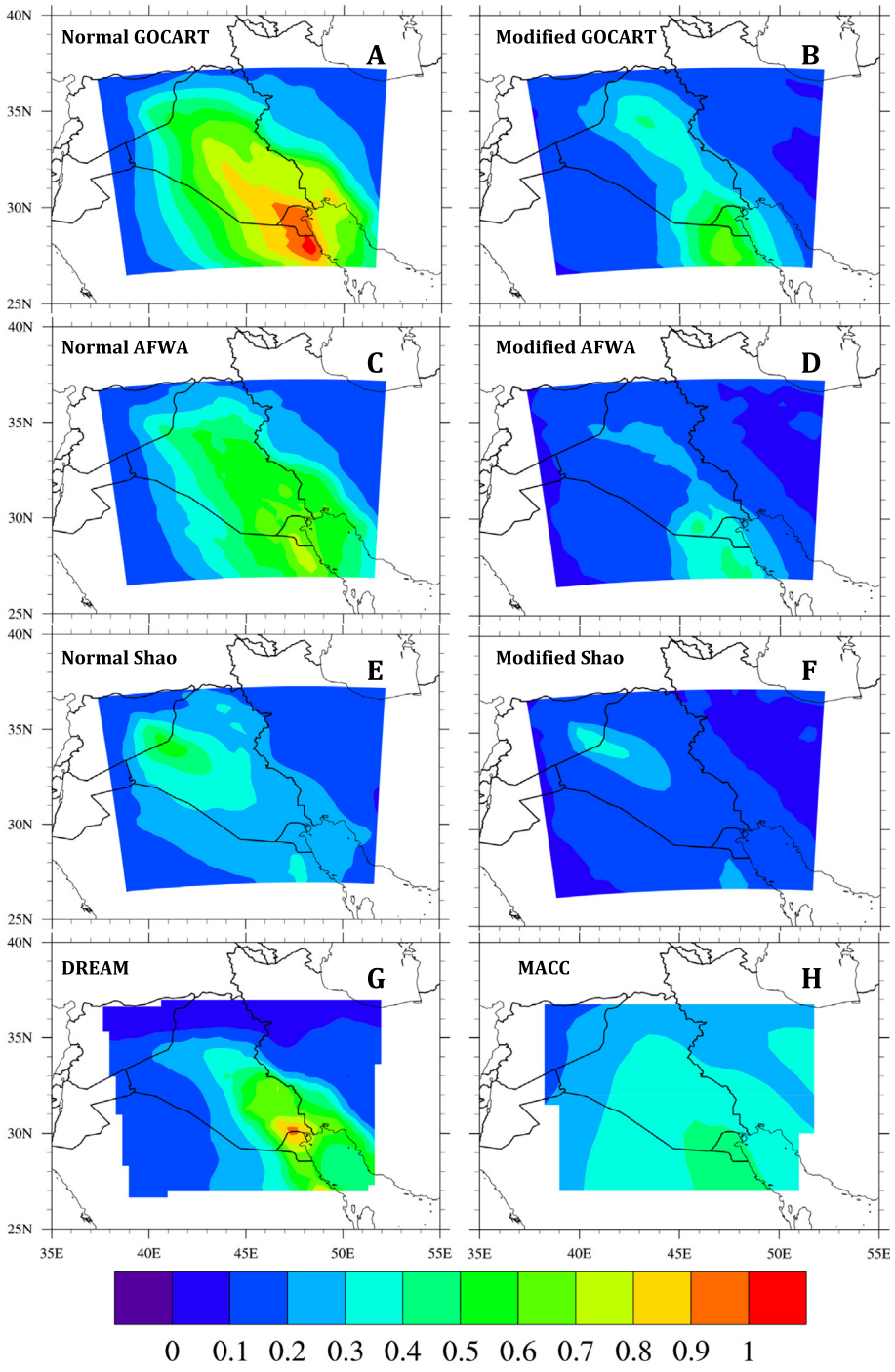

Fig. 6. Averaged AODs at 550 nm simulated by control and modified runs of GOCART (A and B), AFWA (C and D), and Shao (E and F). G and H are, respectively, simulated and reanalyzed DODs from DREAM and MACC. They all are averaged over summertime between 2008 and 2012.

WRF-chem simulations are executed twice as control (with GSF) and modified (WASF) runs for each dust scheme, GOCART (dust_opt = 1) AFWA (dust_opt = 3), and Shao 2011 (dust_opt = 4 and dust_schme = 3), during summertime (Jun, July and August) of five years between 2008 and 2012. It is when West Asia has witnessed a significant upsurge of dust storms (Nabavi et al., 2016). Because WRF is computationally expensive, simulation period was split to 15 monthly runs. So, both control and modified runs are monthly reinitialized. We exclude simulations of the first day of each month as model spin up time.

2.4. Verification data and methods

WRF-chem forecasts dust concentration in the first place. This parameter is, however, very hard to verify directly. There exist observation operators, however, that calculate simulated Aerosol Optical Depth (AOD) at 550 nm from the forecast dust concentration fields (Chin et al., 2002). AOD can be measured both from ground based as well as satellite platforms.

The AErosol RObotic NETwork (AERONET) is a worldwide measurement network intended for gathering optical and physical properties of aerosols. It is commonly used for the verification of other remotely sensed datasets (Bibi et al., 2015) or model simulations (Ginoux et al., 2001). However, only a small number of AERONET stations are established over the study area, especially over dust sources. Because of this, additional verifications of simulations are done by the use of two remotely sensed datasets including MODIS DB AOD and Multi-angle Imaging SpectroRadiometer (MISR) AODs at 550 nm. In order to retrieve aerosol optical thickness over bright areas, like deserts, Hsu et al. (2004) developed DB AOD algorithm. Here we used daily MODIS DB AOD from AQUA platform named MYD04_L2. This product is accessible at a high-resolution of 10 km from 2003 to present (http://ladsweb.nascom.nasa.gov/data/search.html). The MISR instrument installed on the TERRA satellite has provided aerosol optical properties over the oceans and the continents from 1999 to present (Lee and Chung, 2012). Daily MISR AOD 550 nm (MIL3DAE v4) were downloaded at a resolution of 0.5° by 0.5° from the NASA Goddard online visualization and analysis tool (Giovanni, http://giovanni.gsfc.nasa.gov/giovanni/). The comparison of these two products with AERONET AOD has previously shown that they could successfully represent the concentration of dust clouds over different regions (Bibi et al., 2015). In order to check if these results are also valid for West Asia, DB and MISR AODs are compared with AERONET AOD at 550 nm acquired from four stations (Fig. 3) including Dhandah (25.5 N and 56.31E), Kuwait University (29.31 N and 47.96E), Solar Village (24.9 N and 46.38E), and Mezaira (23 N and 53.76E). Except Kuwait University, the other three AERONET stations are out of study area. Fig. 4 shows that both MISR and DB AODs have got high values of SCCs at all stations. The agreement of WRF-chem AOD at 550 nm with these two products is measured through calculation of SCC, Root Mean Square Error (RMSE) (Eq. (8)) and bias (Eq. (9)):

$$RMSE = \sqrt{\frac{1}{n}\sum_{i=1}^{n}\left(AOD_{(WRF-chem)} - AOD_{(MISR)}\right)^2} \quad (8)$$

$$Bias = \frac{AOD_{(WRF-chem)}}{AOD_{(MISR)}} \quad (9)$$

where n is the number of observations.

Since the observation operator applied to WRF-chem dust concentrations only provides AOD 550 nm (not DB AOD 550 nm), RMSE and bias are calculated only for comparisons with the MISR product and the SCC is calculated for both MISR and MODIS.

The vertical distribution of dust particles in the WRF control and modified simulations are verified by comparing simulated extinction coefficients at 550 nm with observations acquired from Cloud-Aerosol LIDAR and Infrared Pathfinder Satellite Observations (CALIPSO). CALIPSO is a two-wavelength (532 and 1064 nm) polarization LIDAR that provides profile information of aerosols during daytime and nighttime for the atmospheric cross section of an orbit. Because daytime data are affected by sunlight (Adams et al., 2012), here, only nighttime profiles of extinction coefficients at 532 nm are used. This product is accessible at vertical and horizontal resolutions of 60 m and 5 km, respectively, and with a revisit time of 16 days from 2006 to present (Ma et al., 2013; Adams et al., 2012).

In addition to optical observations, the performance of model predictions is also examined by the use of weather codes of 6 synoptic stations located in the northwest of Iraq, as one of the main dust sources in the region (Fig. 3). To do so, simulated AODs were categorized as dust and no-dust events and compared against meteorological dust codes, 6–9 and 30–35 (WMO, 2011). The dust and no-dust cases are discriminated by applying the threshold of AOD 550 nm > 0.5 on simulations (Mahowald and Dufresne, 2004). Considering that each dataset (model simulations) has its own bias to observations, this threshold has been first adjusted by being multiplied by its bias (Eq. (9)). In the next step a contingency table is prepared between simulated and observed dust cases. In this method, variables "a", "b", "c", and "d" represent true positives, false positives, false negatives, and true negatives, respectively. True positives are the number of dust events detected by both synoptic observations and model simulations. False positives are the number of times where observations, indicate "no dust," but simulations indicate "dust". False negatives are the number of times where synoptic observations indicate "dust," but simulated AODs indicate "no dust". True negatives are the number of times where both datasets indicate "no dust". These four elements provide components of three validation methods: Probability Of Correct positive Detection (POCD), Probability Of False positive Detection (POFD) and Peirce Skill Score (PSS) (Ciren and Kondragunta, 2014). They are defined as follows:

$$POCD(\%) = \frac{a}{a+c} * 100 \quad (10)$$

$$POFD(\%) = \frac{b}{b+d} * 100 \quad (11)$$

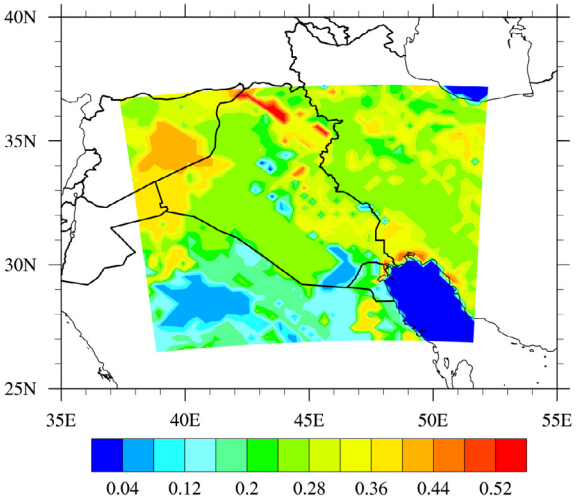

Fig. 7. The fraction of clay, acquired from WRF terrestrial inputs, in the study region.

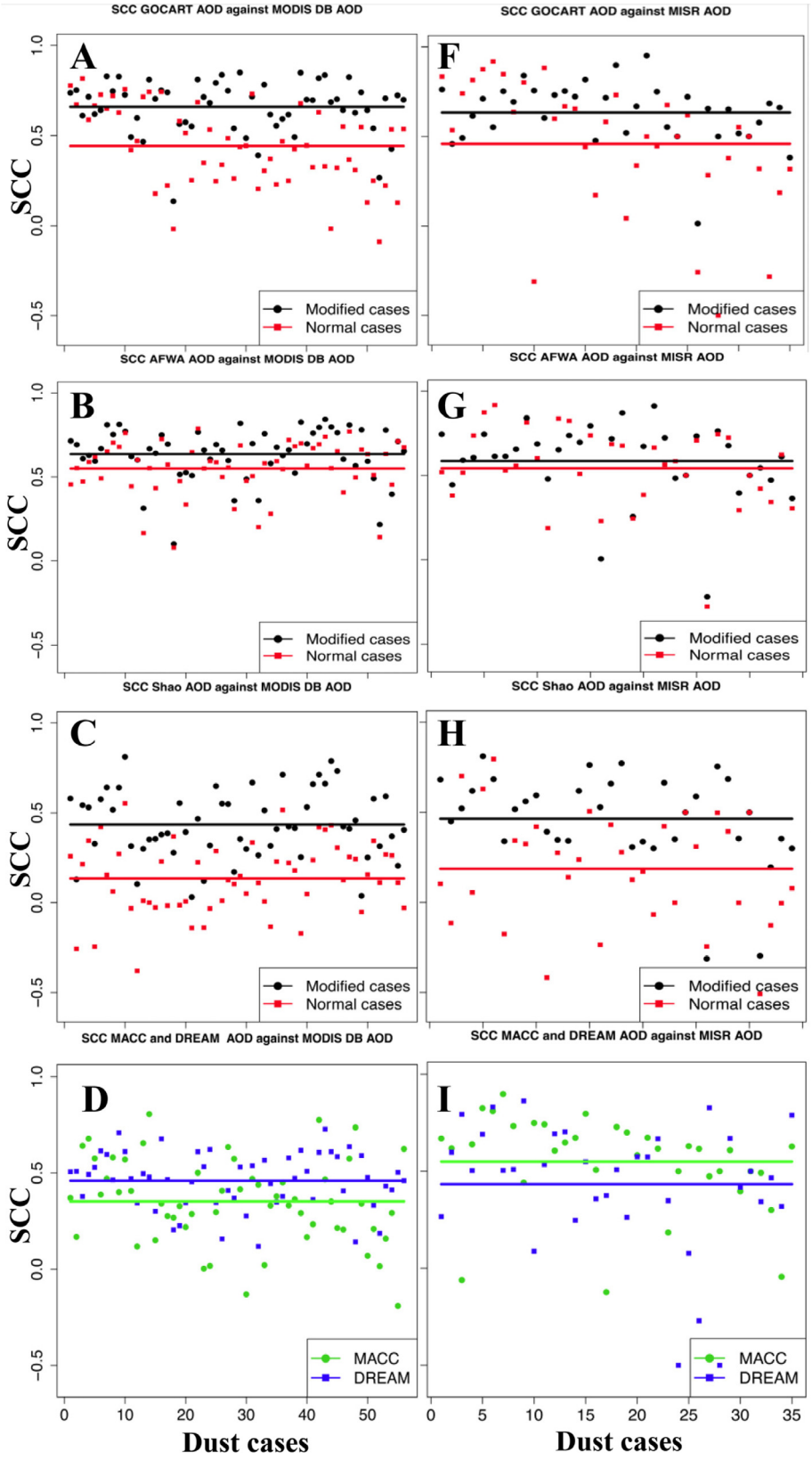

Fig. 8. For figures A–C and F–H: spatial SCCs of modified (black dotes) and control (red squares) cases against DB (A–C) and MISR (F–H) AODs. Red and black lines are, respectively, averaged SCC between control cases and observations and averaged SCC of modified cases and observations. For figures D and I: green dots are SCCs between MACC DODs and observations with an average shown by green line. Blue squares are SCCs between DREAM DODs and observations with an average shown by blue line. (For interpretation of the references to colour in this figure legend, the reader is referred to the web version of this article.)

$$PSS(\%) = POCD - POFD \quad (12)$$

In order to draw an inter-comparison between dust models, WRF-chem simulations are compared with DOD at 550 nm acquired from Monitoring Atmospheric Composition and Climate (MACC) program and Dust Regional Atmospheric Model (DREAM). At the time, GSF is used as source function for DREAM predictions (Basart et al., 2012) while it is considered as a constant ($2*10^{-11}$ kg s^2 m^{-5}) in MACC (Morcrette et al., 2009). Before the presentation of dust simulations, we will discuss the performance of WRF-chem in the simulation of soil moisture (at 0–10 cm depth), air temperature (at 2 m), and wind speed (at 10 m) in the following section. This is because any changes in these factors can influence the amount of dust emission and the range of dust transportation. These kinds of comparisons are normally done by using ground-based observations. However, because of lack of observations in West Asia, particularly in Iraq and Syria, we have acquired above-mentioned data from ECMWF reanalysis dataset (ERA-Interim) in the resolution of 0.75°. In addition, surface soil moisture from European Space Agency Climate Change Initiative (ESA-CCI), with a resolution of 0.25°, was also used as complementary information in soil moisture analysis. We used the ESA-CCI COMBINED dataset which is accessible from 1979 to 2014 (Klingmüller et al., 2016).

3. Results and discussion

Compared to ECMWF, WRF-chem underestimated soil moisture and air temperature whereas this model overestimated wind speed during study period (Fig. 5). Although ESA-CCI measurements cannot be taken as the representative of sub-surface soil moisture, as WRF-chem and ECMWF simulations are, the positive trend of soil moisture in this dataset is better simulated by WRF-chem than ECMWF. Unlike air temperature and wind speed which have the same range of variations in both datasets, WRF-chem produced more variable soil moisture than ECMWF. To sum up, the simultaneous overestimation of wind speed and underestimation of soil moisture by WRF-chem are favorable for dust emission. In fact, if all other variables are kept constant, WRF-chem overestimations can result in the overestimation of emitted dust than dust models which they use ECMWF simulations as inputs. It should be noted, that the forecast skill and biases of these parameters is very similar for the control and modified runs of WRF-chem.

Fig. 6 shows averaged AOD 550 nm acquired from WRF-chem and averaged DOD 550 nm from DREAM simulations and MACC reanalyzed data. The most obvious feature of all modified runs (Fig. 6B, D and F) is the underprediction of AOD, compared to control runs (Fig. 6A, C and E), DREAM (Fig. 6G) and MACC (Fig. 6H) datasets. While averaged AOD of modified runs, at most, reach to 0.6, it is higher than 1 for other datasets. In fact, the implementation of WASF, which generally yields smaller erodibility than GSF, caused a significant decrease in dust emission and, subsequently, resulting AODs.

In spite of this difference, all runs depict a dust path through the middle of the study area with a northwest-southeast direction. This pattern conforms the prevailing wind of the region during summertime, called Shamal, blowing from northwest to southeast of Iraq (Hamidi et al., 2013). Moreover, all AODs, except AOD from the Shao dust scheme, show higher dust intensity in the southeast of Iraq. It can be attributed to the fact that this region is not only the origin of dust storms but it is also hit by depositing dust particles coming from upstream sources in the northwest of Iraq. However, the location of the highest AOD simulated by Shao scheme is clearly located in Western Iraq and east of Syria (Fig. 6E–F). Considering Eq. (7) and clay fraction data used in WRF-chem (Fig. 7), it can be concluded that Shao scheme produced the highest AOD over

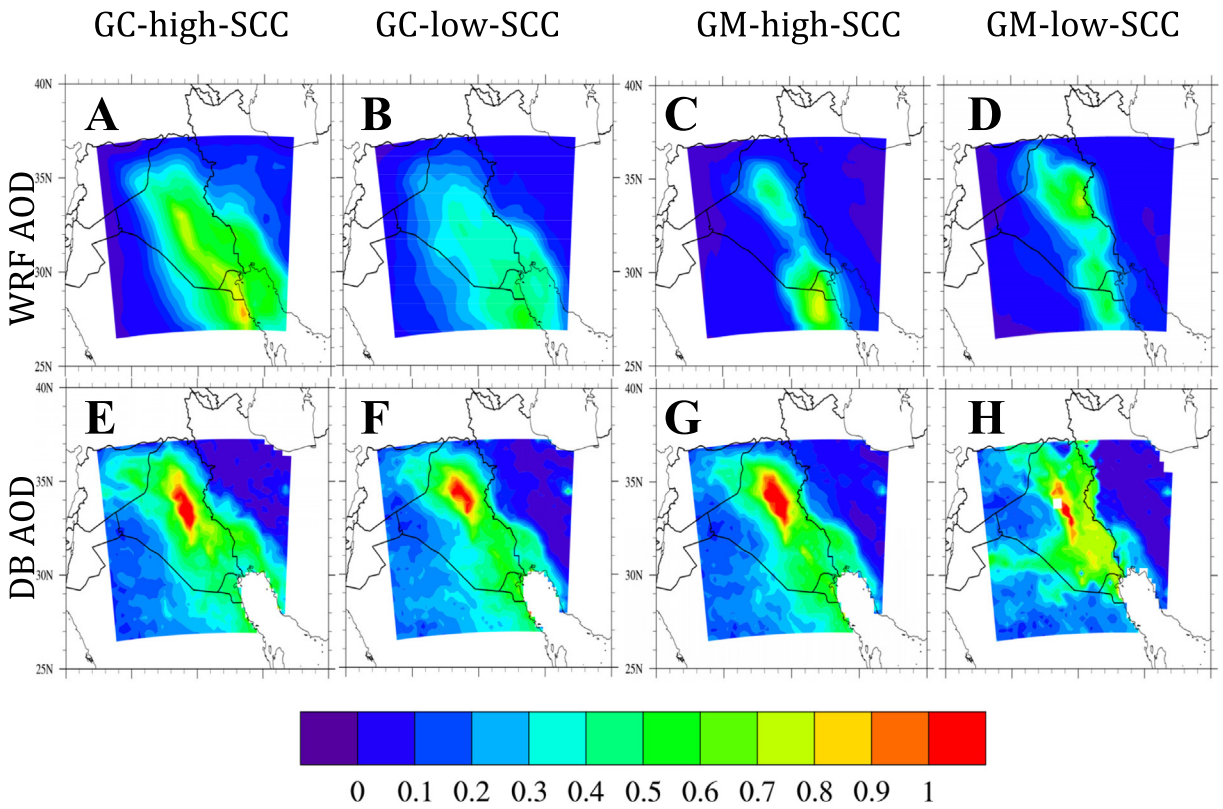

Fig. 9. The averaged AODs of GOCART modified (GM) and control (GC) dust cases simultaneous with high DB-based SCCs (A and C) and low DB-based SCCs (B and D). E, F, G and H, respectively show averaged DB AOD of aforementioned dust cases.

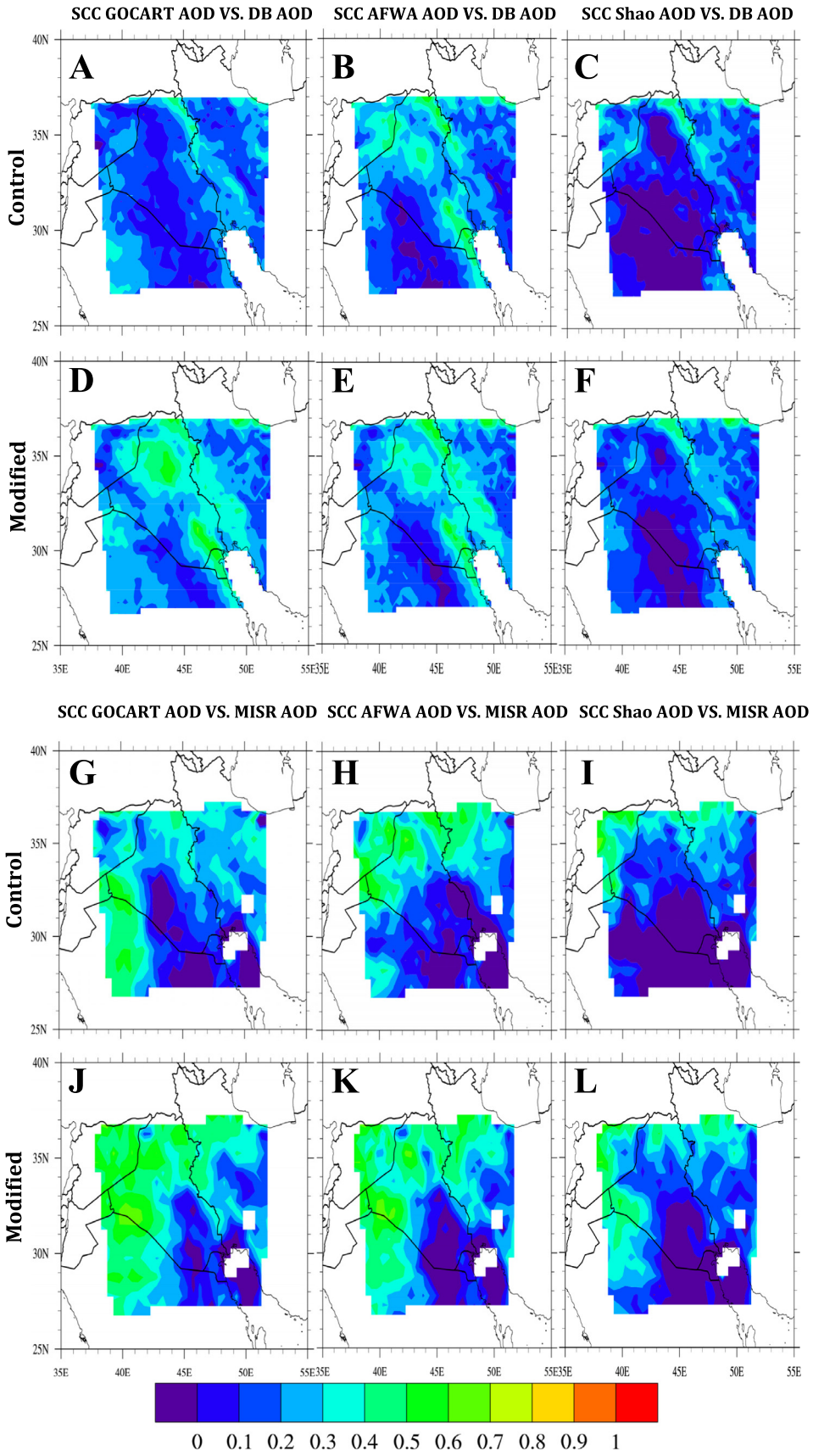

Fig. 10. SCCs between DB AOD and control and modified runs of GOCART (A and D), AFWA (B and E), and Shao (C and F). In the same order, MISR–based validations are shown in figures G and J (GOCART), H and K (AFWA) and I and L (Shao).

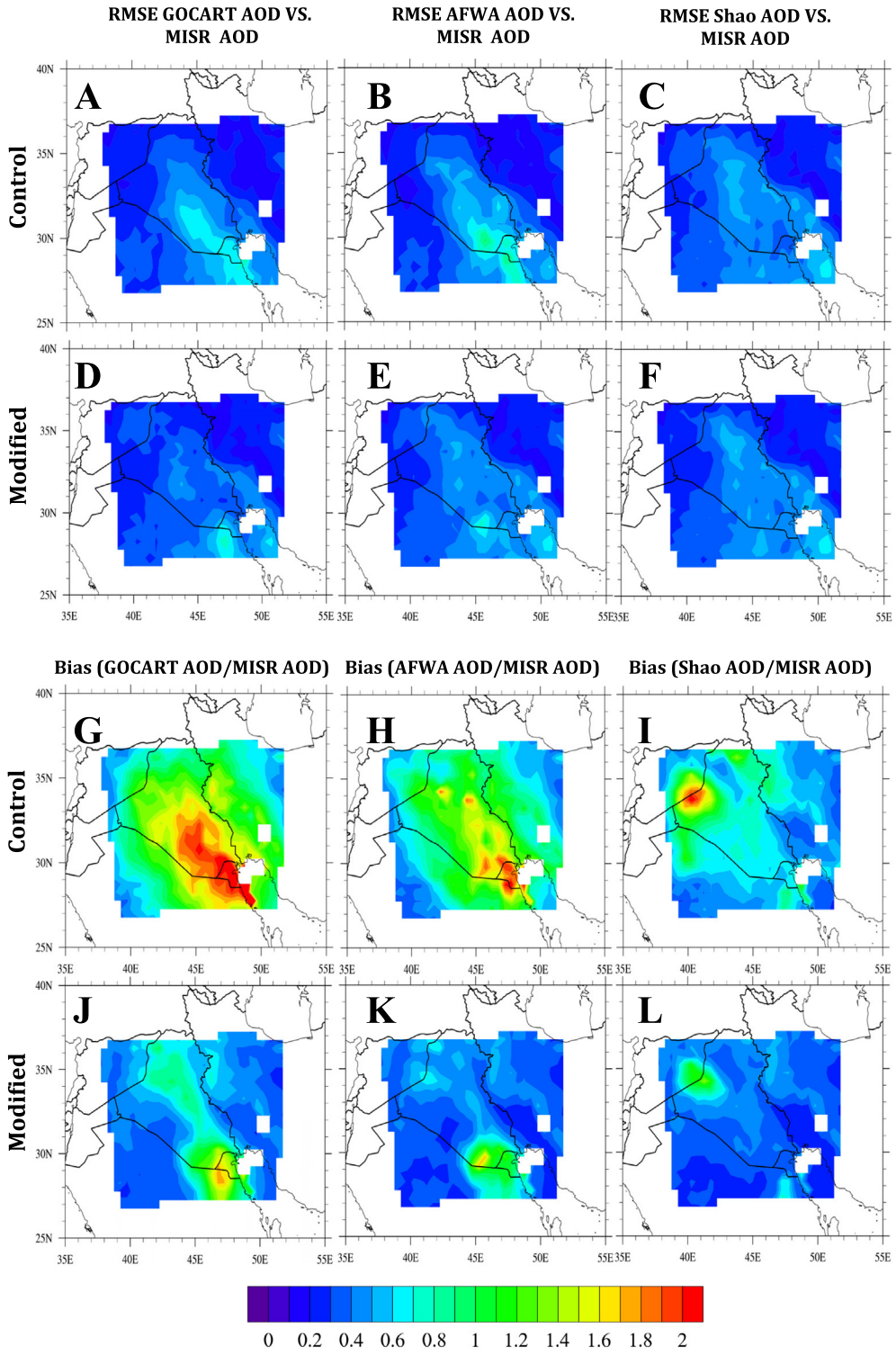

Fig. 11. MISR-based RMSEs of control and modified runs of GOCART (A and D), AFWA (B and E), and Shao (C and F). Corresponding biases are shown in figures G and J (GOCART), H and K (AFWA) and I and L (Shao).

the region where there is high percentage of clay in the soil. In fact, fine-grained soil escalated the amount of $p_m(d)$ which directly increased dust entrainment in Western Iraq and east of Syria. It should be also reminded that this scheme uses source function only to constrain the boundary of dust sources (not to compute dust emission). This means that two different erodibility functions with a same geographical extent will not affect the simulated AOD of Shao dust scheme. Because of this, Shao modified run simulated a thin cloud of AOD over areas out of WASF boundaries and a hot-spot of dust emission in the region intersected between boundaries of WASF and clayey soil.

In order to examine the effect of GSF and WASF on WRF-chem performance and compare it with DREAM and MACC, 56 dust cases are subjectively selected (based on intensity and areal extensity)

and verified through spatial SCC against DB and MISR AODs at 550 nm (Fig. 8). Because of data gaps in MISR dataset, only 32 cases (out of 56) were verified against this instrument.

Results show a significant improvement in the accuracy of WRF-chem predictions after implementation of WASF as source function in all modified runs. According to Fig. 8A–B and F–H, most of modified cases (black dotes) got higher SCC against both remotely sensed observations, than control cases (red squares). This is accentuated by the averaged SCC of modified cases (black line) that is always higher than that of control cases (red line). Further examinations show that AFWA has the best performance among control runs, with the average of 0.55 (against DB) and 0.54 (against MISR). The best performance, however, is achieved with the modified GOCART yielding SCCs of 0.65 (against DB) and 0.63 (against MISR). Although the Shao dust scheme yields the lowest agreement with observations either among control runs, 0.13 (against DB) and 0.16 (against MISR), or modified runs, 0.43 (against DB) and 0.46 (against MISR), it got the highest improvement after modification of source function. The comparison of DREAM and MACCs DODs against DB and MISR AODs has respectively returned averaged SCCs of 0.46 and 0.35 and 0.43 and 0.55 (Fig. 8D and I). In other words, MACC DOD, with a trivial difference to AFWA, has the best performance if it is only verified by MISR AOD and compared to control runs. For other cases, i.e. verification against DB AOD and comparison with modified runs, AFWA normal cases and GOCART modified cases yield the best performance, respectively.

In terms of the spread of SCCs, while the standard deviation of DB-based SCCs of GOCART, AFWA and Shao control cases are 0.22, 0.16, and 0.19, they decline to 0.14, 0.15, and 0.18 in modified cases, respectively. In the same order, the standard deviation of MISR-based SCCs has been reduced from 0.36 to 0.17, 0.24 to 0.23 and 0.31 to 0.25. Briefly, the modification of the source function not only increased the agreement between WRF-chem simulations and observations, it also decreased the variation of this agreement, indicating that the number of bad dust forecasts has strongly decreased. The spread of SCCs of DREAM and MACC have increased from 0.14 and 0.22 to 0.33 and 0.24 when the base of verifications is MISR AOD. In fact, the agreement between MACC DOD and MISR AOD which yielded the highest SCC shows high variations, as well.

To investigate reasons causing the spread of SCCs, the AOD composite of dust cases simultaneous with high and low SCCs are compared with corresponding observations. Low and high SCCs were defined as SCCs lower than 0.4 for control runs, MACC and DREAM and 0.5 for modified runs and higher than 0.7 for all datasets, respectively. Although this analysis has done on all dataset, to avoid redundancy, the comparison of GOCART simulations and DB AOD are shown here. Of 56 studied dust cases, 5 simulated cases of all datasets (WRF, DREAM, and MACC) on 24 August 2008, 14 July 2009, 23 July 2009, 7 June 2012, and 31 July 2012 have low agreement with DB AOD. The simultaneous reduction of accuracy in all datasets implies the presence of inaccuracies in observations. Further examinations revealed that it is caused by the position of

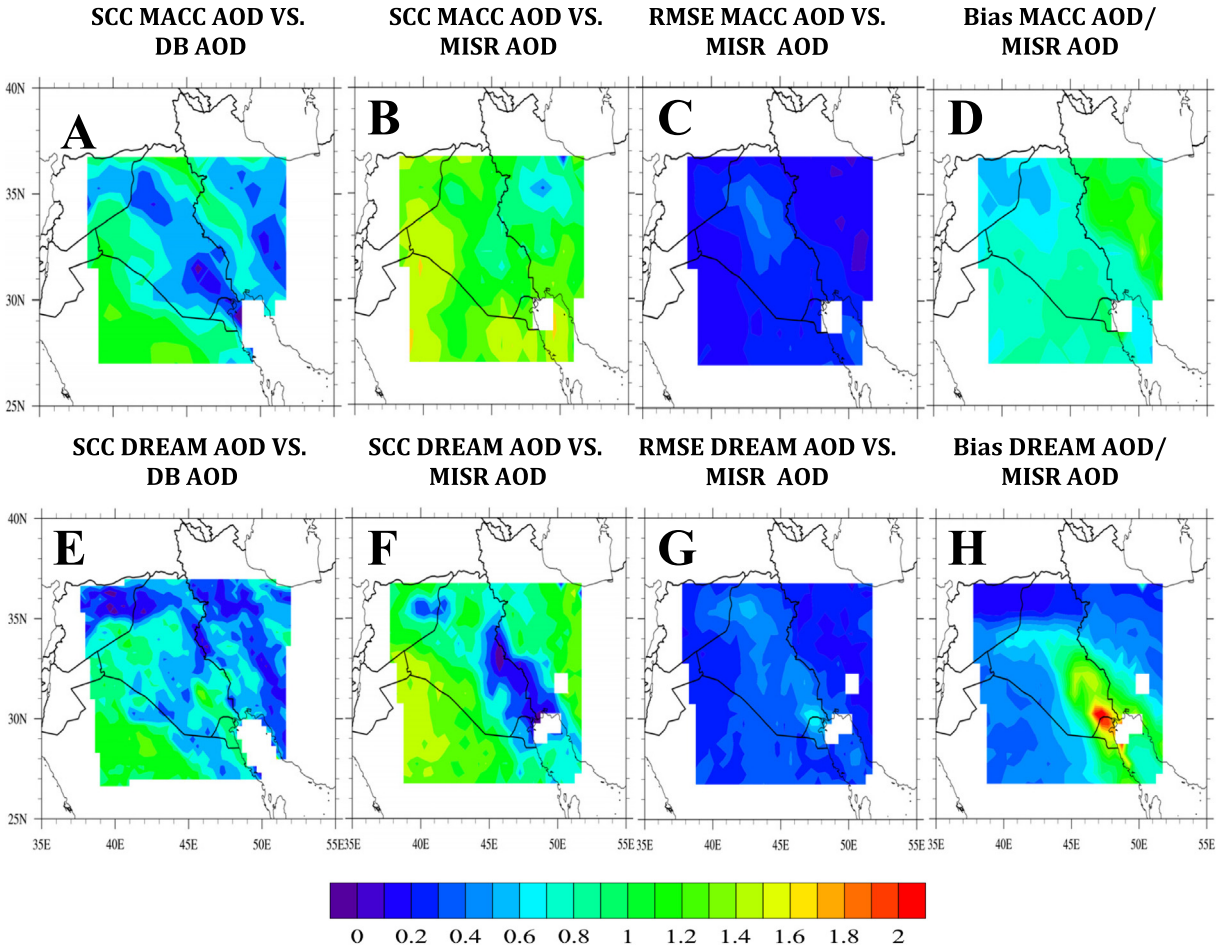

Fig. 12. A and B: SCCs between DB and MISR AODs and MACC DOD, respectively. C and D are MISR-based RMSE and bias of this product. In the same order, SCCs, RMSE and bias of DREAM are shown in figures E–H.

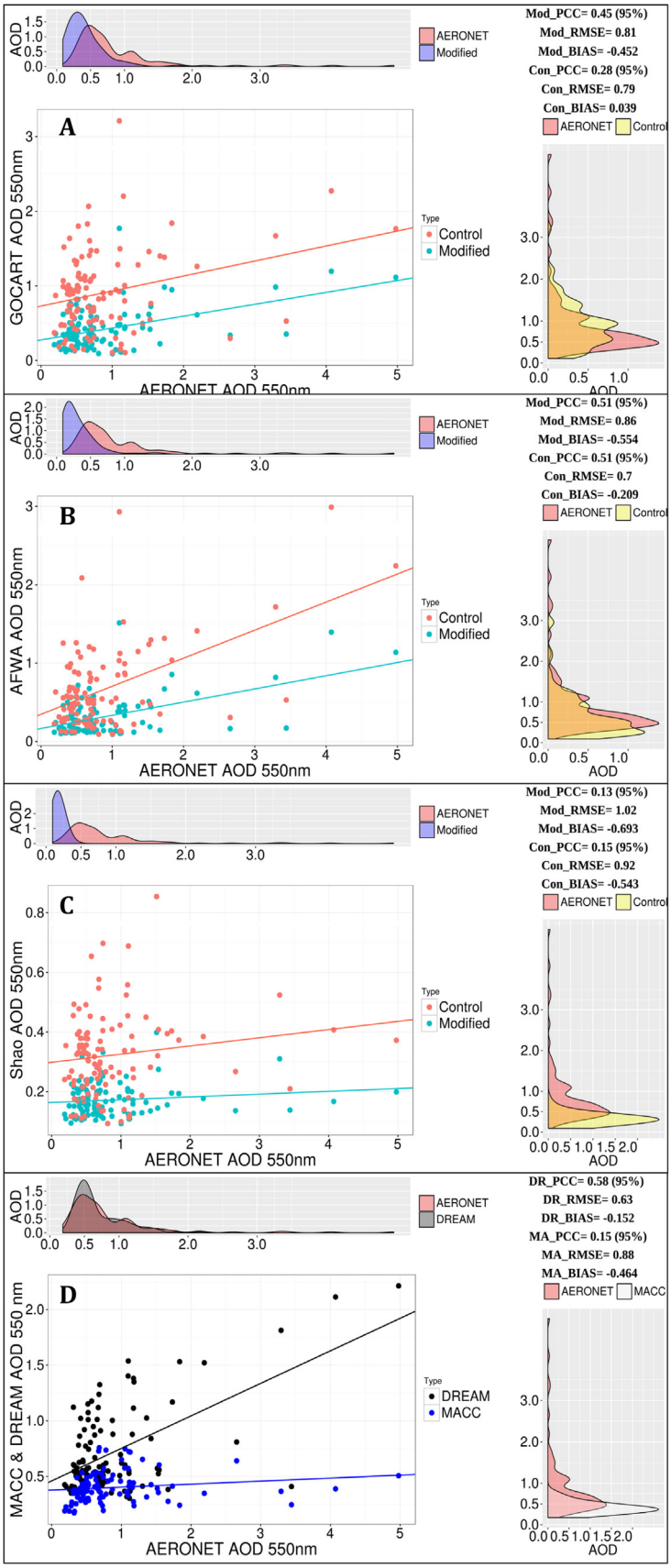

Fig. 13. Scatter plots between AOD 550 nm of Kuwait University AERONET station and control (red dots) and modified (green dots) runs of GOCART (A), AFWA (B) and Shao (C) schemes. Scatter plots of MACC (blue dots) and DREAM (black dots) DODs 550 nm and AERONET AOD 550 nm are shown in D. Distribution of control and modified AODs are respectively shown by yellow and purple curves in figures A–C. It is black and white, respectively, for DREAM and MACC in D and it is red for AERONET in A–D. Solid lines are regression line. (For interpretation of the references to colour in this figure legend, the reader is referred to the web version of this article.)

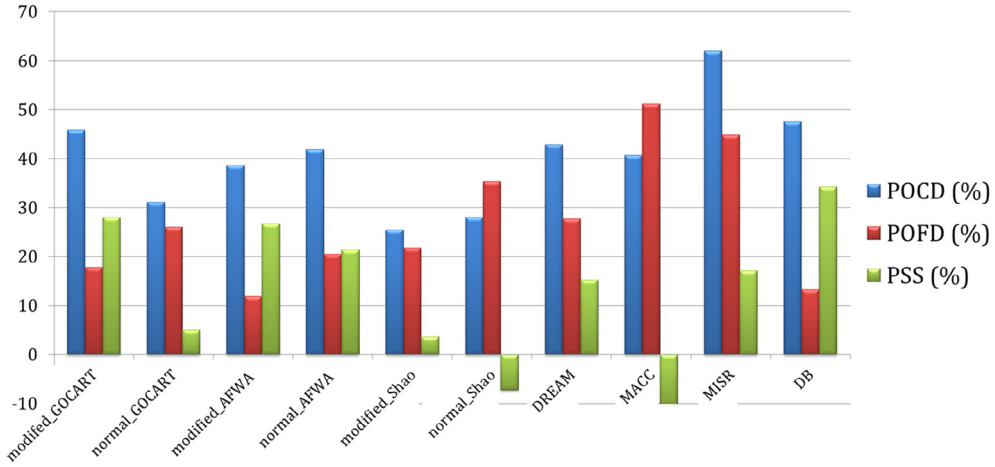

Fig. 14. The validation of WRF-chem AODs and DREAM and MACC DODs with dust codes of 6 synoptic stations in the north west of Iraq via the numbers of correct (POCD) and false (POFD) detections and skill score (PSS) acquired from contingency table.

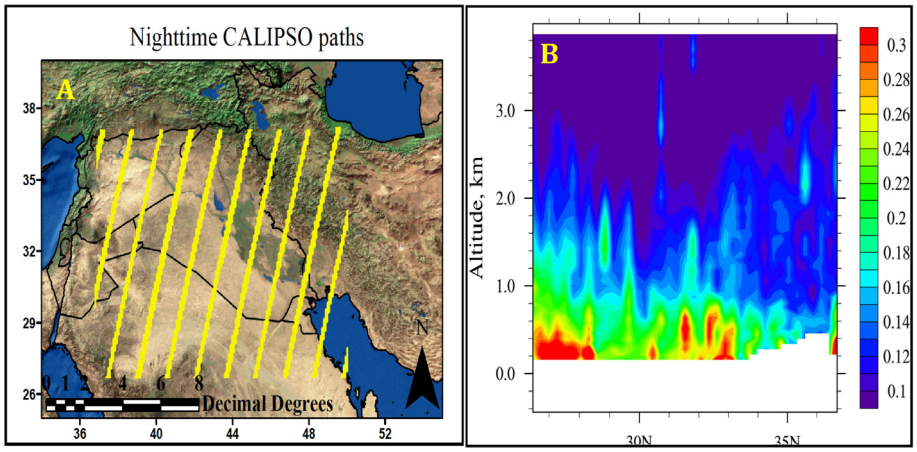

Fig. 15. A: Nighttime CALIPSO paths. B: the zonal average of CALIPSO extinction coefficient at 532 nm between 34E to 52E over the study period.

dusty pixels in the margin of MODIS senses. In fact, the increase of sensor zenith angle, defined as the angle between the satellite and a line perpendicular to the Earth's surface at the view point,[1] decreased the accuracy of observed DB AOD. Fig. 9A and C are the averaged AODs of control and modified cases which are highly correlated (SCC > 0.7) with corresponding DB AODs shown in 9-E and 9-G, respectively. According to these figures, high SCCs are recorded for those cases in which dust clouds formed over areas with high erodibility (dust sources) defined in GSF and WASF, respectively. In contrast, low correlated control and modified dust cases, shown in Fig. 9B and D, seem to be affected by the mismatch of dust hotspots against corresponding observations (Fig. 9F and 9-H). Conclusively, the higher number of highly correlated cases of modified runs (Fig. 8) indicated that WASF could more accurately represent the location of dust formation than GSF. It is worth noting that the performance of WASF during 2008 is not as good as the rest of study period. This seems to be because of an unprecedented drought in this year which turned all Iraq's plains into dust-prone areas (Trigo et al., 2010). The extraordinary expansion of dust sources resulted in a relatively erroneous performance of WASF (Fig. 9D) which is based on the climatology (not extreme events) analysis of dust storms.

In addition to case-by-case analysis, temporal SCC is computed over the whole study period. As is the case with spatial SCC, temporal SCC between dust cases and observations increased after the use of WASF in all three dust schemes. The comparison of simulations with DB and MISR AODs are shown in Fig. 10A–F and G–L, respectively. Verifying against DB AOD, the best results belong to GOCART modified run especially over WASF-defined dust sources in northwest and southeast of Iraq (Fig. 10A VS. D). This relative improvement can be also seen in AFWA (Fig. 10B VS. E) and even Shao (Fig. 10 VS. F) modified runs. The pattern of SCC is different in verifications against MISR AOD and no significant improvement is seen in the southeast of Iraq. This can be because of low spatial (0.5 degree) and temporal (global coverage in 9 days) resolution of MISR AOD and its sensitivity to surface reflectance which is high over deserts area of southern Iraq and east of Saudi Arabia. However, MISR-based verification also affirms that the performance of WRF-chem improved in the north and northwest of study area.

Unlike temporal SCC, MISR-based RMSEs (Fig. 11A–F) and biases (Fig. 11G–L) of simulations indicate the better performance of GOCART (Fig. 11D) and AFWA (Fig. 11E) modified runs over the southeast of study area. Although RMSE of Shao modified cases (Fig. 11F) got lower values over the hotspot of this scheme, in the west of Iraq and east of Syria, it did not change over the rest of region. As expected, all modified runs underestimate (bias < 1) AOD in almost whole study area except the main dust sources. Oppositely, control runs have yielded overestimation (bias > 1) which reaches the highest values over the south east of Iraq and

[1] http://www.seaspace.com/technical/protected/html/man1/angles.html

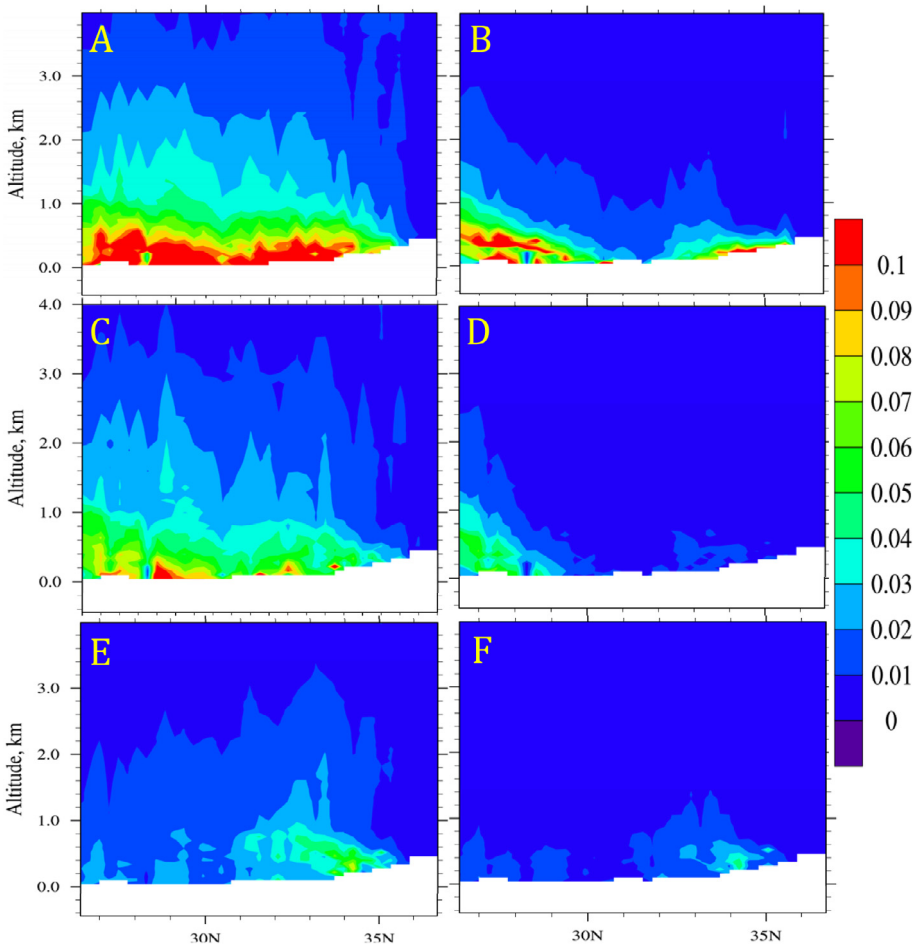

Fig. 16. A, C and E: the zonal average of extinction coefficient at 550 nm acquired from control runs of GOCART, AFWA and Shao between 34E to 52E over the study period. B, D, and F: As before but for modified runs.

Kuwait. Having done analyses above on MACC (Fig. 12A–D) and DREAM (Fig. 12E–H) DODs, the DB-based SCC of MACC DOD shows that this product has a good performance over the west of the study region, but much less so over dust sources and paths in Iraq.

However, MACC DOD has yielded the lowest MISR-based RMSE and bias over the whole region. DB-based SCC of DREAM DOD indicates that this model has an acceptable performance over deserts areas of Saudi Arabia and, to some extent, in the northwest and southeast of Iraq, whereas MISR-based SCC, RMSE and bias show the increase of uncertainties approaching the southeast of the region.

In order to make sure that the above-mentioned discrepancies in MISR and DB-based analyses are only caused by differences in instrumental specifications, WRF-chem simulations are a compared to ground-based observations. All datasets are validated by the only AERONET station (Kuwait University station) in the study area and 6 meteorological stations in the northwest of Iraq. According to Fig. 13, the Pearson Correlation Coefficient (PCC) of AERONET AOD and GOCART simulations (Fig. 13A) increased (from 0.28 to 0.45) after using WASF. In addition, AFWA (Fig 13B) and Shao (Fig 13C) modified runs have yielded approximately the same correlations to control runs. Finally, the higher correlation of DREAM DOD with DB AOD than that of MACC is replicated in the correlation between DREAM and AERONET datasets (Fig. 13D). The comparison of AOD distributions between simulations and AERONET observations (red curves in Fig. 13A–D) reconfirms that all modified runs (purple curves in Fig. 13A–C) underestimated AOD. Conversely, the distribution of AODs simulated by control runs (yellow curves in Fig. 13A–C) has better agreement with observations. Fig. 13D shows that the distribution of DREAM AOD (black curve) is much closer to reality than MACC (white curve) and all other simulations. This is quantitatively presented by corresponding RMSEs and biases.

As explained in Section 2, the validations of aforementioned datasets against dust codes of meteorological stations is done by using three parameters acquired from contingency table including: POCD, POFD and PSS (Fig. 14). Concerning the number of correct detections, modified GOCART got the highest percentage of POCD (45.8%) and Shao control run has received the least POCD of 28%. The highest and lowest false detections belong to MACC (51.15) and modified AFWA (11.88), respectively, which confirms findings of DB-based SCCs (Fig. 12A). Because of having high false detections, MACC and Shao bearded the lowest PSS (skill score). Conversely, low number of POFD increased the skill score of modified GOCART and AFWA runs. In fact, these two runs produced the most accurate results and MACC got the poorest performance over the northwest of Iraq, regarding both correct and false detections. Finally, the comparison of remotely sensed observations indicates that, as expected, DB AOD has higher accuracy (PSS) than MISR AOD.

In the last step of the study, we aim to verify also the vertical dust distribution in WRF-chem simulations by comparing simulated extinction coefficients with CALIPSO 532 nm extinction coefficient profiles. Considering low observation frequency of CALIPSO

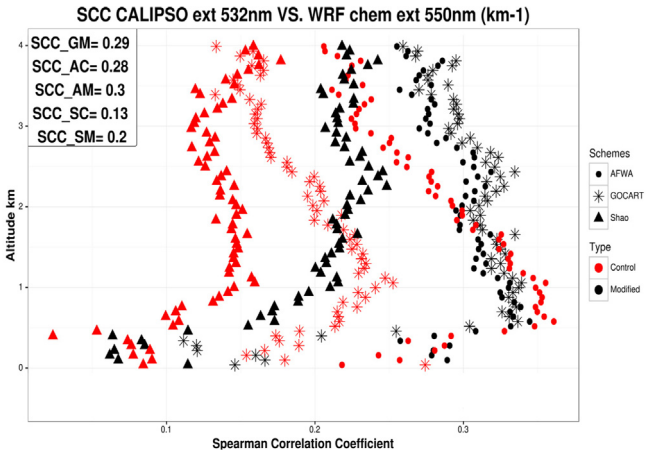

Fig. 17. Spatio-temporal SCC of WRF-chem extinction coefficient (km -1) at 550 nm with corresponding quantities produced by CALIPSO during study period over 75 vertical levels between land surface to 4 km. Values in the box on top left are the average of spatio-temporal SCCs through vertical levels between CALIPSO and Ginoux Modified (GM) and Control (GC) runs, AFWA Modified (AM) and Control (AC) runs and Shao Modified (SM) and Control (SM) runs.

(18 passes during study period), SCC between simulations and CALIPSO observations is calculated across time and space. Because we did not have access to needed data[2] for interpolating MACC and DREAM datasets to the same spatial resolution of CALIPSO, only WRF-chem simulations are tested. Fig. 15A shows the nighttime paths of CALIPSO bounded by study area. The zonal average of CALIPSO extinction coefficient at 532 nm (Fig. 15B) shows two main hotspots located between 31 N to 33 N and lower than 29 N. It seems that the former are dust plumes which are locally originated from the southeast of Iraq and advected from upstream dust sources in the northwest of study area. The second hotspot, which is more intensive, formed over deserts areas of Saudi Arabia and Kuwait.

At first glance, a significant difference is observable between concentration and vertical distribution of modified simulations and observations. While the concentration of observed extinction coefficients increased to around 0.3 over dust hotspots, the highest modified simulations are around 0.1 (Fig. 16B–D–F). In addition, the vertical extent of simulated extinction coefficient is not more than 1 km, whereas it reaches to more than 3 KM in CALIPSO profiles. It is escalated in Shao modified run with a thin dust cloud formed around 34 N which is, however, compatible with 2-dimensional analysis (Fig. 6F). In fact, the significant reduction of dust emission of modified runs, caused by less grade of erodibility in WASF, is also reflected in vertical distribution of dust storms. In spite of dissimilarities between modified runs and CALIPSO profiles, the quantitative comparison indicated that modified simulations have higher agreement with observations than control runs (Fig. 16A–C–E). As the spatio-temporal SCC of simulations of GOCART, AFWA and Shao dust schemes increased respectively from 0.26, 0.41, and 0.24 to 0.42, 0.42, and 0.31 after the implementation WASF. However, the level of agreement decreases when spatio-temporal SCCs are calculated separately over vertical levels through time. According to Fig. 17, spatio-temporal SCCs of both modified and control runs are less than 0.3 over most of the vertical levels. While all runs get highest agreement with observations around 1 km, modified runs reach another peak around 2.5 km. Despite the fact that comparison of WRF-chem outputs and CALIPSO observations indicates the poor performance of WRF-chem in the simulation of vertical distribution of extinction coefficient, the simulations of all three dust schemes improved after modifications.

[2] MACC does not provide extinction coefficient at vertical levels. DREAM extinction coefficient 550 nm is not accompanied by pressure or elevation data needed for interpolation.

4. Conclusion

A climatological study on dust storms of West Asia (Nabavi et al., 2016) showed that northwest and southeast of Iraq and eastern Saudi Arabia are the main dust sources of the region. According to preliminary studies, these regions are not well depicted by topography-based Ginoux source function (GSF), currently used in WRF-chem simulations. Hence, this study aimed to propose a local source function, called WASF, that was implemented in three dust schemes of WRF-chem. In order to evaluate the effect of WASF on WRF-chem performance, the simulations of control and modified runs were compared against remotely sensed observations, including MODIS DB AOD and MISR AOD at 550 nm and profile data of CALIPSO extinction coefficient at 532 nm. Results clearly show that WRF-chem performance, regardless of which dust scheme is considered, is significantly improved after the implementation of WASF. As an example, while the comparison of 56 control dust cases of GOCART, AFWA and Shao runs with DB AOD yielded the averaged spatial SCCs of 0.44, 0.55 and 0.13, they increased respectively to 0.65, 0.63, and 0.43 in modified runs. Although the use of WASF improved RMSE and bias of simulations, especially in GOCART outputs, because of its general reduction of erodibility than GFS, a significant underestimation is found in all modified simulations. The inter-comparison of WRF-chem simulations with DREAM and MACC DODs shows that modified runs outperformed these well-known datasets over dust source areas, while these two datasets have a better performance over the rest of region. These results are corroborated by the validation of all studied datasets with ground-based observations acquired from AERONET station in Kuwait and synoptic stations in the northwest of Iraq. The vertical validation of WRF-chem simulations affirms that modified runs have higher agreement with CALIPSO extinction coefficient 532 nm. This comparison has yielded SCCs of 0.26 0.41, and 0.24 for control runs and 0.42, 0.42, and 0.31 for modified runs of GOCART, AFWA and Shao dust schemes, respectively. However, the level of agreement decreases if spatio-temporal SCCs are calculated separately over vertical levels through time.

Although the use of WASF could improve the performance of WRF-chem especially over dust sources, it still faces with high uncertainty over the rest of study area. This can be because of unknown dust sources in other parts of West Asia. In fact, WASF only considered pixels as dust sources where dust frequency exceeds empirical thresholds. This means that there can be plenty of dust sources which are omitted by WASF. We also hypothesize that possible uncertainties in soil moisture data, as a critical parameter for the determination of erosion threshold, limits the performance WRF-chem. We assume that the transportation of dust away from the surface as well as the deposition models in WRF-chem need improvement. This is, however, beyond the scope of this study.

Acknowledgements

This work has been financially supported by EU 7th framework program ERA-CLIM (No. 265229) and the Austrian Science Funds FWF (Project P25260-N29).

References

Ackerman, S.A., 1989. Using the radiative temperature difference at 3.7 and 11 μm to tract dust outbreaks. Remote Sens. Environ. 27, 129–133.
Ackerman, S.A., 1997. Remote sensing aerosols using satellite infrared observations. J. Geophys. Res.: Atmos. (1984–2012) 102, 17069–17079.

Adams, A.M., Prospero, J.M., Zhang, C., 2012. CALIPSO-derived three-dimensional structure of aerosol over the Atlantic Basin and adjacent continents. J. Clim. 25, 6862–6879.
Basart, S., Pérez, C., Nickovic, S., Cuevas, E., Baldasano, J.M., 2012. Development and evaluation of the BSC-DREAM8b dust regional model over Northern Africa, the Mediterranean and the Middle East. Tellus B 64.
Beljaars, A., 1995. The parametrization of surface fluxes in large-scale models under free convection. Q. J. R. Meteorol. Soc. 121, 255–270.
Bibi, H., Alam, K., Chishtie, F., Bibi, S., Shahid, I., Blaschke, T., 2015. Intercomparison of MODIS, MISR, OMI, and CALIPSO aerosol optical depth retrievals for four locations on the Indo-Gangetic plains and validation against AERONET data. Atmos. Environ. 111, 113–126.
Boloorani, A.D., Nabavi, S., Azizi, R., Bahrami, H., 2013. Characterization of dust storm sources in Western Iran using a synthetic approach. Advances in Meteorology, Climatology and Atmospheric Physics. Springer.
Boloorani, A.D., Nabavi, S.O., Bahrami, H.A., Mirzapour, F., Kavosi, M., Abasi, E., Azizi, R., 2014. Investigation of dust storms entering Western Iran using remotely sensed data and synoptic analysis. J. Environ. Health Sci. Eng. 12, 1.
Bullard, J.E., Harrison, S.P., Baddock, M.C., Drake, N., Gill, T.E., McTainsh, G., Sun, Y., 2011. Preferential dust sources: a geomorphological classification designed for use in global dust-cycle models. J. Geophys. Res.: Earth Surf. 116.
Cao, H., Amiraslani, F., Liu, J., Zhou, N., 2015. Identification of dust storm source areas in West Asia using multiple environmental datasets. Sci. Total Environ. 502, 224–235.
Cavazos-Guerra, C., Todd, M.C., 2012. Model simulations of complex dust emissions over the Sahara during the West African monsoon onset. Adv. Meteorol. 2012.
Chen, F., Dudhia, J., 2001. Coupling an advanced land surface-hydrology model with the Penn State-NCAR MM5 modeling system. Part I: Model implementation and sensitivity. Mon. Weather Rev. 129, 569–585.
Chin, M., Ginoux, P., Kinne, S., Torres, O., Holben, B.N., Duncan, B.N., Martin, R.V., Logan, J.A., Higurashi, A., Nakajima, T., 2002. Tropospheric aerosol optical thickness from the GOCART model and comparisons with satellite and Sun photometer measurements. J. Atmos. Sci. 59, 461–483.
Chin, M., Rood, R.B., Lin, S.-J., Müller, J.-F., Thompson, A.M., 2000. Atmospheric sulfur cycle simulated in the global model GOCART: Model description and global properties.
Ciren, P., Kondragunta, S., 2014. Dust aerosol index (DAI) algorithm for MODIS. J. Geophys. Res.: Atmos. 119, 4770–4792.
Defries, R., Townshend, J., 1994. NDVI-derived land cover classifications at a global scale. Int. J. Remote Sens. 15, 3567–3586.
Gerivani, H., Lashkaripour, G.R., Ghafoori, M., Jalali, N., 2011. The source of dust storm in Iran: a case study based on geological information and rainfall data. Carpathian J. Earth Environ. Sci. 6.
Gillete, D., 1979. Environmental factors affecting dust emission by wind erosion. Saharan Dust, 71–94.
Gillette, D.A., Passi, R., 1988. Modeling dust emission caused by wind erosion. J. Geophys. Res.: Atmos. 93, 14233–14242.
Ginoux, P., Chin, M., Tegen, I., Prospero, J.M., Holben, B., Dubovik, O., Lin, S.J., 2001. Sources and distributions of dust aerosols simulated with the GOCART model. J. Geophys. Res.: Atmos. 106, 20255–20273.
Ginoux, P., Prospero, J.M., Gill, T.E., Hsu, N.C., Zhao, M., 2012. Global-scale attribution of anthropogenic and natural dust sources and their emission rates based on MODIS Deep Blue aerosol products. Rev. Geophys. 50.
Hamidi, M., Kavianpour, M.R., Shao, Y., 2013. Synoptic analysis of dust storms in the Middle East. Asia-Pac. J. Atmos. Sci. 49, 279–286.
Hsu, N.C., Tsay, S.-C., King, M.D., Herman, J.R., 2004. Aerosol properties over bright-reflecting source regions. IEEE Trans. Geosci. Remote Sens. 42, 557–569.
Karimi, N., Moridnejad, A., Golian, S., Vali samani, J.M., Karimi, D., Javadi, S., 2012. Comparison of dust source identification techniques over land in the Middle East region using MODIS data. Can. J. Remote Sens. 38, 586–599.
Kim, D., Chin, M., Bian, H., Tan, Q., Brown, M.E., Zheng, T., You, R., Diehl, T., Ginoux, P., Kucsera, T., 2013. The effect of the dynamic surface bareness on dust source function, emission, and distribution. J. Geophys. Res.: Atmos. 118, 871–886.
Klingmüller, K., Pozzer, A., Metzger, S., Stenchikov, G.L., Lelieveld, J., 2016. Aerosol optical depth trend over the Middle East. Atmos. Chem. Phys. 16, 5063–5073.
Koven, C.D., Fung, I., 2008. Identifying global dust source areas using high-resolution land surface form. J. Geophys. Res.: Atmos. 113.
Kumar, R., Barth, M., Pfister, G., Naja, M., Brasseur, G., 2014. WRF-Chem simulations of a typical pre-monsoon dust storm in northern India: influences on aerosol optical properties and radiation budget. Atmos. Chem. Phys. 14, 2431–2446.
Lee, J.A., Gill, T.E., Mulligan, K.R., Acosta, M.D., Perez, A.E., 2009. Land use/land cover and point sources of the 15 December 2003 dust storm in southwestern North America. Geomorphology 105, 18–27.
Lee, K., Chung, C., 2012. Observationally-constrained estimates of global small-mode AOD. Atmos. Chem. Phys. Discuss. 12, 31663–31698.
Lo, J.C.F., Yang, Z.L., Pielke, R.A., 2008. Assessment of three dynamical climate downscaling methods using the Weather Research and Forecasting (WRF) model. J. Geophys. Res.: Atmos. 113.
Ma, X., Bartlett, K., Harmon, K., Yu, F., 2013. Comparison of AOD between CALIPSO and MODIS: significant differences over major dust and biomass burning regions. Atmos. Meas. Tech. 6, 2391–2401.
Mahowald, N.M., Dufresne, J.L., 2004. Sensitivity of TOMS aerosol index to boundary layer height: implications for detection of mineral aerosol sources. Geophys. Res. Lett. 31.
Marticorena, B., Bergametti, G., 1995. Modeling the atmospheric dust cycle: 1. Design of a soil-derived dust emission scheme. J. Geophys. Res.: Atmos. 100, 16415–16430.
Morcrette, J.J., Boucher, O., Jones, L., Salmond, D., Bechtold, P., Beljaars, A., Benedetti, A., Bonet, A., Kaiser, J., Razinger, M., 2009. Aerosol analysis and forecast in the European Centre for medium-range weather forecasts integrated forecast system: forward modeling. J. Geophys. Res.: Atmos. 114.
Moridnejad, A., Karimi, N., Ariya, P.A., 2015a. A new inventory for middle east dust source points. Environ. Monit. Assess. 187, 1–11.
Moridnejad, A., Karimi, N., Ariya, P.A., 2015b. Newly desertified regions in Iraq and its surrounding areas: significant novel sources of global dust particles. J. Arid Environ. 116, 1–10.
Nabavi, S.O., Haimberger, L., Samimi, C., 2016. Climatology of dust distribution over West Asia from homogenized remote sensing data. Aeolian Res. 21, 93–107.
Parajuli, S.P., Yang, Z.L., Kocurek, G., 2014. Mapping erodibility in dust source regions based on geomorphology, meteorology, and remote sensing. J. Geophys. Res.: Earth Surf. 119, 1977–1994.
Prospero, J.M., Ginoux, P., Torres, O., Nicholson, S.E., Gill, T.E., 2002. Environmental characterization of global sources of atmospheric soil dust identified with the Nimbus 7 Total Ozone Mapping Spectrometer (TOMS) absorbing aerosol product. Rev. Geophys. 40. 2-1-2-31.
Roskovensky, J., Liou, K., 2005. Differentiating airborne dust from cirrus clouds using MODIS data. Geophys. Res. Lett. 32.
Samadi, M., Boloorani, A.D., Alavipanah, S.K., Mohamadi, H., Najafi, M.S., 2014. Global dust Detection Index (GDDI); a new remotely sensed methodology for dust storms detection. J. Environ. Health Sci. Eng. 12, 1.
Shao, Y., 2004. Simplification of a dust emission scheme and comparison with data. J. Geophys. Res.: Atmos. 109.
Shao, Y., Ishizuka, M., Mikami, M., Leys, J., 2011a. Parameterization of size-resolved dust emission and validation with measurements. J. Geophys. Res.: Atmos. 116.
Shao, Y., Wyrwoll, K.-H., Chappell, A., Huang, J., Lin, Z., McTainsh, G.H., Mikami, M., Tanaka, T.Y., Wang, X., Yoon, S., 2011. Dust cycle: an emerging core theme in Earth system science. Aeolian Res. 2, 181–204.
Su, L., Fung, J.C., 2015. Sensitivities of WRF-Chem to dust emission schemes and land surface properties in simulating dust cycles during springtime over East Asia. J. Geophys. Res.: Atmos. 120.
Torres, O., Bhartia, P., Herman, J., Ahmad, Z., Gleason, J., 1998. Derivation of aerosol properties from satellite measurements of backscattered ultraviolet radiation: theoretical basis. J. Geophys. Res.: Atmos. (1984–2012) 103, 17099–17110.
Trigo, R.M., Gouveia, C.M., Barriopedro, D., 2010. The intense 2007–2009 drought in the Fertile Crescent: impacts and associated atmospheric circulation. Agric. For. Meteorol. 150, 1245–1257.
Walker, A.L., Liu, M., Miller, S.D., Richardson, K.A., Westphal, D.L., 2009. Development of a dust source database for mesoscale forecasting in southwest Asia. J. Geophys. Res.: Atmos. 114.
WMO 2011. Manual on Codes. I.1.
Zaitchik, B.F., Santanello, J.A., Kumar, S.V., Peters-Lidard, C.D., 2013. Representation of soil moisture feedbacks during drought in NASA unified WRF (NU-WRF). J. Hydrometeorol. 14, 360–367.
Zender, C.S., Bian, H., Newman, D., 2003. Mineral Dust Entrainment and Deposition (DEAD) model: description and 1990s dust climatology. J. Geophys. Res.: Atmos. 108.

5 Prediction of Aerosol Optical Depth in West Asia using Dust Models and Machine Learning Algorithms

Seyed Omid Nabavi[1], Leopold Haimberger[1], Reyhaneh Abbasi[2], Cyrus Samimi[3,4]

[1] Department of Meteorology and Geophysics, University of Vienna, Faculty of Earth Sciences, Geography and Astronomy, UZA II Althanstrasse 14, A-1010 Vienna, Austria

[2]Acoustics Research Institute, Austrian Academy of Sciences, Wohllebengasse, 12-14, 1040 Vienna, Austria

[3] Faculty of Biology, Chemistry and Earth Sciences, University of Bayreuth, Universitätsstr. 30, 95447 Bayreuth, Germany

[4] Bayreuth Center of Ecology and Environmental Research, BayCEER, Dr. Hans-Frisch-Straße 1-3, 95448 Bayreuth, Germany

Atmospheric Environment (submitted)

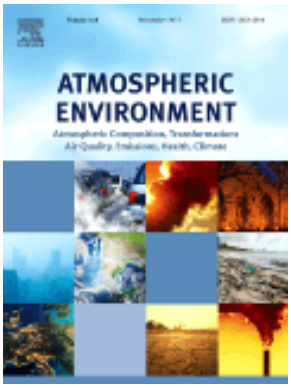

This chapter is to test Hypothesis 3. Various variable datasets and different types of FSC are examined to determine the most influential factors of dust formations needed for building MLAs. This step of the study aims to prepare a comparative examination of MLAs and DMs for the prediction of dust abundance in West Asia. Using MODIS DB as the response variable, results show that MLAs, even with standard settings, especially SVM and MARS, have significantly outperformed DMs. In addition, SF found to be critical in the prediction accuracy of MLAs.

- Conception of research approach: **Nabavi, S. O.** (major); Haimberger, L. (minor); Abbasi, R. (major); Samimi, C. (minor)
- Development of research methods: **Nabavi, S. O.** (major); Haimberger, L. (minor); Abbasi, R. (major); Samimi, C. (minor)
- Data collection and data preparation: **Nabavi, S. O.** (major); Haimberger, L. (minor); Abbasi, R. (minor); Samimi, C. (minor)
- Execution of research: **Nabavi, S. O.** (major); Haimberger, L. (minor); Abbasi, R. (minor); Samimi, C. (minor)
- Analysis/Interpretation of data or preliminary results: **Nabavi, S. O.** (major); Haimberger, L. (major); Abbasi, R. (minor); Samimi, C. (minor)
- Writing or substantive rewriting of the manuscript: **Nabavi, S. O.** (major); Haimberger, L. (major); Abbasi, R. (major); Samimi, C. (minor)
- Role of **Nabavi, S. O.**: leading contribution (70 %)

Prediction of Aerosol Optical Depth in West Asia using Dust Models and Machine Learning Algorithms

Seyed Omid (first name) Nabavi (family name) (1), Leopold (first name) Haimberger (family name) (1), Reyhaneh (first name) Abbasi (family name) (2), and Cyrus (first name) Samimi (family name) (3)

(1) Department of Meteorology and Geophysics, University of Vienna, Vienna, Austria,
(2) Acoustics Research Institute, Austrian Academy of Sciences, Vienna, Austria.
(3) Department of Geography, University of Bayreuth, Bayreuth, Germany.

Abstract[1]

Because of the lack of ground-based observations, mineral dust is mainly monitored by using remote sensing techniques that in most cases deliver Aerosol Optical Depth (AOD) at 550nm as a product that can be considered as observation. AOD is also predicted by so-called dust models (DMs), which are numerical weather prediction models that are extended to predict not only standard meteorological variables but also concentration of dust. AOD is calculated in DMs from 3D dust concentration fields using an observation operator that describes the complex interaction between dust and solar radiation. The skill of DMs in reproducing remotely sensed observations on monthly time scales over West Asia is rather limited due to significant uncertainties in inputs and complexity of dust.

Machine Learning Algorithms (MLAs), which require much less computational expenses than DMs, can be used for monthly dust forecasts as well. MLAs focus on the statistical relationships between potential predictors, such as soil erodibility and wind speed, and the predicted variable, in this case AOD. The importance of the predictors for AOD forecasts is evaluated during an extensive training period (2003-2010). During the feature selection process, the dust source function turned out to be the most important factor in dust prediction whereas some less important predictors could be pruned.

Abbreviations: DMs, Dust Models; MLAs, Machine Learning Algorithms; DB, Deep Blue; FSC, Feature Selection Criteria; MARS, Multivariate Adaptive Regression Splines; SVM, Support Vector Machines; MLR, Multiple Linear Regression; ANN, Artificial Neural Networks; RF, Random Forest; DUP, Dust Uplift Potential; SM, Soil Moisture; ST, Soil Temperature; SF, Source Function; WASF, West Asia Source Function; SPEI, Standardized Precipitation-Evapotranspiration Index; PCC, Pearson Correlation Coefficient; SCC, Spearman Correlation Coefficient; MI, Mutual Information; RFE, Recursive Feature Elimination.

For a testing period (2011-2013) the performance of two DMs and five MLAs was compared using Moderate Resolution Imaging Spectroradiometer (MODIS) Deep Blue (DB) AOD as the representative of response variable. MLAs, especially Multivariate Adaptive Regression Splines (MARS) and Support Vector Machine (SVM), outperformed DMs on monthly time scales. In addition, findings disclosed that DMs, especially MACC, have failed to simulate the amount of dust over western Iran where the Zagros Mountains prevent advection of dust clouds to the east of the study area. High prediction errors of MLAs and DMs along with major DB AOD peaks can be traced back to the rough resolution of variable datasets, uncertainties in dust emission regulated by the dust source function, omission of some unknown influential factors and the scarcity of extreme cases. It also remains to be tested in how far the results presented can be generalized to other regions.

Keywords: Machine learning algorithms; Deterministic models, Dust Models; Feature selection criteria; Dust Source Function.

1. Introduction

Numerical weather prediction models which simulate dust's lifecycle, including emission in sources, transport in the atmosphere, and wet and dry deposition, are referred to as Dust Models (DMs) (Tegen, 2003). They are classical tools for the prediction of dust storms (Marticorena and Bergametti, 1995, Liu et al., 2007, Kumar et al., 2014). For short-range (up to three days) operational forecasts where there is nearly complete theoretical knowledge about the nature of the relationships between prognostic variables and boundary conditions, they are quite powerful prediction tools. The improvement of DMs' structure and computational power will assist their strong physical basis for more accurate short-term predictions in the forthcoming years (Taheri Shahraiyni and Sodoudi, 2016).

While near-surface aerosol concentrations are the most important output of such models, since those affect human health, they are rarely observed over West Asia with sufficient accuracy and frequency and thus are of limited use for model validation. Monthly mean AOD is another important output parameter which, besides being relevant for climate, is well observed by satellites and is therefore a valuable benchmark for any method trying to predict it. So far DMs still have difficulties reproducing AOD on a monthly time scale because of limitations in both model formulation and observation operators (Liu et al., 2011a).

DMs are not the only way to predict monthly mean AOD. As any observable AOD can be seen as stochastic variable that depends on several potential predictands such as soil moisture,

temperature or wind at least in a statistical sense. These dependencies can be estimated if there exists a significant number of observations of both predictors and predictands. Machine Learning Algorithms (MLAs) have shown promising performance inferring such relationships, particularly in engineering problems, for more than three decades (Carbonell et al., 1983, Cortes and Vapnik, 1995, Kotsiantis et al., 2007, Hempel et al., 2012, Abbasi et al., 2014, LeCun et al., 2015). MLAs can identify the underlying behavior of a system from long-term observations at relatively low computational cost (Lary et al., 2016). MLAs are already used for the prediction of air quality in urban areas (Taheri Shahraiyni and Sodoudi, 2016) and have also been applied to the adjustment of satellite AOD (Hyer et al., 2011, Albayrak et al., 2013) to have a better fit to ground-based observations.

However, to the best of our knowledge, there has so far been no scientific attempts to predict monthly mean AOD over a whole region through MLAs. Yet we consider such an effort very useful (i) to demonstrate the feasibility of using MLAs for predicting monthly mean AOD, (ii) to detect the most influential predictors, (iii) to check whether the estimated dependencies between predictors and AOD can be found also in DMs. This might help improving DMs which are known to be deficient in predicting monthly mean AOD, at least over West Asia.

A rather large class of algorithms may be referred to as Machine Learning Algorithms. Probably the best known way to estimate statistical relationships between predictors and predictands is Multiple Linear Regression (MLR). Klingmüller et al. (2016) modeled annual Deep Blue (DB) AOD as the representative of vertically averaged dust concentration, in a coarse resolution of 2 degrees using different predictors and MLR. In order to evaluate the importance of predictors, they applied the Akaike Information Criterion (AIC). Results point to soil moisture as the dominant factors for AOD over dust sources in Saudi Arabia and Iraq. Yu et al. (2015) used a similar technique for seasonal prediction of dust storms. They predicted seasonal dust activity in Saudi Arabia as a function of antecedent-accumulated rainfall over the Arabian Peninsula and North Africa, and antecedent-averaged SST of Mediterranean Sea, tropical eastern Pacific and Indian oceans. Temporal correlations of 0.7 and 0.74 between predictions and observations could be achieved for summer and spring, respectively. Kaboodvandpour et al. (2015) have compared the performance of MLR in dust prediction with Artificial Neural Networks (ANN), and Adaptive Neuro-Fuzzy Inference System (ANFIS). They have chosen $PM_{10} > 200$ μg m^{-3} at Sanandaj station (dust receptor in Iran) as the indicator of dust occurrence (response variable). The meteorological variables, including air pressure, temperature, humidity, wind speed, and wind direction, from the station Damascus (dust source

in Syria), on the day before the storm observed at Sanandaj station during 2009-2011, have been taken as predictors. Results show that ANN and ANFIS have yielded the highest agreement (the highest coefficient of determination (R^2) = 0.86) and the highest consistency (the lowest Root Mean Squared Error (RMSE) = 0.07) with observations, respectively, whereas MLR has performed poorly (R^2 = 0.416 and RMSE = 0.0965).

Although the discussed studies could shed light on the applicability of MLAs in dust prediction, the determination of an efficient MLA based prediction tool requires the inter-comparison of different MLAs over a long-term period. The low spatial and temporal resolutions of MLA predictions are other shortcomings of existing research work. In addition, there is a lack of comparative studies evaluating DM and MLA performance in dust prediction. Finally yet importantly, it seems that the research on this subject so far underestimated the importance of feature selection criteria (FSC) needed for developing MLAs. Selection of predictors has mostly been based on simple correlations between predictors and response variables or based on expert judgment.

The present study aims to make a more comprehensive and objective comparison of AOD prediction methods for West Asia. Output from five MLAs and two DMs has been compared at higher spatial and temporal resolutions than can be found in the literature. The input variables of MLAs have been selected by considering the results of different FSC. The descriptions of research data and methods are presented in section 2. Section 3 and 4 are allotted to results and conclusions, respectively.

2. Data and methods

The setup of MLAs requires access to long-term measurements of response variable and nominated predictors. The general process of MLA training and prediction is shown in figure 1.

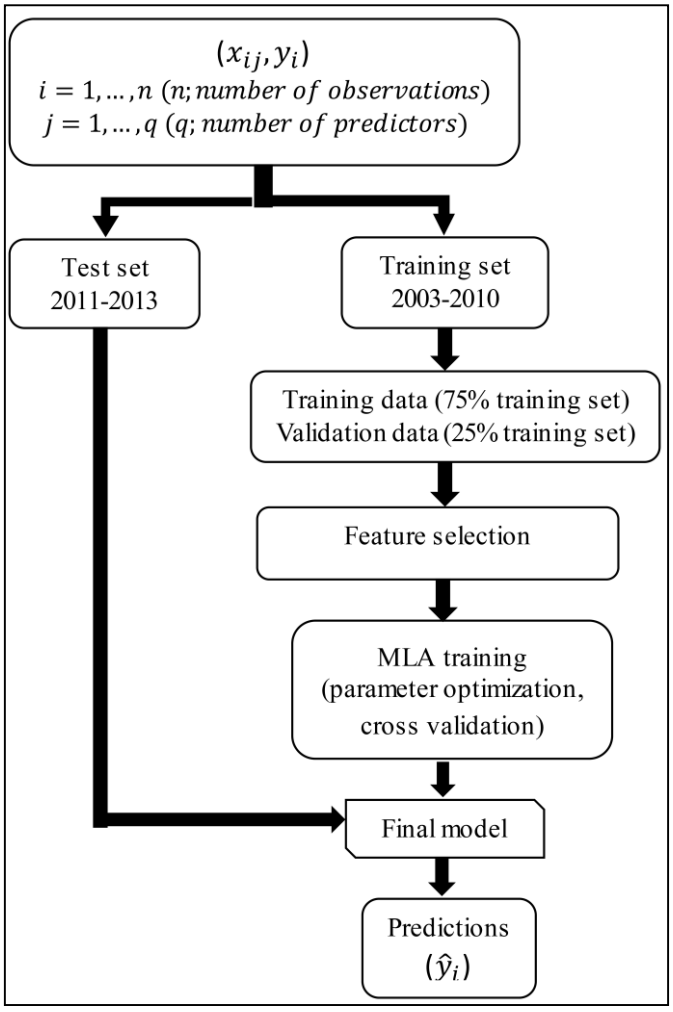

2.1. Figure 1 Flow chart of MLA prediction. During the training process parameters are automatically optimized using cross validation until the final model is defined. This model is applied to the test set. Variable datasets

Since MLAs require a significant number of observations for training, the first priority is to use observation datasets with high spatial and temporal resolution. In addition, dust storms are the result of complex interactions between atmosphere and land surface, so its predictors should be also representatives of both environments. In this study, the Moderate Resolution Imaging Spectroradiometer (MODIS) DB AOD (Hsu et al., 2004) collection 6 (Sayer et al., 2014) is chosen as long-term record of dust quantity in West Asia (Fig. 2-A).

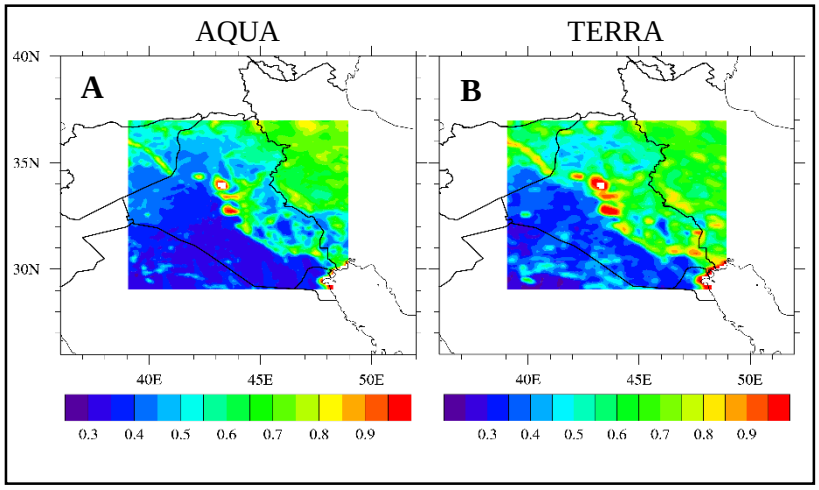

Figure 2 Fraction of missing data of AQUA (A) and TERRA (B) DB AOD between 2003 and 2013. The red spots in the middle of Iraq are related to water reservoirs behind major dams (e.g. Mossul dam).

While TERRA DB AOD (Fig. 2-B) is available since 1999, we used MODIS daily DB AOD from the AQUA platform, available since 2003, since it has much less missing data. The spatial resolution is 10 km. In figure 2, the color portion shows the study area located between latitudes 29 °- 37 ° N and longitudes 39 ° - 49 ° E.

For training and application of the MLAs, we apply the natural logarithm to DB AOD data to make the data distribution more symmetric. This transformation reduces the negative effect of high extreme values on MLA predictions, as will be discussed later. This implies, however, that the MLAs also predict the logarithm of DB AOD, which has to be transformed back (with the exponential function) in order to compare it with observed AOD.

A general insight into the influential factors which are governing the dust cycle is needed as first step to develop MLAs. In other words, we first need to roughly determine those factors which are of high importance in dust emission, transportation, and deposition. Some of these potential predictors may, however, be redundant and should be eliminated afterwards by FSC (subsection 2.2). Following the literature and the authors' experiences, nine environmental parameters are chosen as potential predictors for dust: (i) 10m wind, (ii) vertical velocity (omega), (iii) soil temperature, (iv) albedo, (v) soil moisture, (vi) precipitation, (vii) vegetation cover, (viii) drought intensity, and (ix) susceptibility of dust emission. The first four parameters are acquired from the European Centre for Medium-Range Weather Forecasts (ECMWF) ERA-Interim reanalysis dataset, accessible from 1979 to present, with a grid resolution of 0.75 degrees (Dee et al., 2011). The low-level horizontal erosive speed of air parcels is represented by Dust Uplift Potential (DUP) at 10 m. According to Cowie et al. (2015), DUP is calculated as follows:

Equation 1

$$DUP = \begin{cases} U^3(1+\frac{U_t}{U})(1+\frac{{U_t}^2}{U^2}), & if\ U > U_t \\ 0, & otherwise \end{cases}$$

where U is wind speed at 10 meter and U_t is a threshold for dust emission. Here U_t is defined as the long term average of 10-meter wind speed simultaneous with DB AOD > 0.7. We also expect that the uplift from near the surface to higher levels is related to omega at 850 hPa from ERA-Interim, therefore we include this field as predictor as well. The top layer (1-7cm) soil temperature is provided by the ERA-Interim "soil temperature level 1" (ST) parameter which is available every three hours. Surface albedo from ERA-Interim is used to feed the high surface reflectance of dust-prone areas into MLAs. All mentioned ECMWF datasets are analyses at 6 am (around 9 am local time). The selection of this time of the day is because visual examination of MODIS images shows that the first dust plumes of study area are mostly formed in the early morning. European Space Agency Climate Initiative (ESA-CCI) has provided daily surface soil moisture (SM) based on satellite mounted active and passive microwave sensors. In this study, the COMBINED data set, on the grid resolution of 0.25 degree, is used (Liu et al., 2011b, Liu et al., 2012, Wagner et al., 2012). Precipitation has been taken from the Global Precipitation Climatology Centre (GPCC) dataset (Schneider et al., 2011). It provides monthly 0.5° × 0.5° precipitation (Total Full V7) from quality controlled station data during 1901 to 2013. In order to incorporate the variations of vegetation cover in dust predictions, we have used the normalized difference vegetation index (NDVI) dataset from the Global Inventory Modeling and Mapping Studies (GIMMS), called NDVI3g. Tucker et al. (2004) have provided this refined product from 15-day maximum NDVI values. NDVI3g, derived from AVHRR sensor data of NOAA 7 to 18 satellites, has 1/12° spatial and bi-monthly temporal resolutions and it covers the time period from 1981 to 2015. The impact of successive droughts on dust outbreaks is considered by using the 9-month aggregated Standardized Precipitation-Evapotranspiration Index (SPEI). SPEI is a simple measure of the water surplus or deficit that is calculated based on the monthly (or weekly) difference between precipitation and potential evapotranspiration (Vicente-Serrano et al., 2010).

The uneven potential of dust emission in arid areas necessitates the use of a spatially varying dust Source Function (SF) in dust models. In fact, SF allocates a certain potential of dust release to each place. Following Nabavi et al. (2016), we have used the West Asia Source Function (WASF) which is determined from the long-term study of Aerosol Index (AI) and MODIS DB AOD (Fig. 3-A). They have analyzed AI for the large-scale, binary determination of dust

sources. Subsequently, the potential of identified sources is quantitatively defined as the long-term fraction of dust occurrence determined by DB AOD > 0.7.

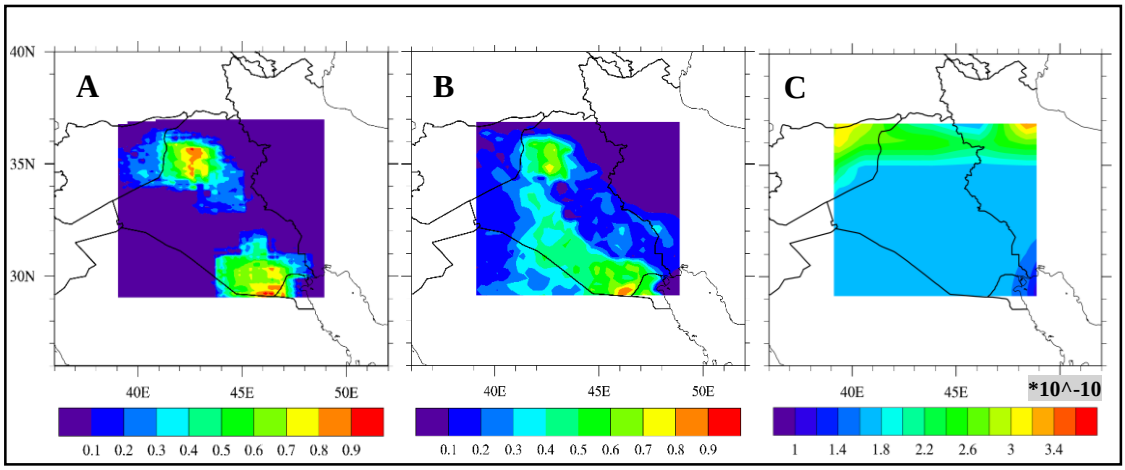

Figure 3 A and B are respectively the original (Nabavi et al., 2017) and modified WASF, calculated based on the fraction of dust occurrence. C depicts the source function as used by MACC (in units kg s^2 m^{-5}).

In comparison with original WASF, we made two modifications. First, the threshold of dust occurrence within dust sources was decreased to 0.6 (instead of 0.7) to detect any active dust sources. Second, we considered the possibility of dust occurrence away from major dust sources by applying a dust threshold DB AOD > 0.8 for these regions (Fig 3-B). They got higher thresholds (than major dust sources) to make sure that high AOD over these areas is not because of transporting dust originated from upstream dust sources. The original WASF assumes no dust emission out of dust sources, which is likely too stringent. It is worth mentioning that all discussed datasets are interpolated or aggregated to a 0.25 degree and, if needed, are averaged to get monthly means. It should be noted that all MLAs and the Weather Research and Forecasting Model coupled with chemistry (WRF-chem) applied here use WASF as source function whereas The Monitoring Atmospheric Composition and Climate (MACC) uses source functions shown in panel C of Fig. 3.

The study period is the warm months of the year (Apr-Sep) between 2003 and 2013. In these months dust storms are most frequent in West Asia (Boloorani et al., 2014) and all datasets are available. Figure 4 shows that the MODIS DB Angstrom exponent is less than 1, which is used as a criterion to discriminate dust particles from other types of aerosols (Dubovik et al., 2002), over most of the study area. DB Angstrom exponents more than one occur in the Northeast of the study region, where the Zagros Mountains act as barrier against the entrance of dust particles to the west of Iran. The two partitions of 2003 to 2010 and 2011 to 2013 are chosen as training and test sets, respectively.

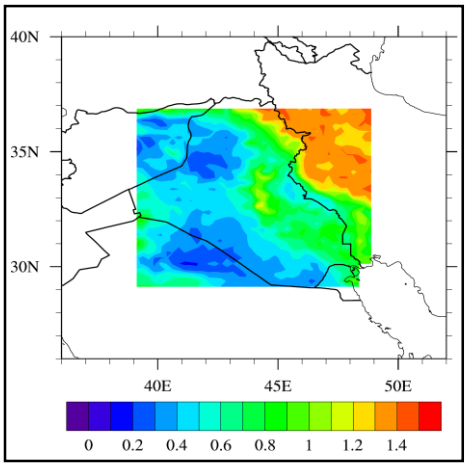

Figure 4: Averaged DB angstrom exponent as defined in Dubovik et al., (2002) during warm months (Apr-Sep) of 2003 to 2013. DB angstrom exponents less than 1 indicate that the aerosol mostly consists of dust.

2.2. Feature selection criteria (FSC)

Machine learning algorithms generally optimize the combination of potential predictors to get the best statistical forecasts of a particular predictand, in our case DB AOD. Computational expense of MLAs is extremely sensitive on the number of predictors. The process of feature selection aims to choose the optimal set of predictors from a (much) larger set of potential predictors. Regardless of which MLAs are used for prediction, feature selection is a critical step, which has a direct effect on the level of accuracy and, at the same time, complexity of model. It also regulates the generalizability/overfitting of MLAs. This process is now described with the advisable brevity.

The FSC are principally categorized into filter, wrapper, and embedded types. Filter-type methods estimate the importance of explanatory variables regardless of the model performance. These methods are computationally effective and robust against overfitting. However, the relationships between potential features are neglected by filter-type methods, which can result in the selection of redundant predictors. Therefore, they are mainly used as preprocessing methods (Chandrashekar and Sahin, 2014). Pearson correlation coefficient (PCC) and Mutual Information (MI) are two well-known filter-type methods. Correlation ranking simply considers the linear relationship between each predictor X_j and response variable Y:

Equation 2

$$PCC(j) = \frac{cov(X_j,Y)}{\sqrt{var(X_j)\times var(Y)}}$$

where cov and var represent the covariance and variance, respectively. MI is the measure of a relationship between two random variables that are sampled simultaneously (Paninski, 2003). In other words, MI measures how much information random variables have about each other

(Eq. 3). Zero MI means predictor X_j and response variable Y are independent whereas high MI indicates that there is large amount of information shared. The MI of two continuous variables X_j and Y whose joint distribution is defined by P (x_j, y) is as follows;

Equation 3 $$MI(X_j, Y) = \int_Y \int_{X_j} P(x_j, y) log \frac{P(x_j,y)}{P(x_j)P(y)} dx_j dy$$

$P(x_j)$ and $P(y)$ are the marginal distributions of X_j and Y.

Unlike filter-type methods, wrapper-type methods evaluate the performance of variable subsets which helps to recognize the possible interactions between variables (Chandrashekar and Sahin, 2014). Wrapper-type methods consider the predictors and model performance, respectively, as the inputs and the output to be optimized. Recursive Feature Elimination (RFE) is one of the most commonly used wrapper-type methods. To implement this algorithm the given model is first executed with all predictors. Then, the importance of each predictor is separately determined by applying ranking methods which differ from model to model. Random forest (RF) and Multivariate Adaptive Regression Splines (MARS) have built-in FSC (discussed in subsection 2.2), whereas ANN and MLR use combinations of the absolute values of the weights and the absolute value of the "t" statistic for each model parameter, respectively. Support Vector Machines (SVM) consider coefficient of determination (R^2) for ranking predictors. This statistic is calculated by fitting a LOESS (LOcally wEighted Scatter-plot Smoother) between the response variable and the predictors (Kuhn, 2012a). Having determined the importance of each variable, the top ranked subset of variables is iteratively used as the input to refit. In figure 5, the importance of variable subsets is represented by S. It is the sequence of importance-ordered numbers which are candidate values for the number of predictors to retain (S1 > S2,…). The performance of each subset is assessed and the value of S_i with the best performance is determined to fit the final model (Kuhn, 2012b). RMSE, calculated between predictions and observations over the study area, is used as criterion to evaluate the model performance and, subsequently, variable subsets.

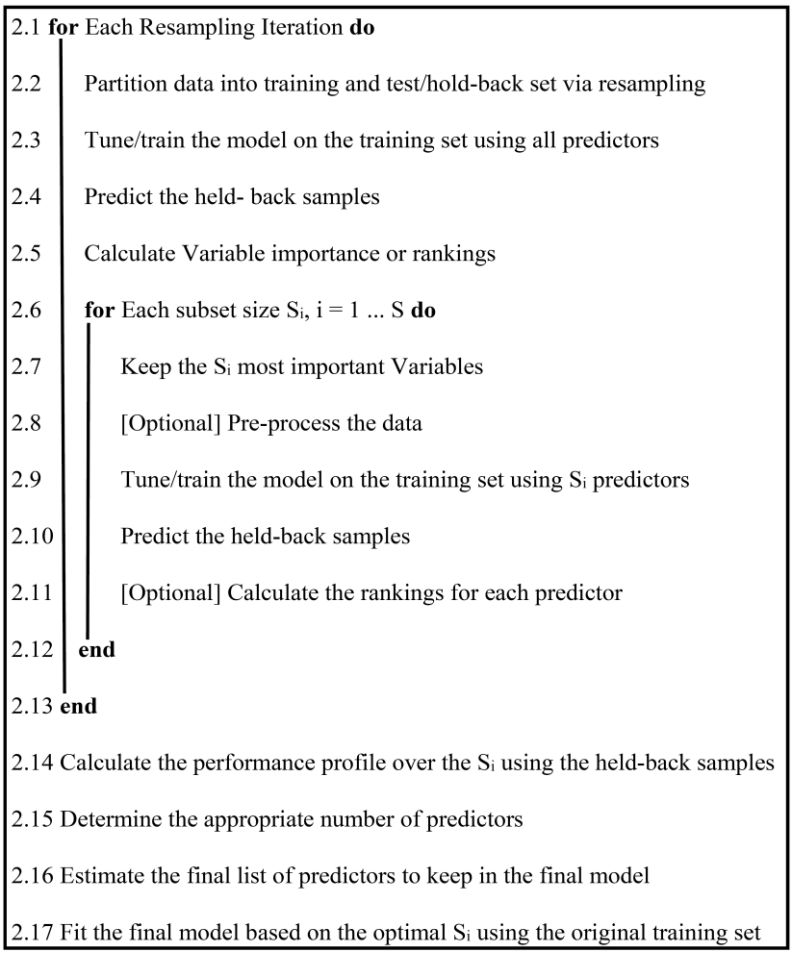

Figure 5 Flow chart of recursive feature elimination (RFE, (Kuhn, 2012b)).

The applicability of wrapper-type methods is limited because of two main issues. The risk of over-fitting increases when the number of observations is insufficient. On the other hand, these methods are computationally expensive when dealing with a large number of inputs. Embedded-type methods are recently proposed as compound algorithms, which utilize the advantages of both previous methods. They can significantly reduce the computation time required by wrapper methods (Chandrashekar and Sahin, 2014). This is because wrapper methods find the final model by the evaluation of multiple variable subsets against model performance whereas embedded methods evaluate the number of subsets already reduced as part of the training process. Battiti (1994) defined the optimal subset as a variable subset in which maximum and minimum MI occur respectively between each feature and the output and newly selected feature and so far selected futures. Figure 6 shows the differences between embedded-type methods and two other types.

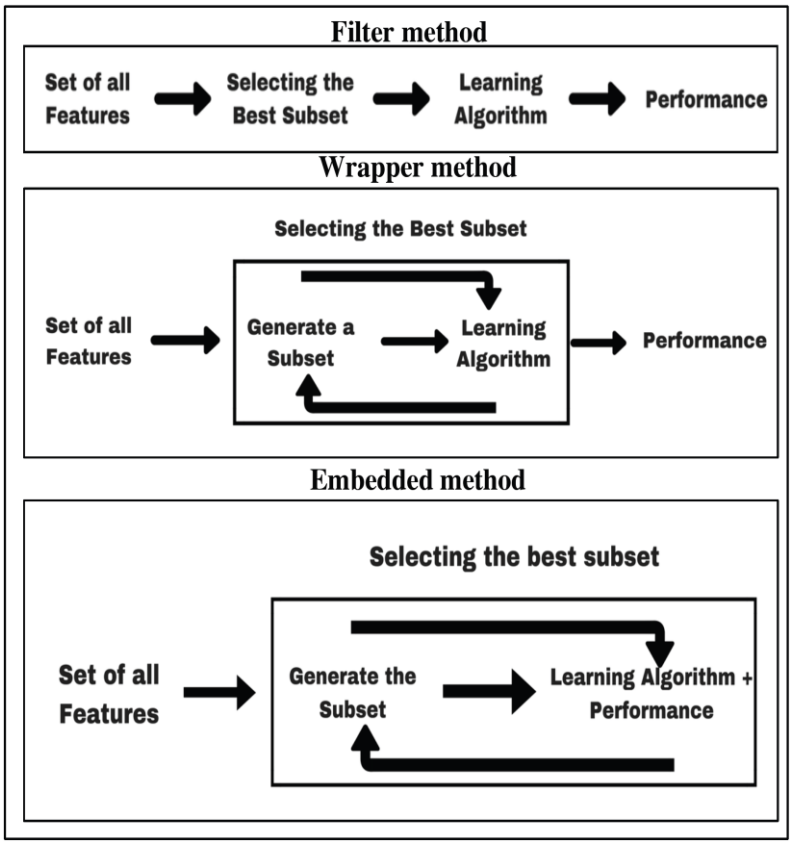

Figure 6 Flow charts of three types of FSC (Hamon, 2013).

Since embedded-type methods consider the feature selection step as a main part of MLAs, we will discuss them in the next subsection.

2.3. Machine learning algorithms

In this subsection, first we discuss RF and MARS which utilize two different embedded-type methods for feature selection. They will be followed by three other machine learning algorithms, including SVMs, ANN, and MLR, which have no built-in FSC.

- Random forest

Breiman (2001) proposed RF as an ensemble of decision trees algorithm. The latter is to increase the predictability of output by splitting observations (root nodes) into new classes (sub-nodes). It evaluates the splits of all available variables at each node and, then, it selects the split (variable) which results in less inhomogeneity. This is repeated recursively until data has been categorized into homogenous groups. However, the prediction of response value through a single tree mostly yields high bias and/or variance (over-fitting). To deal with this problem, RF constructs numerous trees using different bootstrap (Efron and Tibshirani, 1994) samples of the data. In addition, it adds an additional layer of randomness by choosing the

potential variable among a subset of predictors. In regression problems, the feature with the least residual sum of squares (RSS) of sub-nodes is selected (Eq. 4).

Equation 4
$$RSS = \sum left\,(y_i - y_L)^2 + \sum right\,(y_i - y_R)^2$$

where y_L and y_R are the mean y-value for right and left nodes, respectively. The y_i are the observed values. As mentioned before, random forest uses an embedded-type FSC. In this method, the Mean Squared Error (MSE) of out-of-bag (OOB)/held-back data is the basis of feature selection. On the average, each data point would be around 36% of the times excluded from training process because of bootstrapping. At each bootstrap iteration, OOB data are predicted, aggregated and compared with observed data (MSE_{OOB}) (Eq. 5)

Equation 5
$$MSE_{OOB} = o^{-1} \sum_1^o \{ y_i - \hat{y}_i^{OOB} \}^2,$$

where $\hat{y}_i^{OOB}$ is the average of the OOB predictions for the i_{th} observation. o is the number of OOB data. Subsequently, the importance of each variable is determined by measuring how much the prediction error increases when OOB data for that variable is permuted while all others are left unchanged (Eq. 6).

Equation 6
$$MSE_{per-OOB} = \frac{MSE_{per} - MSE_{OOB}}{MSE_{OOB}} \times 100$$

Here MSE_{OOB} and MSE_{per} are the representatives of calculated MSE between OBB data and real values before and after permutation, respectively. This criterion can be interpreted as follows: if a predictor is important in the current model, then assigning other values for that predictor randomly but realistically (permutation) should result in higher $MSE_{per-OOB}$.

- MARS

MARS is a nonparametric statistical method that makes no assumptions about the functional relationship of the variables. In order to improve the prediction of non-linear system, MARS splits the linear relationship between explanatory and response variables into separate piecewise linear segments (splines) of differing gradients (Zhang and Goh, 2016).

Equation 7
$$f(X) = \beta_0 + \sum_{m=1}^{M} \beta_m \lambda_m(X),$$

where each λ_m is a basis function (BF), β_m is a coefficient of parameter, and $X = (X_1, \ldots, X_q)$ is a matrix of q input variables. The term β_0 is a constant coefficient, estimated using the least-squares method. BF can be one spline function or the interaction of two or more BFs, depending on the order of $f(X)$. BFs are connected through the connection/interface points called knots.

During forward phase of MARS, candidate knots are placed at random positions to define a mirrored pair of BFs (Eq. 8).

Equation 8

$$Direct: Max(0, x - c) = \begin{cases} x - c, if\ x \geq c \\ 0, \quad otherwise \end{cases}$$

$$Mirror: Max(0, c - x) = \begin{cases} c - x, if\ c \geq x \\ 0, \quad otherwise \end{cases}$$

Equation 8, also known as hinge function, shows how continuously the variable *x* is transformed using a constant "c" as a knot. At each step, the model picks up that knot and its corresponding pair of BFs (direct and mirror) which yield the minimum error. This process continues until the model reaches a predetermined error level or/and a threshold number of BFs, which usually results in a purposely complicated and overfitted model. Due to this, the backward phase is used to improve the model by pruning the less significant terms. At the end of the backward phase, the model with lowest Generalized Cross-Validation (GCV) value is selected as the final model. The GCV criterion trades off goodness-of-fit against model complexity (Zarandi et al., 2013). For the training data with n observations, the GCV is calculated as (Eq. 9):

Equation 9

$$GCV = \frac{\frac{1}{n}\sum_{i=1}^{n}[y_i - \hat{y}_i]^2}{\left[1 - \frac{M + d \times (M-1)/2}{n}\right]^2}, d = \begin{cases} 3, & if\ degree > 1 \\ 2, & otherwise \end{cases}$$

Here M is the number of BFs, d is a penalty for each BF, and $\hat{y}_i$ represents the i_{th} predicted value. Thus, the numerator and denominator are, respectively, the MSE of the model and penalty for the prediction variance because of model complexity (Zhang and Goh, 2016). Here we used the varImp function (Kuhn, 2012a), implemented in R, to calculate the importance of each variable based on GCV. According to the help page, it accumulates the reduction in the GCV (or other statistics) when each predictor's feature is added to the model. The total reduction of GCV is used as the measure of variable importance. The more GCV decreases, the higher importance score each variable receives. Conversely, if a predictor was never used in any of the MARS basis functions in the final model (after pruning), it has an importance value of zero.

- Support Vector machines

SVMs, proposed by Vapnik (1995), have been applied successfully to both pattern recognition and more recently also to regression (Parrella, 2007) problems. For linear regression, SVM is formulated as follows (Eq. 10):

Equation 10 $$f(x) =< w, x > +b \qquad w, x \in R^q , b \in R$$

Where <,> denotes the inner vector product, b is bias, w represents weight for each variable, q is the number of variables, and x represents input variables. In case of nonlinearity between response and explanatory variables, SVM kernels (Φ), like Gaussian (radial), are used to map the data into a feature space in which the problem becomes linearly separable (Eq. 11).

Equation 11 $$y = f(x) =< w, \Phi(x) > +b$$

Vapnik (1995) suggested the following regularized cost function (Eq. 12) to estimate optimal w and b:

Equation 12 $$\frac{1}{2}\,||w||^2 + \frac{C}{n}\sum_{i=1}^{n} |y_i - f(x_i)|\varepsilon$$

The factor *C* trades off training error against the complexity of the model. A large (small) value for *C* will decrease (increase) the number of training errors. However, a large *C* can also lead to overfitting and high variance of prediction error. The bigger (smaller) ε results in the wider (narrower) ε-insensitive zone, which is used to fit the fewer (more) support vectors and, on the other hand, more flat (overfitted) estimates (Cortes and Vapnik, 1995). In fact, both *C* and ε values control model complexity (but in a different way). The second term of equation 12 can be defined as:

Equation 13 $$|y - f(x)|\varepsilon = \begin{cases} 0, & if\ |y - f(x)| < \varepsilon \\ |y - f(x)| - \varepsilon, & otherwise \end{cases}$$

The optimal weights are found by conversion of equation 12 and the corresponding constraints (Eq. 13) to a Lagrange function by introducing a dual set of variables. By some manipulations with Lagrange multiplier and dual optimization, one obtains:

Equation 14 $$w = \sum_{i=1}^{n}(\alpha_i - \alpha_i^*)\Phi(x_i)$$

α_i and α_i^* are Lagrange multipliers. Feeding equation14 into the equation 11, SVM predictions $f(X)$ are obtained for a test data point X. According to Mercer's condition (Burges, 1998), the inner product $\Phi(X)$ and $\Phi(x_i)$ can be defined through a kernel $\mathrm{K}(\mathrm{X}, x_i)$.

Equation 15 $$f(X) = \sum_{i=1}^{n}(\alpha_i - \alpha_i^*)\mathrm{K}(\mathrm{X}, x_i)+\mathrm{b}$$

with

Equation 16 $$K(\mathrm{X}, x_i) =< \Phi(x_i), \Phi(X) >$$

Here we chose the radial (Gaussian) basis function as SVM kernel, while other choices (Polynomial and Sigmoid) would also have been possible.

- Artificial neural network

Neural networks are multivariate nonlinear models. Feed-forward back propagation neural network (FFBP) is one of the most commonly used ANN models which consists of three layers; an input layer, one or more hidden layers, and an output layer (Konate et al., 2015). Each layer has processing units known as neurons or nodes. The neurons are interconnected by connection strengths called weights. In addition, there is a bias neuron with input 1 and corresponding weight connected to each processing unit in the hidden and output layers. The number of input neurons is equal to the number of independent variables while the output neuron(s) represent the dependent variable(s). The ANN model with one hidden layer can be written as

Equation 17 $$y = \alpha_0 + \sum_{i=1}^{h} \alpha_i f(\sum_{j=1}^{q} \beta_{ji} X_j + \beta_{0i}) + \varepsilon$$

where q is the number of input variables, h is the number of hidden neurons, β_{0i} (α_0) and β_{ji} (α_i) represent bias of the hidden layer (output layer) and weights of connections from input (hidden) neurons to hidden (output) neurons, respectively. The sigmoid transfer function (Eq. 18):

Equation 18 $$\mathrm{sgm(x)} = \frac{1}{1+e^{-x}}$$

is most commonly used for f. It is worth mentioning that Equation 18 assumes a linear transfer function in the output node for forecasting problems. In order to obtain the best weights for training a neural network, the back propagation algorithm uses MSE as cost function.

- Multivariable linear regression:

Linear models are the most simple and commonly used machine learning algorithms. They try to find a linear relationship, if any, between one or more predictors and a response variable by fitting a linear equation to observed data. MLR is used for the cases that the number of predictors is more than one variable (Eq. 19)

Equation 19 $$y_i = \beta_0 + \beta_1 x_{i,1} + \beta_2 x_{i,2} + \cdots + \beta_{q-1} x_{i,q-1} + \varepsilon_i$$

where q is the number of coefficients β in the model including the intercept (β_0). ε_i is the prediction error of the model. The coefficients are estimated by minimizing the sum of the squares.

2.4. MLA configuration

Although one may discuss that MLAs are designed to make a machine system that automatically builds models from data without human involvement, the best performance of MLAs only occurs when their optimal parameters are obtained through tuning. In this study, the optimal parameters are tuned based on the automated evaluation of prediction errors (RMSE) resulting from 10-fold cross-validation. Both the tuning and training of MLAs are done by using the Caret package (Kuhn, 2008), implemented in R. In table 1 tuned parameters of MLAs are presented. Names of parameters are replicated to be easily found in the help page.

Table 1 Optimal parameters of MLAs as result of tuning. Parameter mtry is the number of variables randomly sampled as candidates at each split, ntree is the number of trees, nprune is the maximum number of terms (including intercept) in the pruned model, degree is the maximum degree of interaction, sigma is the width of radial kernel (also known as smoothing parameter), C is the constant of the regularization term in the Lagrange formulation, size is the number of units in the hidden layer, and the decay is parameter for weight decay (Kuhn, 2008).

MLA	**Parameter(s)**	**RMSE**
RF	mtry = 3, ntree=100	0.16
MARS	nprune = 16, degree = 1	0.315
SVM	sigma=0.237, C = 1	0.273
ANN	size = 15, decay = 0.01	0.059

2.5. Dust models

Dust models are the present standard tool for predicting important processes of the dust cycle such as dust emission, transport as well as dry and wet deposition. Physical or empirical laws are employed to parameterize those mostly sub-grid scale processes. In most cases the dust models are deterministic, i.e. no stochastic forcing is present in the forecast equations. The initial state of the dust forecasts is computed with different degrees of sophistication as will be described below. From this state short term forecasts are performed to predict dust concentrations and AOD a few days ahead.

In this paper we use forecasts from two quite different state of the art dust modeling systems to get fields of monthly mean AOD:

- WRF-chem (Grell et al., 2005, Fast et al., 2006, Skamarock et al., 2008) can be run with various aerosol species, with a variety of schemes available to parameterize mineral dust cycle including the Goddard Chemistry Aerosol Radiation and Transport (GOCART) (Ginoux et al., 2001), the Air Force Weather Agency (AFWA) (Su and Fung, 2015) and the University of Cologne (UoC) (Shao et al., 2011). Nabavi et al. (2017) have shown that the parameterized dust fluxes into the atmosphere are rather sensitive to the dust source function and that dust forecast skill near dust sources can be considerably improved if the dust source function is well represented. In the present paper WRF-chem 3.6.1 is executed for the study period using the configuration explained by Nabavi et al. (2017). It is run over the domain shown in figure 2 with the GOCART dust scheme modified to use WASF, as described above, as source function. ERA-Interim analyses are used as lateral boundary conditions for forecasts of the warm months (Apr-Sep). Newtonian nudging toward ERA-Interim is used to keep the forecasts close to observed atmospheric state. This is a well proven method especially for so-called hindcasts (forecasts of past weather) that allows to avoid explicit and expensive analysis steps (Deng et al., 2007). Soil moisture is provided from National Centers for Environmental Prediction (NCEP) Final (FNL) Operational Global Analysis data and precipitation is a standard forecast product. Total column dust concentration is the primary forecast variable which is converted into AOD at 550nm using a radiative transfer code (a so-called observation operator, (Chin et al., 2002). AOD is then averaged to yield a monthly mean.
- The MACC (2003-2012) project and its successor the Copernicus Atmospheric Monitoring Service (CAMS) (July 2012 to present) have been and are devoted to air quality monitoring. Many chemical species but also five aerosol species, including mineral dust, are monitored and forecast. The basic meteorological forecast system used for data assimilation is the Integrated Forecasting System (IFS) of ECMWF. The formulation of the aerosol model (including dust) has remained largely similar during the transition from MACC to CAMS, based on Morcrette et al. (2009). It is a global forecasting system and as such has limited spatial resolution. Contrary to WRF-chem as used here, MACC assimilates satellite observations (Benedetti et al., 2009). The MACC dust product is thus not a forecast but an analysis where dust-sensitive observations, namely MODIS AOD, have been assimilated, which certainly strengthens this product. MACCs primary focus is on atmospheric chemical species, not so much

mineral dust. The parameterizations for dust have been tuned relatively little. A time-invariant climatological source function is used in the dust emission parameterization. However it varies between different geographical regions to parameterize their different characteristics as dust sources. A global base value of 10^{-11} kg m^{-2} s^{-1} is used, corresponding to "theoretical" dust emissions with 1 m s^{-1} wind speed and with albedo of 1, and then multiplied by albedo and by the regional factors (0.5 for West Asia, see Fig. 3-C). The total column dust concentration analyses are converted into AOD using an observation operator and then are averaged to yield a monthly mean. The products are freely available from apps.ecmwf.int

Nabavi et al (2017) also included results from the Dust REgional Atmospheric Model (DREAM) modeling system (Basart et al., 2012), which yielded skill scores similar to MACC. In this paper, which is more stringent in the choice of predictands, we decided not to include DREAM since it provides only dust optical depth (DOD) but not AOD as output field.

Still, in order to maintain the consistency of the comparisons, AOD yielded by WRF-chem and MACC needs to be converted into DB AOD using a linear regression which is computed between MODIS DB AOD and AOD 550nm of three AErosol RObotic NETwork (AERONET) stations, including Dhandah (25.5N, 56.3E), Kuwait University (29.3N, 47.96E), Solar Village (24.9N, 46.4E). Comparing MACC dust optical depth with both MISR AOD and MODIS DB AOD at 550 nm, Nabavi et al. (2017) found that this product has higher agreement with the former instrument. However, they have also pointed out that the differences are generally small over dust sources. Therefore, we have assumed that the evaluation of MACC outputs against MODIS DB AOD (not against MISR AOD) cannot distort our examinations especially over hot spots. MACC AOD is available from 2002 to 2012. Therefore, this dataset is six months shorter than WRF-chem and MLA predictions, which are available during the whole study period.

3. Results and discussion

In this section we first report about the determination of predictors of DB AOD used by MLAs using the feature selection criteria described above, and then about the prediction of DB AOD by MLAs and DMs (3.2).

3.1. Potential predictors of DB AOD

As discussed before, RFE can simultaneously determine the importance of each single variable and of variable subsets. To this end, it evaluates the performance of different variable subsets

which are already created by the orderly elimination of variables from the least to the most important one. Because each MLA uses a different ranking method for determining the importance of variables (step 2.5, Fig. 5 and subsection 2.2), RFE assigns different levels of importance to each single variable. To reduce these differences, we have modified the standard RFE and have named it as modified RFE. In this method, all five MLAs were iteratively trained and validated while variables are eliminated one by one at each iteration. The main differences between modified RFE and standard RFE are that the former eliminates only one variable (not a subset of variables) at each iteration considering no priority ranking and that it evaluates the performance of MLAs by using test data (not validation data recorded during training period). Modified RFE uses the averaged Spearman Correlation Coefficient (SCC) and averaged RMSE between MLA predictions and DB AOD of the test dataset to determine the importance of variables and, consequently, variable subsets. According to figure 7, the elimination of SF has caused the highest decrease in SCC. Conversely, the averaged SCC increased when SPEI, SM, and ST are eliminated. Using RMSE as a measure leads to the same conclusion. It increases most significantly if SF is eliminated but actually decreases when SPEI, SM, and ST are eliminated.

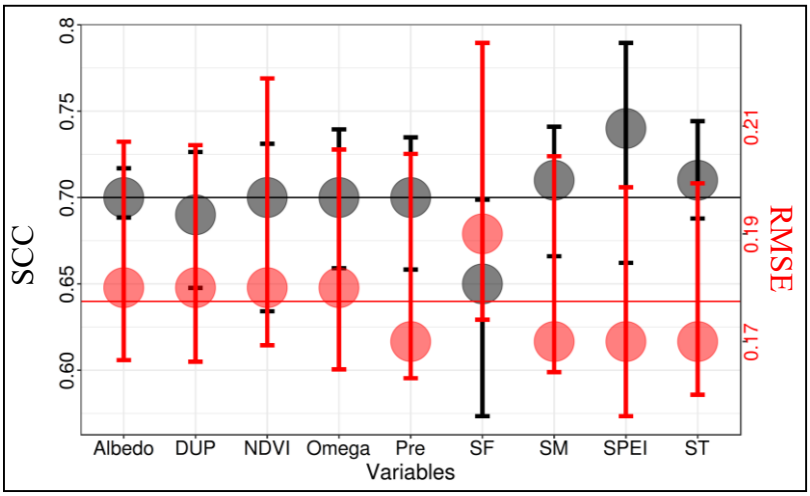

Figure 7 the averaged SCC (black filled circle) and RMSE (red filled circle) between MLA predictions and test observations. Error bars are limited between the maximum and minimum values of SCC (black bars) and RMSE (red bars) resulted from separate comparison of five MLA predictions and observations. The average of averaged SCC and RMSE are shown by the black and red lines, respectively.

The overall outcome of MI and PCC (filter-type methods) have also assigned the least importance to SPEI and SM (Fig. 8). The biggest discrepancy occurs when, unlike modified RFE, MI and PCC have selected omega and ST as the third least and most important features, respectively. In order to clarify this ambiguity, we have examined the levels of variable importance assigned by standard RFE. It disclosed that ST has generally had a higher

importance than omega in the prediction accuracy of MLAs (not shown here). Conclusively, six features including Albedo, DUP, NDVI, ST, precipitation, and SF are selected to train MLAs during 2003 and 2010.

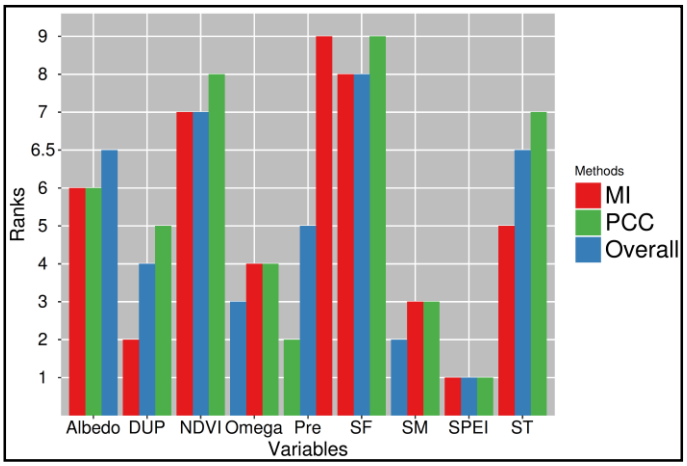

Figure 8 The importance of variables determined by MI and PCC. The overall outcome is prepared by the average of variable ranks assigned by mentioned methods. High rank means high importance.

3.2. The prediction of AOD by MLAs and DMs

It should be first noted that, here, the comparison of MLA and DM performance is discussed based on their statistics during the test period. This is because MLAs are trained such that they always yield the least possible errors compared to training observations which cannot be generalized to the test set (predictions). The performance of MLAs and DMs during the training period is presented in the supplement (Fig. S1). Figure 9-A shows time series of MLA (dashed line) and DM (dotted lines) predictions of DB AOD during 2011 to 2013 together with observations. The visual investigation of time series indicates that both MLAs and DMs roughly managed to simulate the general variations of observed DB AOD. However, MLAs have yielded higher SCC and lower centered RMSE compared to DMs (Fig. 9-C). Except ANN, the good agreement of standard deviations of MLA predictions to that of observations (0.23) implies that they have more accurately simulated the amplitude of DB AOD. Except MACC, the most obvious feature of all time series is that major peaks are not well captured especially in 2012. Besides the fact that these prediction errors may be partly attributed to non-linearities between the dust abundance and DB AOD intensity over the study area (Nabavi et al., 2016) and/or instrumental miscalculations (Albayrak et al., 2013), three main reasons could cause underpredicting high extreme values. The lack of variables which thoroughly explain the variance of DB AOD (dust storm) can be seen as the primary reason. In other words, selected features for training MLAs and numerical solutions of DMs, especially WRF-chem in this case,

do not perfectly estimate dust emission. This requires further studies for the improvement of our knowledge about the mechanism of dust formation which is beyond the scope of this paper. Secondly, the scarcity of extreme high values results in poor performance of both MLAs (Zhang et al., 2015) and DMs (Kumar et al., 2014) in the prediction of extraordinary cases. In fact, models are trained or formulated so that they yield the least overall bias with observations. That is, achieving the highest level of prediction accuracy does not necessarily mean that models accurately estimate the whole range of measured quantities but it means they are successful in the simulation of more frequent cases. For the prediction of phenomena which have a positively skewed frequency distribution, like dust abundance, this problem is known to be particularly serious. Using Synthetic Minority Over-sampling Technique (SMOTE), Torgo et al. (2013) tried to deal with this issue by under-sampling of frequent cases (irrelevant cases) and over-sampling of rare quantities (relevant cases) used for training MLAs. However, the extent of over-sampling/under-sampling requires researcher intervention and it changes case by case. Therefore, we decided not to manipulate the original distribution and to concede part of uncertainties related to the unbalanced distribution of DB AOD.

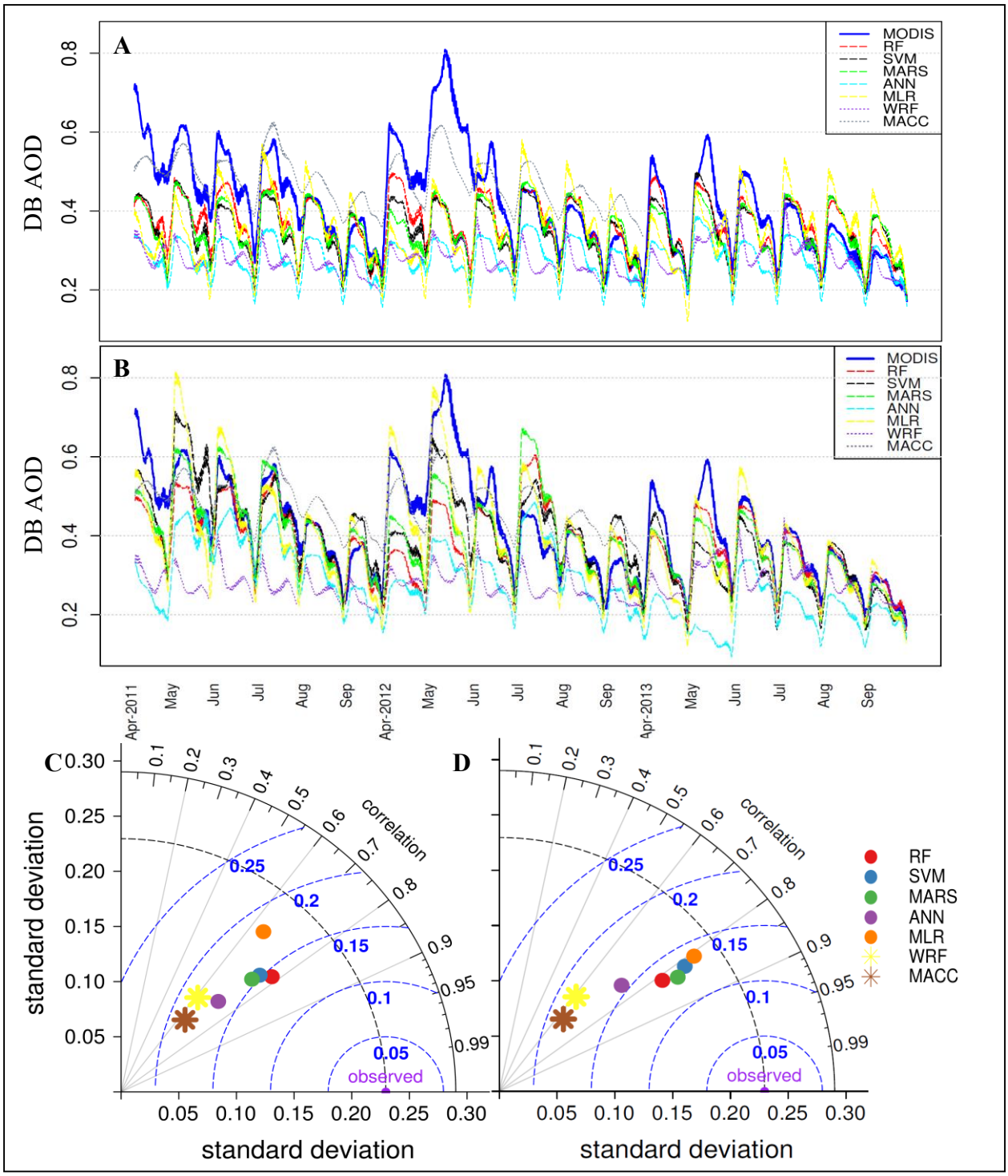

Figure 9 A: observed (blue) and predicted DB AODs throughout study area (32x40 pixels) during the testing period (18 time steps). Dashed and dotted lines show 200-point moving average of MLA and DM predictions, respectively. B: the same as A but after the inclusion of five area-averaged predictors. The statistics of predictions, calculated between prediction and observation vectors within the study area, including centered RMSE (dashed blue line), standard deviation (dashed black line) and SCC correlation (solid black line) are presented in C (before the inclusion of area-averaged predictors) and D (after the inclusion of area-averaged predictors).

The third reason of differences between predicted and observed peaks can be attributed to the fact that a significant portion of AOD values at each pixel, especially over surrounding areas

of dust sources, is related to the amount of dust particles advected from upstream sources. Using WRF-chem for dust prediction, Nabavi et al. (2017) showed that shortcomings in the prediction of dust transport and deposition result in significant overestimation/underestimation of dust concentration over affected areas. They linked a great deal of AOD over West Asia to dust plumes originating from source points in the northwest of Iraq, not to their local potential of dust emission. Therefore, we have conducted a sensitivity experiment taking the area-averaged observed DB AOD over northwest of Iraq (area between latitudes 34°- 37 ° N and longitudes 37 ° - 40 ° E) as additional input for MLAs throughout the study area. This input can be also be seen as an alternative of transportation and deposition schemes, used in DMs, to regulate the amount of advected dust. As expected, it caused a significant improvement in the prediction of extreme values by MLAs (not shown here). In order to keep the MLAs independent of the response variable, this predictor (area-averaged DB AOD) is replaced by the area average of five predictors (except SF) over the mentioned region and, then, MLAs are retrained using 11 predictors (6 normal datasets + 5 corresponding area-averaged datasets). The effect of this modification on MLA performance can be seen in figures 9–B and 9-D. Although a few peaks are overestimated by MLR, MLAs in general managed to capture or get closer to the most of extreme high values. Interestingly, all MLAs have yielded high agreement with observations in the second run as the least and highest SCC are 0.76 and 0.83 belonging to ANN and MARS, respectively. In contrast, the SCC of DM predictions, which are produced under a same setting in both runs, at most reach 0.65 for MACC simulations. The analogy of standard deviation of MLA predictions (ranging from 0.14 to 0.2) and of observations (0.23) in the second run shows the importance of the newly added predictors in the more accurate simulation of DB AOD amplitude, compared to MACC and WRF-chem (0.06 and 0.07). Similarly, the centered RMSE between MLA predictions and observations decrease to less than 0.15 in the second run whereas DMs have yielded centered RMSE of 0.18. In order to examine the performance of models in the course of time, area-averaged monthly RMSE and bias (prediction/observation) are compared with corresponding observed DB AOD (blue line) (Fig. 10-A and B) over test period. As expected, DMs have yielded higher RMSE than MLAs in most of the times. The noticeable point is that RMSE did not follow any tangible positive trend by approaching the end of test period. In other words, if MLAs get overfitted over training period, the level of prediction errors will increase by getting distance from the start point of test period which is not the case in our examinations. The juxtaposition of DB AOD with simulations show that prediction error meaningfully increase when DB AOD reach a peak. This is because of DB AOD underestimation which is escalated during the upsurge of dust storms

around May (Fig 10-B). Apart from this period, all MLAs except ANN, have no significant bias against observations. In contrast, WRF-chem has left two different periods of underestimation and overestimation before and after June 2012, respectively. MACC has yielded very significant overestimation during entire test period (until the last available data point in Sep 2012). Further examinations show that this model has high prediction error (Fig. 10-C) and bias (Fig. 10-D) mainly for low values of DB AOD. Therefore the overall performance statistics for MACC are relatively modest although it performs well in cases of high observed DB AOD (Fig. 10-D). WRF-chem has also yielded high bias for quantities of DB AOD < 0.2, but because it is canceled by significant underestimation of higher values, unlike MACC, it is not reflected in the spatially-averaged bias in figure 10-B. Besides this, all DMs and MLAs, especially WRF-chem and ANN, have yielded higher RMSE and significant underestimation by approaching higher values of DB AOD indicating having difficulties for the prediction of high DB AOD (intense dust storms). The point-to-point comparison (Fig. 11) of simulations and observations also show the better performance of MLAs as their predictions are mainly congested around regression lines, which can be interpreted as high correlation between observations and predictions. The lower bias of MLAs, except ANN, predictions shown in figure 10-B, is also represented by the proximity of their regression and identity lines. The juxtaposition of observed and predicted histograms indicates that the frequency distribution of MLA predictions, especially SVM, is very similar to that of observations (Figs. 11-A, C, E, F, and G). In contrast, the larger bias of DM predictions and their low agreement with observations can be diagnosed from the significant tilt between the regression line and the identity line and higher spread of simulations, respectively (Figs. 11-B and D). The significant bias of simulated DB AOD by MACC against observations can be also seen in figure 11-D where simulated DB AOD start from 0.3. In the following, the spatial analysis of the discussed statistics characterizes more clearly the performance of DMs and MLAs over the study area and it also discloses the reason of overestimation of low DB AOD by DMs.

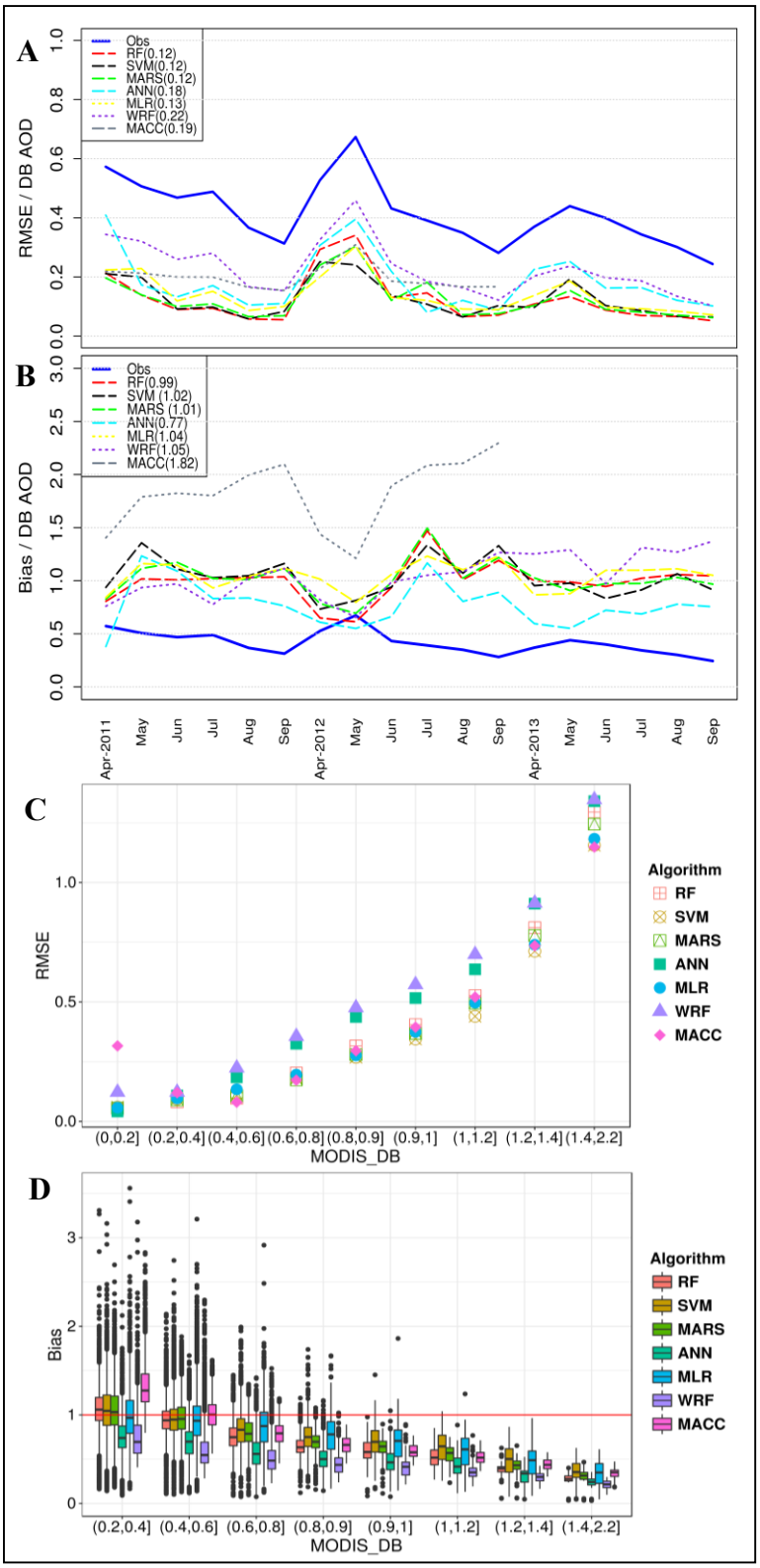

Figure 10 A and B are showing RMSE and bias over test period. Blue lines in A and B are area-averaged monthly observed DB AOD. Panel C shows RMSE values for different classes of MODIS DB AOD. Panel D shows the ratios between observed and predicted DB AOD for different classes of DB AOD on a logarithmic scale.

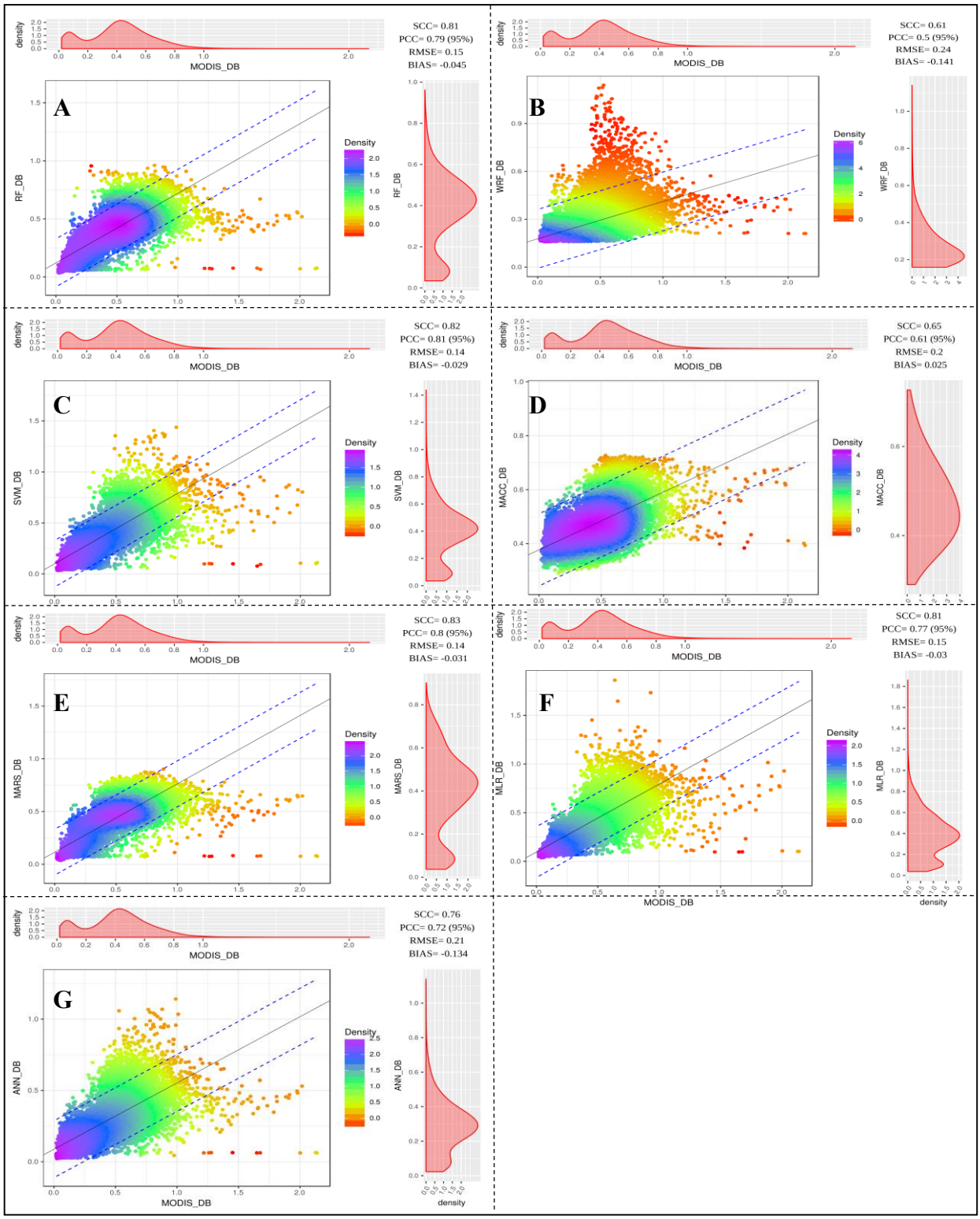

633

634 Figure 11 scatter plots between MODIS DB AOD values (all 25x25km pixels of the study area, all months of test
635 period) and predictions of MLAs; RF (A), SVM (C), MARS(E), ANN (G) and MLR (F) and DMs; WRF-chem
636 (B) and MACC (D). The histograms of observations and predictions are at top and right margins of each plot,
637 respectively. Colors represent the estimate of the density function.

Figure 12 presents the temporal average of observed and predicted DB AOD (figs. 12 AA-AH), and temporal average of SCC (figs. 12 BA-BG), RMSE (figs. 12 CA-CG), and bias (figs. 12 DA-DG) between observations and simulations, during the test period. The distribution of observed DB AOD clearly depicts a dust hot spot in northwest of Iraq and a dust path with northwest-southeast direction. This pattern is to some extent reflected in the simulations of all models, which conforms the northwest-southeast prevailing wind of the region during summertime, called Shamal. According to these plots, MACC and, to some extent, WRF-chem do not resolve Zagros Mountains, in western Iran, as barrier against transportation of dust particles from plains in Iraq to the east of the study area which is represented by low DB AOD in observations and simulations of other models. In fact the main reason of DM overestimation of DB AOD < 0.2 is that they do not resolve the effect of elevations in the deposition of dust particles in western Iran. The inter-comparison of MLAs shows that ANN is the only algorithm which could not well simulate AOD quantities, while other MLAs have provided a realistic distribution of DB AOD over northwest of Iraq and the dust path. Although the general distribution of AOD is also simulated by DMs, they fail to estimate accurately the absolute quantities of DB AOD particularly over main dust source of the study area (northwest of Iraq). It should be also noted that the agreement of MLR and MARS predictions with observations over the dust path is higher than other algorithms. Although RMSEs between predictions and observations increase over dusty areas of Iraq, because of underestimation high dust concentrations, in all algorithms, MLAs have generally produced much less RMSE than DMs over these areas. Similarly, the bias of MLA predictions, except ANN, is interestingly around 1 (no bias) whereas DMs have yielded very high overestimation over Western Iran, as discussed above, and moderate underestimation over dust sources and dust path. In fact, dust schemes of DMs, used for the estimation of dust emission, deposition, and transportation, underestimated emitted dust, which can be attributed to a suboptimal representation of the source function over dust sources and to overestimated dust advection into Iran, delineated with high RMSE and bias in figures 12-DF and 12-DG. The analysis of SCC between predictions and observations shows that the eastern half of study area, more or less, has received lower SCC in all predictions. As discussed before, these uncertainties can be attributed to suboptimal dust deposition by DMs and, moreover, lower predictability of MLA predictors in dust transportation and deposition (affecting the west of Iran) than dust emission (over Iraq).

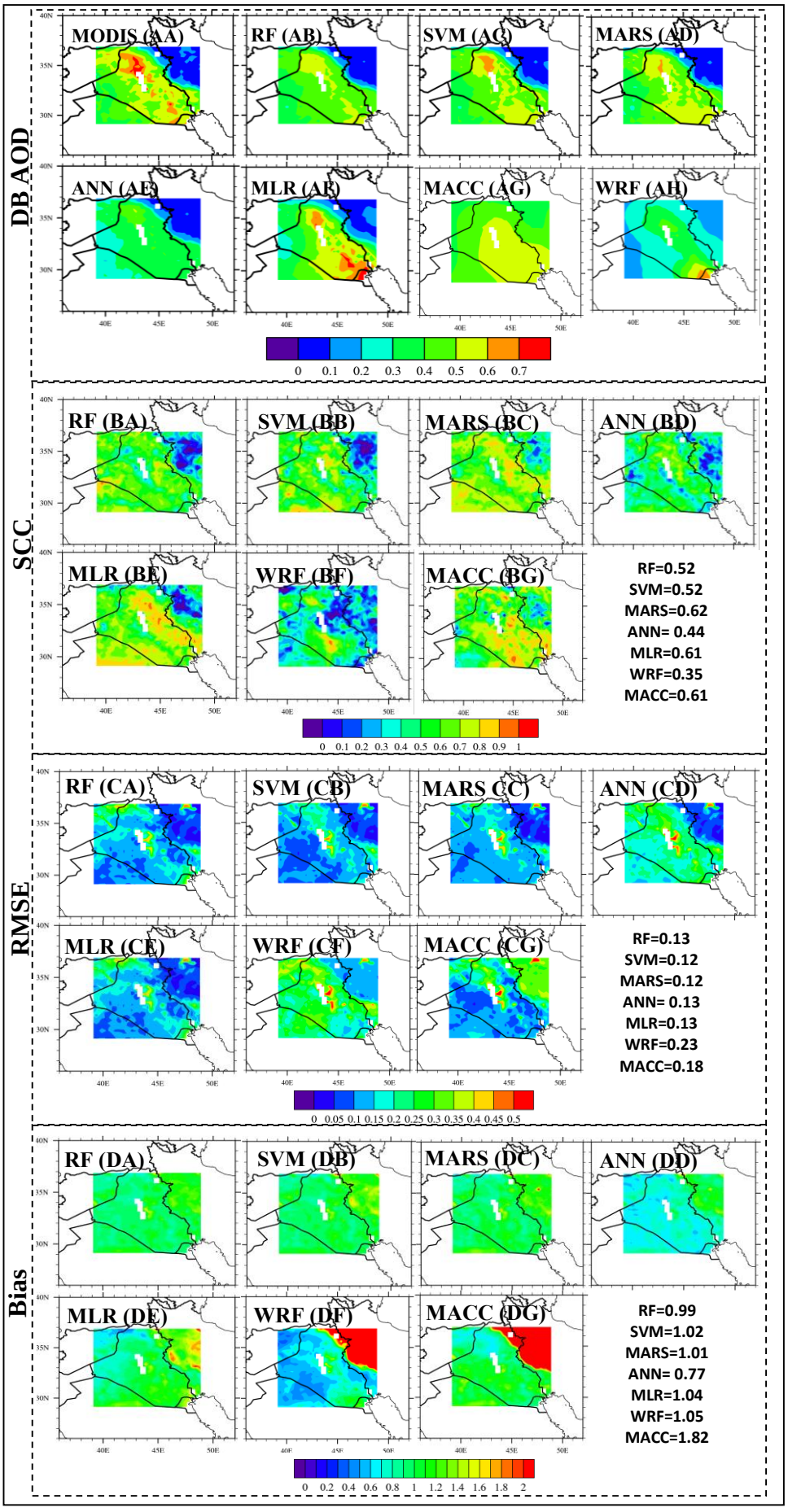
DB AOD
MODIS (AA)
RF (AB)
SVM (AC)
MARS (AD)
ANN (AE)
MLR (AF)
MACC (AG)
WRF (AH)
0 0.1 0.2 0.3 0.4 0.5 0.6 0.7
SCC
RF (BA)
SVM (BB)
MARS (BC)
ANN (BD)
MLR (BE)
WRF (BF)
MACC (BG)
RF=0.52
SVM=0.52
MARS=0.62
ANN= 0.44
MLR=0.61
WRF=0.35
MACC=0.61
0 0.1 0.2 0.3 0.4 0.5 0.6 0.7 0.8 0.9 1
RMSE
RF (CA)
SVM (CB)
MARS (CC)
ANN (CD)
MLR (CE)
WRF (CF)
MACC (CG)
RF=0.13
SVM=0.12
MARS=0.12
ANN= 0.13
MLR=0.13
WRF=0.23
MACC=0.18
0 0.05 0.1 0.15 0.2 0.25 0.3 0.35 0.4 0.45 0.5
Bias
RF (DA)
SVM (DB)
MARS (DC)
ANN (DD)
MLR (DE)
WRF (DF)
MACC (DG)
RF=0.99
SVM=1.02
MARS=1.01
ANN= 0.77
MLR=1.04
WRF=1.05
MACC=1.82
0 0.2 0.4 0.6 0.8 1 1.2 1.4 1.6 1.8 2

669

Figure 12 maps of temporal averages of observed (AA) and predicted DB AOD (AB-AD). Averaging period: warm season (April-September) of years 2011-2013. Following rows are maps of temporal statistics (SCC, RMSE, and Bias compared to observed DB AOD), calculated between MLA and DM predictions. Values in white box are the area average of corresponding statistics. Acronyms are explained in the text.

Conclusions

The successful application of MLAs in various classification and regression problems and the necessity of dust prediction with mesoscale (25x25km) spatial and monthly temporal resolution in West Asia were two main motivations to attempt dust prediction with MLAs. Due to the lack of ground-based observations, MODIS DB AOD was selected as the response variable to be predicted and eight monthly datasets including ST, SM, SPEI, albedo, NDVI, Precipitation, omega at 850 hPa, and DUP at 10 meter were used as potential predictors. In addition, we made use of a time-invariant variable "SF" to regulate the potential of dust emission at each 25x25km pixel. Using three types of Feature Selection Criteria, SF was determined as the most important factor of dust forecast. On the contrary, SPEI, SM, and omega were designated as the least important variables and they were eliminated. Because advected dust has a large influence on AOD of dust-affected areas, the area average of time-variant variables over main dust source of study area, northwest of Iraq, were taken as complementary predictors. Five MLAs, including MLR, RF, SVM, MARS, and ANN, were trained and compared with two DMs, including WRF-chem and MACC. In a nutshell, predictions of AOD by MLAs, especially SVM and MARS, outperformed DMs on the time scales considered in the present work. The analysis of statistics shows that MLAs have high agreement with observations and they, except ANN, yielded the smallest prediction errors over dust sources. Since the Source Function gained high weights in the feature selection it is quite likely that its careful specification as WASF has been a big advantage for MLAs. It helped their predictions to be more accurate in the representation of dust source distribution in West Asia than those of DMs, which mostly put less emphasis on specification of the Source Function. Although both MLAs and DMs were relatively successful in the simulation of general variations of aerosol concentration, they still all underestimated major DB AOD peaks. The rough resolution of used datasets, the scarcity of extreme values and the omission of some unknown influential predictors and remaining deficiencies in the specification of the source function are likely the main reasons. In addition, DMs, especially MACC, have failed to resolve the effect of Zagros Mountains as a natural barrier preventing the transportation of dust to the west of Iran which is reflected as a very high

overestimation of low DB AODs. This is the main reason why the overall performance scores for MACC are relatively low.

We emphasize here that the results found are valid for the space and time scales considered here. For short term forecasts on the daily scale with good knowledge of the initial atmospheric state and of initial surface properties such as soil moisture, DMs are still considered the method of choice since the physical laws for short term predictions are well known and well implemented in such models. On time scales where the instantaneous initial conditions play less role the more uncertain input parameters and physical relationships become more important. Under these circumstances MLAs perform quite well. While the authors have invested quite some efforts into optimizing deterministic dust forecasts (Nabavi et al., 2017) these could not beat the MLA based predictions. We still put the caveat here that the validation has been done with AOD, which is not a state variable of DMs but has to be calculated with an observation operator. It is likely that the advantage of MLAs would be smaller if validation were done against in situ measurements of aerosol concentrations or even spectra. In the study area those do barely exist and typically do not separate between mineral and other types of aerosol, particularly the black carbon in urban areas, which makes it difficult to prove this conjecture.

The results of this study do indicate, however, that MLAs are a promising forecast tools in the environmental sciences which should be developed and tested further for more general use cases. We plan to identify potential missing factors of dust predictions and to optimize MLA as well as DM parameters used for dust forecast. We also plan to investigate the performance of MLAs and global numerical aerosol models in large scale simulations of air pollutants including dust particles. We believe these types of studies will help to identify influential factors reducing uncertainties of aerosol predictions over sources and receptors.

Acknowledgements

This work has been financially supported by EU 7th framework program ERA-CLIM (No. 265229) and the Austrian Science Funds FWF (Projects P25260-N29). We acknowledge scientists involved in the production of the MODIS, AERONET ECMWF ERA-Interim and MACC datasets used in this research work.

Reference

ABBASI, R., MORADI, M. H. & MOLAEEZADEH, S. F. Long-term prediction of blood pressure time series using multiple fuzzy functions. Biomedical Engineering (ICBME), 2014 21th Iranian Conference on, 2014. IEEE, 124-127.

ALBAYRAK, A., WEI, J., PETRENKO, M., LYNNES, C. & LEVY, R. C. 2013. Global bias adjustment for MODIS aerosol optical thickness using neural network. *Journal of Applied Remote Sensing,* 7**,** 073514-073514.

BATTITI, R. 1994. Using mutual information for selecting features in supervised neural net learning. *IEEE Transactions on neural networks,* 5**,** 537-550.

BENEDETTI, A., MORCRETTE, J. J., BOUCHER, O., DETHOF, A., ENGELEN, R., FISHER, M., FLENTJE, H., HUNEEUS, N., JONES, L. & KAISER, J. 2009. Aerosol analysis and forecast in the European centre for medium-range weather forecasts integrated forecast system: 2. Data assimilation. *Journal of Geophysical Research: Atmospheres,* 114.

BOLOORANI, A. D., NABAVI, S. O., BAHRAMI, H. A., MIRZAPOUR, F., KAVOSI, M., ABASI, E. & AZIZI, R. 2014. Investigation of dust storms entering Western Iran using remotely sensed data and synoptic analysis. *Journal of Environmental Health Science and Engineering,* 12**,** 124.

BREIMAN, L. 2001. Random forests. *Machine learning,* 45**,** 5-32.

BURGES, C. J. 1998. A tutorial on support vector machines for pattern recognition. *Data mining and knowledge discovery,* 2**,** 121-167.

CARBONELL, J. G., MICHALSKI, R. S. & MITCHELL, T. M. 1983. An overview of machine learning. *Machine learning.* Springer.

CHANDRASHEKAR, G. & SAHIN, F. 2014. A survey on feature selection methods. *Computers & Electrical Engineering,* 40**,** 16-28.

CHIN, M., GINOUX, P., KINNE, S., TORRES, O., HOLBEN, B. N., DUNCAN, B. N., MARTIN, R. V., LOGAN, J. A., HIGURASHI, A. & NAKAJIMA, T. 2002. Tropospheric aerosol optical thickness from the GOCART model and comparisons with satellite and Sun photometer measurements. *Journal of the atmospheric sciences,* 59**,** 461-483.

CORTES, C. & VAPNIK, V. 1995. Support-vector networks. *Machine learning,* 20**,** 273-297.

COWIE, S. M., MARSHAM, J. H. & KNIPPERTZ, P. 2015. The importance of rare, high-wind events for dust uplift in northern Africa. *Geophysical Research Letters,* 42**,** 8208-8215.

DEE, D., UPPALA, S., SIMMONS, A., BERRISFORD, P., POLI, P., KOBAYASHI, S., ANDRAE, U., BALMASEDA, M., BALSAMO, G. & BAUER, P. 2011. The ERA-Interim reanalysis: Configuration and performance of the data assimilation system. *Quarterly Journal of the Royal Meteorological Society,* 137**,** 553-597.

DENG, A., STAUFFER, D. R., DUDHIA, J., OTTE, T. & HUNTER, G. K. Update on analysis nudging FDDA in WRF-ARW. 8th Annual WRF User's Workshop, National Center for Atmospheric Research, Boulder, Colorado, 2007. 11-15.

DUBOVIK, O., HOLBEN, B., ECK, T. F., SMIRNOV, A., KAUFMAN, Y. J., KING, M. D., TANRÉ, D. & SLUTSKER, I. 2002. Variability of absorption and optical properties of key aerosol types observed in worldwide locations. *Journal of the atmospheric sciences,* 59**,** 590-608.

EFRON, B. & TIBSHIRANI, R. J. 1994. *An introduction to the bootstrap*, CRC press.

FAST, J. D., GUSTAFSON, W. I., EASTER, R. C., ZAVERI, R. A., BARNARD, J. C., CHAPMAN, E. G., GRELL, G. A. & PECKHAM, S. E. 2006. Evolution of ozone, particulates, and aerosol direct radiative forcing in the vicinity of Houston using a fully coupled meteorology-chemistry-aerosol model. *Journal of Geophysical Research: Atmospheres,* 111.

GINOUX, P., CHIN, M., TEGEN, I., PROSPERO, J. M., HOLBEN, B., DUBOVIK, O. & LIN, S. J. 2001. Sources and distributions of dust aerosols simulated with the GOCART model. *Journal of Geophysical Research: Atmospheres,* 106**,** 20255-20273.

GRELL, G. A., PECKHAM, S. E., SCHMITZ, R., MCKEEN, S. A., FROST, G., SKAMAROCK, W. C. & EDER, B. 2005. Fully coupled "online" chemistry within the WRF model. *Atmospheric Environment,* 39**,** 6957-6975.

HAMON, J. 2013. *Optimisation combinatoire pour la sélection de variables en régression en grande dimension: Application en génétique animale.* Université des Sciences et Technologie de Lille-Lille I.

HEMPEL, S., SHETTY, K. D., SHEKELLE, P. G., RUBENSTEIN, L. V., DANZ, M. S., JOHNSEN, B. & DALAL, S. R. 2012. Machine learning methods in systematic reviews: identifying quality improvement intervention evaluations.

HSU, N. C., TSAY, S.-C., KING, M. D. & HERMAN, J. R. 2004. Aerosol properties over bright-reflecting source regions. *IEEE Transactions on Geoscience and Remote Sensing,* 42**,** 557-569.

HYER, E., REID, J. & ZHANG, J. 2011. An over-land aerosol optical depth data set for data assimilation by filtering, correction, and aggregation of MODIS Collection 5 optical depth retrievals. *Atmospheric Measurement Techniques,* 4**,** 379-408.

KABOODVANDPOUR, S., AMANOLLAHI, J., QHAVAMI, S. & MOHAMMADI, B. 2015. Assessing the accuracy of multiple regressions, ANFIS, and ANN models in predicting dust storm occurrences in Sanandaj, Iran. *Natural Hazards,* 78**,** 879-893.

KLINGMÜLLER, K., POZZER, A., METZGER, S., STENCHIKOV, G. L. & LELIEVELD, J. 2016. Aerosol optical depth trend over the Middle East. *Atmospheric Chemistry and Physics,* 16**,** 5063-5073.

KONATE, A. A., PAN, H., KHAN, N. & YANG, J. H. 2015. Generalized regression and feed-forward back propagation neural networks in modelling porosity from geophysical well logs. *Journal of Petroleum Exploration and Production Technology,* 5**,** 157-166.

KOTSIANTIS, S. B., ZAHARAKIS, I. & PINTELAS, P. 2007. Supervised machine learning: A review of classification techniques.

KUHN, M. 2008. Caret package. *Journal of Statistical Software,* 28**,** 1-26.

KUHN, M. 2012a. Variable importance using the caret package.

KUHN, M. 2012b. Variable selection using the caret package. *URL {http://topepo.github.io/caret/index.html}*.

KUMAR, R., BARTH, M., PFISTER, G., NAJA, M. & BRASSEUR, G. 2014. WRF-Chem simulations of a typical pre-monsoon dust storm in northern India: influences on aerosol optical properties and radiation budget. *Atmospheric Chemistry and Physics,* 14**,** 2431-2446.

LARY, D. J., ALAVI, A. H., GANDOMI, A. H. & WALKER, A. L. 2016. Machine learning in geosciences and remote sensing. *Geoscience Frontiers,* 7**,** 3-10.

LECUN, Y., BENGIO, Y. & HINTON, G. 2015. Deep learning. *Nature,* 521**,** 436-444.

LIU, M., WESTPHAL, D. L., WALKER, A. L., HOLT, T. R., RICHARDSON, K. A. & MILLER, S. D. 2007. COAMPS real-time dust storm forecasting during Operation Iraqi Freedom. *Weather and forecasting,* 22**,** 192-206.

LIU, X., HUNEEUS, N., SCHULZ, M., BALKANSKI, Y., GRIESFELLER, J., PROSPERO, J., KINNE, S., BAUER, S., BOUCHER, O. & CHIN, M. 2011a. Global dust model intercomparison in AeroCom phase I. *Atmospheric Chemistry and Physics,* 11**,** 7781.

LIU, Y., DORIGO, W. A., PARINUSSA, R., DE JEU, R. A., WAGNER, W., MCCABE, M. F., EVANS, J. & VAN DIJK, A. 2012. Trend-preserving blending of passive and active microwave soil moisture retrievals. *Remote Sensing of Environment,* 123**,** 280-297.

LIU, Y. Y., PARINUSSA, R., DORIGO, W. A., DE JEU, R. A., WAGNER, W., VAN DIJK, A., MCCABE, M. F. & EVANS, J. 2011b. Developing an improved soil moisture dataset by blending passive and active microwave satellite-based retrievals. *Hydrology and Earth System Sciences,* 15**,** 425.

MARTICORENA, B. & BERGAMETTI, G. 1995. Modeling the atmospheric dust cycle: 1. Design of a soil-derived dust emission scheme. *Journal of Geophysical Research: Atmospheres,* 100**,** 16415-16430.

MORCRETTE, J. J., BOUCHER, O., JONES, L., SALMOND, D., BECHTOLD, P., BELJAARS, A., BENEDETTI, A., BONET, A., KAISER, J. & RAZINGER, M. 2009. Aerosol analysis and forecast in the European Centre for medium-range weather forecasts integrated forecast system: Forward modeling. *Journal of Geophysical Research: Atmospheres,* 114.

NABAVI, S. O., HAIMBERGER, L. & SAMIMI, C. 2016. Climatology of dust distribution over West Asia from homogenized remote sensing data. *Aeolian Research,* 21**,** 93-107.

NABAVI, S. O., HAIMBERGER, L. & SAMIMI, C. 2017. Sensitivity of WRF-chem predictions to dust source function specification in West Asia. *Aeolian Research,* 24**,** 115-131.

PANINSKI, L. 2003. Estimation of entropy and mutual information. *Neural computation,* 15**,** 1191-1253.

PARRELLA, F. 2007. Online support vector regression. *Master's Thesis, Department of Information Science, University of Genoa, Italy*.

SAYER, A., MUNCHAK, L., HSU, N., LEVY, R., BETTENHAUSEN, C. & JEONG, M. J. 2014. MODIS Collection 6 aerosol products: Comparison between Aqua's e-Deep Blue, Dark Target, and "merged" data sets, and usage recommendations. *Journal of Geophysical Research: Atmospheres,* 119.

SCHNEIDER, U., BECKER, A., FINGER, P., MEYER-CHRISTOFFER, A., RUDOLF, B. & ZIESE, M. 2011. GPCC full data reanalysis version 6.0 at 0.5: monthly land-surface precipitation from rain-gauges built on GTS-based and historic data. doi: 10.5676/DWD_GPCC. *FD_M_V6_050*.

SHAO, Y., ISHIZUKA, M., MIKAMI, M. & LEYS, J. 2011. Parameterization of size-resolved dust emission and validation with measurements. *Journal of Geophysical Research: Atmospheres,* 116.

SKAMAROCK, W., KLEMP, J., DUDHIA, J., GILL, D., BARKER, D., DUDA, M., HUANG, X., WANG, W. & POWERS, J. 2008. A description of the Advanced Research WRF Version 3, NCAR technical note, Mesoscale and Microscale Meteorology Division. *National Center for Atmospheric Research, Boulder, Colorado, USA*.

SU, L. & FUNG, J. C. 2015. Sensitivities of WRF-Chem to dust emission schemes and land surface properties in simulating dust cycles during springtime over East Asia. *Journal of Geophysical Research: Atmospheres,* 120.

TAHERI SHAHRAIYNI, H. & SODOUDI, S. 2016. Statistical modeling approaches for PM10 prediction in urban areas; A review of 21st-century studies. *Atmosphere,* 7**,** 15.

TEGEN, I. 2003. Modeling the mineral dust aerosol cycle in the climate system. *Quaternary Science Reviews,* 22**,** 1821-1834.

TORGO, L., RIBEIRO, R. P., PFAHRINGER, B. & BRANCO, P. Smote for regression. Portuguese conference on artificial intelligence, 2013. Springer, 378-389.

TUCKER, C., PINZON, J. & BROWN, M. 2004. Global inventory modeling and mapping studies. *Global Land Cover Facility, University of Maryland, College Park, Maryland*.

VAPNIK, V. N. 1995. Introduction: Four periods in the research of the learning problem. *The Nature of Statistical Learning Theory.* Springer.

VICENTE-SERRANO, S. M., BEGUERÍA, S. & LÓPEZ-MORENO, J. I. 2010. A multiscalar drought index sensitive to global warming: the standardized precipitation evapotranspiration index. *Journal of climate,* 23**,** 1696-1718.

WAGNER, W., DORIGO, W., DE JEU, R., FERNANDEZ, D., BENVENISTE, J., HAAS, E. & ERTL, M. 2012. Fusion of active and passive microwave observations to create an essential climate variable data record on soil moisture. *ISPRS Annals of the Photogrammetry, Remote Sensing and Spatial Information Sciences (ISPRS Annals),* 7**,** 315-321.

YU, Y., NOTARO, M., LIU, Z., WANG, F., ALKOLIBI, F., FADDA, E. & BAKHRJY, F. 2015. Climatic controls on the interannual to decadal variability in Saudi Arabian dust activity: Toward the development of a seasonal dust prediction model. *Journal of Geophysical Research: Atmospheres,* 120**,** 1739-1758.

ZARANDI, M. F., ZARINBAL, M., GHANBARI, N. & TURKSEN, I. 2013. A new fuzzy functions model tuned by hybridizing imperialist competitive algorithm and simulated annealing. Application: Stock price prediction. *Information Sciences,* 222**,** 213-228.

ZHANG, W. & GOH, A. T. 2016. Multivariate adaptive regression splines and neural network models for prediction of pile drivability. *Geoscience Frontiers,* 7**,** 45-52.

ZHANG, Z., MA, C., XU, J., HUANG, J. & LI, L. 2015. A Novel Combinational Forecasting Model of Dust Storms Based on Rare Classes Classification Algorithm. *Geo-Informatics in Resource Management and Sustainable Ecosystem.* Springer.

PART III: SYNTHESIS AND OUTLOOK

6 Synthesis

This chapter is to combine findings of the individual manuscripts and to examine if conducted research could successfully address the research questions and hypotheses. In the following, each hypothesis is discussed using related achievements. The first hypothesis has challenged the applicability of remotely sensed data in the long-term study of the spatio-temporal distribution of dust storms in West Asia:

Hypothesis 1: The combination of remote sensing products such as TOMS-OMI AI, and SeaWiFS and MODIS DB AOD can reveal the climatology of dust storms in West Asia. It is expected that research findings indicate a significant increase of dust occurrence and expansion of dust sources in the region.

Manuscript 1 is prepared to test the first hypothesis by using long-term records (1980-2014) of Aerosol Index (AI) from TOMS and OMI instruments. Because of AI discontinuity, some preprocessing measures are taken. They contain the replacement of original values with a binary signal (dust/no dust) based on Varying Threshold (VT), the homogenization of binarized AI through the consideration of two separate VTs for TOMS and OMI eras, and the exclusion of invalid data between 2002 and 2004. Results show that the application of VT could amend artificially high/low values of AI particularly over western Saudi Arabia where highlands host a constant high boundary layer (AI). In addition, the evaluation of the refined AI against synoptic weather codes proves that it is able to reproduce changes in the dust frequency and extent of dust sources in a large scale. The tally of VT-based dust cases shows the frequent dust entrainment from sources in the east of Saudi Arabia during the study period, called permanent dusty areas. It also reveals the recent spatio-temporal expansion of dust sources in the east of Syria and northwest of Iraq, called emerging dusty areas. While June and July have been normally the peak period of dust activity in emerging areas, it is recently expanded into the whole studied warm months (Apr-Sep). The positive trend of dust storms in entire West Asia is mainly attributed to extreme droughts in the Fertile Crescent, with a peak during 2007–2012. Using MODIS DB AOD, the local-scale hot spots of dust emission in emerging and permanent areas are found to be concentrated in a

desert region called Al-jazireh and northern Saudi Arabia, respectively. Dust storms formed in these hot spots are transported to the south of Turkey and northwest of Iran by a Frontal lifting mechanism during spring. During summer, Shamal atmospheric pattern sweeps dust plumes from the northwest of Iraq to the southwest of Iran and the Persian Gulf countries.

The characterization of dust sources in West Asia can be seen as the main outcome of the first manuscript. In order to evaluate the reliability of determined dust sources, the second hypothesis has been formulated:

Hypothesis 2: The topography-based algorithm used by GSF cannot provide a realistic distribution of dust sources in West Asia. Instead, WASF as a remote sensing-based source function is more suitable to be used in dust modeling systems.

In the second step of the study, candidate source functions are implemented in three dust schemes of WRF-chem. Control (WRF-chem with GSF) and modified (WRF-chem with WASF) runs are evaluated against remotely sensed observations, including MODIS DB AOD and MISR AOD at 550 nm and profile data of CALIPSO extinction coefficient at 532 nm. Because WASF generally allocates less emission magnitude to dust source points than GSF, all modified runs are biased low to AOD observations. However, findings show the higher agreement (SCC) of modified WRF-chem simulations and observations, regardless of which dust scheme is considered. Among them, modified run of GOCART scheme yields the best performance with SCC of 0.65 and 0.63 against MODIS and MISR observations, respectively. It should be noted that both control and modified runs perform poorly (layer-stratified SCCs < 0.3) in reproducing the vertical distribution of extinction coefficient measured by CALIPSO. In addition, WASF expectedly, due to the allocation of lower emission potential, cause a stronger underestimation of extinction coefficient than GSF. However, like vertically integrated AOD, the agreement of WRF-chem simulations and CALIPSO observations improved at all studied vertical levels after the implementation of WASF. Modified runs, especially GOCART, even outperformed DREAM and MACC DODs over dust sources. These findings are supported by ground-based observations acquired from synoptic stations in the northwest of Iraq where the modified run of GOCART scheme got the highest percentage of correct detection (45.8 %) and the highest

Pierce skill score (28 %). The comparison of simulations with the only available AERONET station in the study area, located in Kuwait, shows that DREAM has yielded the best performance followed by modified AFWA which outperforms other WRF-chem runs and MACC. In spite of aforementioned achievements, modified runs still face high uncertainty over regions away from dust sources. This can be mainly because of remaining unknown dust sources in other parts of West Asia. In addition, the transportation of lifted dust, as well as the deposition schemes in WRF-chem, ought to be improved.

Although the outcomes of the second study leave us with the sense that future improvements can amend existing weaknesses of numerical dust modeling, it is tried to examine the feasibility of dust prediction using MLAs (the third manuscript). The third hypothesis is cautiously optimistic and anticipates the applicability of MLAs in dust prediction as follows:

Hypothesis 3: The promising performance of MLAs in engineering problems can be also achieved in dust prediction. Considering the fact that, here, MLAs are not elaborated and their standard settings are applied (e.g. Gaussian kernel for SVM or linear regression as the output-layer function of ANN) MLAs do not outperform DMs at this stage.

Five MLAs and two DMs are applied to predict dust abundance over West Asia. Due to the lack of ground-based observations, MODIS DB AOD was selected as the response variable to be predicted. Since the selection of influential predictors is a prerequisite for a successful MLA setup, according to literature and authors' experience, nine features are loosely selected as the potential predictors of dust formation. Then the six final inputs including Albedo, DUP, NDVI, soil temperature, precipitation, and SF are chosen through applying three types of feature selection criteria (FSC). Interestingly, all types of FSC determine SF as the most important predictor of dust forecast. Results also show that the level of importance assigned to each parameter, except SF, varies slightly depending on which type of FSC is employed. Although still better than DMs, significant prediction errors are found between the preliminary runs of MLAs and observation. This is found to be caused by the fact that none of the selected features can represent the contribution of advected dust to the total amount of AOD over the downstream region. Hence, the monthly area average of time-variant predictors over northwest of Iraq, as the main dust hot spot, are

taken as complementary predictors. The evaluation of MLA performance in the second run shows that they all yield much better performance than the preliminary runs and, again, DMs. Findings disclose that DMs fail to reproduce the amount of dust advected to the west of Iran which is reflected in the high bias of low DB AODs simulated by MACC and WRF-chem. Most likely, it is triggered by the fact that DMs do not resolve elevations in the west of Iran as a natural barrier against dust transportation. Finally, both DMs and MLAs underestimate DB AOD peaks which can be attributed to the rough resolution of variable datasets, remaining uncertainties in the dust source function, omission of some unknown influential factors and the scarcity of extreme cases.

Generally, it can be concluded that the combination of different satellite sensors is an efficient approach to derive the climatology of dust frequency in West Asia (the first manuscript). However, due to instrumental changes, caution has to be taken when using TOMS-OMI AI dataset as a continuous time series. The combination of AI and DB AOD disclosed a meaningful increase of dust frequency and expansion of dust sources in West Asia approaching the end of study period. The verification of identified dust sources (the second manuscript) testifies that the implementation of more accurate source function can significantly improve the performance of WRF-chem in West Asia, especially over dust sources. However, there may be other dust source points not taken into account by newly proposed source function (WASF) because of limitations in existing remote sensing tools and techniques. In addition, the emission is only one component of dust cycle and the optimization of dust models require the improvement of two other components including dust transport and deposition. The performance investigation of MLAs and DMs (the third manuscript) supports the hypothesis regarding the applicability of MLAs in dust prediction. Since the standard settings of MLAs are applied, it was not expected that MLAs can outperform DMs which is, unexpectedly, documented in the results though. It should be noticed that DMs are still favorable for the short-term forecasts and it is likely that the advantage of MLAs would be smaller if validation were done against in situ measurements of aerosol concentrations or even spectra, instead of using DB AOD at 550 nm.

7 Outlook

Recent progress in the algorithms of dust retrieval implemented on long-operating satellite data, such as TOMS-OMI AI and MODIS DB AOD, let us characterize dust activity in West Asia from 1980 to present (Nabavi et al., 2016). It was found that West Asia has two main dusty areas including the northwest of Iraq and the east of Saudi Arabia. They feed dust particles into Frontal and Shamal systems during cold and warm periods of the year, respectively. While dust sources in Iraq have recently formed because of successive droughts, eastern Saudi Arabia is known as an old origin of local and regional dust storms.

Significant differences between dust source functions obtained from previous analyses (Nabavi et al., 2016) and Ginoux et al. (2001) were inspiring to find out which source function is more realistic. To do so, both source functions were implemented in WRF-chem model. Results attested that newly proposed source function, called WASF, is much more consistent with the current status of dust distribution and it improves the accuracy of dust predictions in the region (Nabavi et al., 2017b).

In the third study it was tried to find the best strategy for the prediction of dust storms in the study area. Preliminary investigations showed that the efficiency of MLAs in regional dust prediction is underestimated by the literature. In fact, numerical dust models (DMs) have been mostly used as the only option for doing dust forecast. Hence, a comparative study of seven state of the art MLAs and DMs was conducted. Although both approaches have difficulties in reproducing extreme cases, findings indicate the higher capability of MLAs in dust prediction at least on a monthly basis. Keeping in mind the fact that any changes in settings of MLAs, study area, explanatory variables, and response variable can leave us with different results, study findings are convincing enough to put more efforts into the application of MLAs for dust prediction in West Asia and other dust-prone regions.

Like often this study faced with some limitations which constrain generalizability and utility of findings. As discussed before, instrumental changes caused discontinuity of AI acquired from TOMS and OMI instruments. The lack of temporal overlap period between reliable TOMS data and OMI data

makes it particularly challenging to apply sophisticated homogenization methods (Haimberger et al., 2012, Mears et al., 2003) on AI records. Therefore, two separate VTs for TOMS and OMI eras were considered which of course cannot deal with all uncertainties raised by this issue. Recently, the DB AOD algorithm has been implemented such that it can be applied to data from AVHRR instrument which can realize the ambition of having access to more consistent, long-term records of dust activity from the 1980s onward (Sayer et al., 2017).

In this study, thresholds, especially those used for the determination of dust occurrence, are determined based on literature (Ginoux et al., 2001, Ginoux et al., 2012, Karimi et al., 2012) or authors' experience which both are very subjective. This may explain some of the differences between findings of presented study and literature and, possibly, future attempts. Because most of these subjective thresholds are used for the specification of dust source function, author plans to replace WASF with other remote sensing-based source functions, like the one proposed by Chen et al. (2017), in future studies. This type of source function provides the total amount of dust emission (not the potential of emission) without using common thresholds.

In the second study, DOD, instead of AOD, provided by MACC and DREAM was used to be compared with WRF-chem simulations. It is because DREAM does not provide AOD and both auxiliary simulations (from MACC and DREAM) should be comparable. Because the study is conducted during summer months when dust is the prominent aerosol in the region, this cannot cause such a big difference in results which degrade the overall reliability of achievements. However, the third manuscript shows that MACC AOD expectedly has a slightly better agreement with AOD observations than its DOD does.

It should be also taken into account that the performance of models are also affected by the time period and area over which the study is conducted. For example, while WRF-chem outperformed MACC in the second study, it is reverse in the third study where the study period is extended from three summer months of 2008-2012 to the six warm months of 2003 to 2013.

Although MLAs could outperform DMs in the monthly prediction of dust abundance, they inherently cannot provide any information about the physical

relationship between predictors and response variables. This requires modelers to put a lot of effort into a deep understanding of true drivers of predictant before they are used as inputs of MLAs. Because none of studies were allotted to the identification of factors inducing dust formation, we should put the caveat here that there may be some influential factors which are omitted during the selection of inputs for MLAs. Because of this, author has recently prepared a proposal in which a significant amount of time is allotted to the selection of predictors governing air pollutants including dust in West Asia.

In addition to aforementioned issues, this study has led to some research recommendations which may be considered by future studies:

1. Conduct similar studies in regions with better in situ observation records
2. Try MLAs with aerosol concentrations rather than AOD as predictands. It is important to understand the cause of poor performance of DMs. Does it come from the observation operators or has already the aerosol concentration been badly predicted?
3. Apply DMs and MLAs to climate model output (both recent past and future). Do climate models driven with observed SSTs have realistic soil moisture and other predictors in the study region. How does dust occurrence behave in future under different climate scenarios?
4. What are the prospects of reducing dust by smart land use (reforestation, irrigation, other measures against erosion, etc.)

8 Bibliography

ABBASI, R., MORADI, M. H. & MOLAEEZADEH, S. F. Long-term prediction of blood pressure time series using multiple fuzzy functions. Biomedical Engineering (ICBME), 2014 21th Iranian Conference on, 2014. IEEE, 124-127.

ABDI VISHKAEE, F., FLAMANT, C., CUESTA, J., OOLMAN, L., FLAMANT, P. & KHALESIFARD, H. R. 2012. Dust transport over Iraq and northwest Iran associated with winter Shamal: A case study. *Journal of Geophysical Research: Atmospheres,* 117.

ADAMS, A. M., PROSPERO, J. M. & ZHANG, C. 2012. CALIPSO-derived three-dimensional structure of aerosol over the Atlantic Basin and adjacent continents. *Journal of Climate,* 25**,** 6862-6879.

ADEFOLALU, D. 1984. On bioclimatological aspects of Harmattan dust haze in Nigeria. *Archives for meteorology, geophysics, and bioclimatology, Series B,* 33**,** 387-404.

AHMAD, S. P., TORRES, O., BHARTIA, P., LEPTOUKH, G. & KEMPLER, S. Aerosol index from TOMS and OMI measurements. Proc. of the 86th AMS Annual Meeting, 2006.

AHMAD, Z., BHARTIA, P. & KROTKOV, N. 2004. Spectral properties of backscattered UV radiation in cloudy atmospheres. *Journal of Geophysical Research: Atmospheres,* 109.

AHRENS, C. D. 2011. *Essentials of meteorology: an invitation to the atmosphere,* Cengage Learning.

ALBAYRAK, A., WEI, J., PETRENKO, M., LYNNES, C. & LEVY, R. C. 2013. Global bias adjustment for MODIS aerosol optical thickness using neural network. *Journal of Applied Remote Sensing,* 7**,** 073514-073514.

ALIZADEH CHOOBARI, O., ZAWAR-REZA, P. & STURMAN, A. 2013. Simulation of the spatial distribution of mineral dust and its direct radiative forcing over Australia. *Tellus B: Chemical and Physical Meteorology,* 65**,** 19856.

ASHRAFI, K., SHAFIEPOUR-MOTLAGH, M., ASLEMAND, A. & GHADER, S. 2014. Dust storm simulation over Iran using HYSPLIT. *Journal of environmental health science and engineering,* 12**,** 9.

AZIZI, G., SHAMSIPOUR, A., MIRI, M. & SAFARRAD, T. 2012. Synoptic and remote sensing analysis of dust events in southwestern Iran. *Natural hazards,* 64**,** 1625-1638.

BAGNOLD, R. A. 2012. *The physics of blown sand and desert dunes,* Courier Corporation.

BASART, S., PÉREZ, C., NICKOVIC, S., CUEVAS, E. & BALDASANO, J. 2012. Development and evaluation of the BSC-DREAM8b dust regional model over Northern Africa, the Mediterranean and the Middle East. *Tellus B: Chemical and Physical Meteorology,* 64**,** 18539.

BENEDETTI, A., MORCRETTE, J. J., BOUCHER, O., DETHOF, A., ENGELEN, R., FISHER, M., FLENTJE, H., HUNEEUS, N., JONES, L. & KAISER, J. 2009. Aerosol analysis and forecast in the European centre for medium-range weather forecasts integrated forecast system: 2. Data assimilation. *Journal of Geophysical Research: Atmospheres,* 114.

BIAN, H., TIE, X.-X., CAO, J.-J., YING, Z. M., HAN, S.-Q. & XUE, Y. 2011. Analysis of a severe dust storm event over China: Application of WRF-dust model.

BIBI, H., ALAM, K., CHISHTIE, F., BIBI, S., SHAHID, I. & BLASCHKE, T. 2015. Intercomparison of MODIS, MISR, OMI, and CALIPSO aerosol optical depth retrievals for four locations on the Indo-Gangetic plains and validation against AERONET data. *Atmospheric Environment,* 111**,** 113-126.

BOLOORANI, A. D., NABAVI, S., AZIZI, R. & BAHRAMI, H. 2013. Characterization of dust storm sources in Western Iran using a synthetic approach. *Advances in Meteorology, Climatology and Atmospheric Physics.* Springer.

BOLOORANI, A. D., NABAVI, S. O., BAHRAMI, H. A., MIRZAPOUR, F., KAVOSI, M., ABASI, E. & AZIZI, R. 2014. Investigation of dust storms entering Western Iran using remotely sensed data and synoptic analysis. *Journal of Environmental Health Science and Engineering,* 12**,** 124.

BREIMAN, L. 2001. Random forests. *Machine learning,* 45**,** 5-32.

BULLARD, J., BADDOCK, M., MCTAINSH, G. & LEYS, J. 2008. Sub-basin scale dust source geomorphology detected using MODIS. *Geophysical Research Letters,* 35.

BULLARD, J. E., HARRISON, S. P., BADDOCK, M. C., DRAKE, N., GILL, T. E., MCTAINSH, G. & SUN, Y. 2011. Preferential dust sources: A geomorphological classification designed for use in global dust-cycle models. *Journal of Geophysical Research: Earth Surface,* 116.

CAO, H., AMIRASLANI, F., LIU, J. & ZHOU, N. 2015. Identification of dust storm source areas in West Asia using multiple environmental datasets. *Science of the Total Environment,* 502**,** 224-235.

CARBONELL, J. G., MICHALSKI, R. S. & MITCHELL, T. M. 1983. An overview of machine learning. *Machine learning.* Springer.

CAVAZOS-GUERRA, C. & TODD, M. C. 2012. Model simulations of complex dust emissions over the Sahara during the West African monsoon onset. *Advances in Meteorology,* 2012.

CHANG, Q., ZHANG, J., JIAO, W. & YAO, F. 2016. A comparative analysis of the NDVIg and NDVI3g in monitoring vegetation phenology changes in the Northern Hemisphere. *Geocarto International***,** 1-20.

CHEN, C., DUBOVIK, O., LAPYONAK, T., HENZE, D. K., CHIN, M., LI, L., DERIMIAN, Y., LITVINOV, P. & DUCOS, F. 2017. Inferring emissions of desert dust and primary carbonaceous aerosol from PARASOL/GRASP retrievals.

CHIN, M., GINOUX, P., KINNE, S., TORRES, O., HOLBEN, B. N., DUNCAN, B. N., MARTIN, R. V., LOGAN, J. A., HIGURASHI, A. & NAKAJIMA, T. 2002. Tropospheric aerosol optical thickness from the GOCART model and comparisons with satellite and Sun photometer measurements. *Journal of the atmospheric sciences,* 59**,** 461-483.

CORTES, C. & VAPNIK, V. 1995. Support-vector networks. *Machine learning,* 20**,** 273-297.

CUEVAS, E., CAMINO, C., BENEDETTI, A., BASART, S., TERRADELLAS, E., BALDASANO, J., MORCRETTE, J., MARTICORENA, B., GOLOUB, P. & MORTIER, A. 2015. The MACC-II 2007–2008 reanalysis: atmospheric dust evaluation and characterization over northern Africa and the Middle East. *Atmos. Chem. Phys,* 15**,** 3991-4024.

DEE, D., UPPALA, S., SIMMONS, A., BERRISFORD, P., POLI, P., KOBAYASHI, S., ANDRAE, U., BALMASEDA, M., BALSAMO, G. & BAUER, P. 2011. The ERA-Interim reanalysis: Configuration and performance of the data assimilation system. *Quarterly Journal of the Royal Meteorological Society,* 137**,** 553-597.

DEFRIES, R. & TOWNSHEND, J. 1994. NDVI-derived land cover classifications at a global scale. *International Journal of Remote Sensing,* 15**,** 3567-3586.

ECK, T., HOLBEN, B., REID, J., DUBOVIK, O., SMIRNOV, A., O'NEILL, N., SLUTSKER, I. & KINNE, S. 1999. Wavelength dependence of the optical depth of biomass burning, urban, and desert dust aerosols. *Journal of Geophysical Research: Atmospheres,* 104**,** 31333-31349.

FAST, J. D., GUSTAFSON, W. I., EASTER, R. C., ZAVERI, R. A., BARNARD, J. C., CHAPMAN, E. G., GRELL, G. A. & PECKHAM, S. E. 2006. Evolution of ozone, particulates, and aerosol direct radiative forcing in the vicinity of Houston using a fully coupled meteorology-chemistry-aerosol model. *Journal of Geophysical Research: Atmospheres,* 111.

FURMAN, H. K. H. 2003. Dust storms in the Middle East: sources of origin and their temporal characteristics. *Indoor and Built Environment,* 12**,** 419-426.

GARCÍA, O., DÍAZ, A., EXPOSITO, F., DIAZ, J., DUBOVIK, O., DUBUISSON, P., ROGER, J. C., ECK, T., SINYUK, A. & DERIMIAN, Y. 2008. Validation of AERONET estimates of atmospheric solar fluxes and aerosol radiative forcing by ground-based broadband measurements. *Journal of Geophysical Research: Atmospheres,* 113.

GERIVANI, H., LASHKARIPOUR, G. R., GHAFOORI, M. & JALALI, N. 2011. The source of dust storm in Iran: a case study based on geological information and rainfall data. *Carpathian Journal of Earth and Environmental Sciences,* 6.

GINOUX, P., CHIN, M., TEGEN, I., PROSPERO, J. M., HOLBEN, B., DUBOVIK, O. & LIN, S. J. 2001. Sources and distributions of dust aerosols simulated with the GOCART model. *Journal of Geophysical Research: Atmospheres,* 106**,** 20255-20273.

GINOUX, P., PROSPERO, J. M., GILL, T. E., HSU, N. C. & ZHAO, M. 2012. Global-scale attribution of anthropogenic and natural dust sources and their emission rates based on MODIS Deep Blue aerosol products. *Reviews of geophysics,* 50.

GOUDIE, A. & MIDDLETON, N. J. 2006. *Desert dust in the global system,* Springer Science & Business Media.

GRELL, G. A., PECKHAM, S. E., SCHMITZ, R., MCKEEN, S. A., FROST, G., SKAMAROCK, W. C. & EDER, B. 2005. Fully coupled "online" chemistry within the WRF model. *Atmospheric Environment,* 39**,** 6957-6975.

HAAS, E., KIDD, R., DORIGO, W., CHUNG, D., DE JEU, R., PARINUSSA, R. & WAGNER, W. Soil Moisture CCI: Production Of The Most Complete And Consistent Global Soil Moisture Data Record. ESA Living Planet Symposium, 2013. 61.

HAIMBERGER, L., TAVOLATO, C. & SPERKA, S. 2012. Homogenization of the global radiosonde temperature dataset through combined comparison with reanalysis background series and neighboring stations. *Journal of Climate,* 25**,** 8108-8131.

HAMON, J. 2013. *Optimisation combinatoire pour la sélection de variables en régression en grande dimension: Application en génétique animale.* Université des Sciences et Technologie de Lille-Lille I.

HAO, X. & QU, J. J. 2007. Saharan dust storm detection using moderate resolution imaging spectroradiometer thermal infrared bands. *Journal of Applied Remote Sensing,* 1**,** 013510.

HEMPEL, S., SHETTY, K. D., SHEKELLE, P. G., RUBENSTEIN, L. V., DANZ, M. S., JOHNSEN, B. & DALAL, S. R. 2012. Machine learning methods in systematic reviews: identifying quality improvement intervention evaluations.

HOLBEN, B. N., ECK, T., SLUTSKER, I., TANRE, D., BUIS, J., SETZER, A., VERMOTE, E., REAGAN, J., KAUFMAN, Y. & NAKAJIMA, T. 1998. AERONET—A federated instrument network and data archive for aerosol characterization. *Remote sensing of environment,* 66**,** 1-16.

HSU, N., GAUTAM, R., SAYER, A., BETTENHAUSEN, C., LI, C., JEONG, M., TSAY, S.-C. & HOLBEN, B. 2012. Global and regional trends of aerosol optical depth over land and ocean using SeaWiFS measurements from 1997 to 2010. *Atmospheric Chemistry and Physics Discussions,* 12**,** 8465-8501.

HSU, N. C., TSAY, S.-C., KING, M. D. & HERMAN, J. R. 2004. Aerosol properties over bright-reflecting source regions. *Geoscience and Remote Sensing, IEEE Transactions on,* 42**,** 557-569.

HYER, E., REID, J. & ZHANG, J. 2011. An over-land aerosol optical depth data set for data assimilation by filtering, correction, and aggregation of MODIS Collection 5 optical depth retrievals. *Atmospheric Measurement Techniques,* 4**,** 379-408.

INNESS, A., BAIER, F., BENEDETTI, A., BOUARAR, I., CHABRILLAT, S., CLARK, H., CLERBAUX, C., COHEUR, P., ENGELEN, R. & ERRERA, Q. 2013. The MACC reanalysis: an 8 yr data set of atmospheric composition. *Atmospheric chemistry and physics,* 13**,** 4073-4109.

KABOODVANDPOUR, S., AMANOLLAHI, J., QHAVAMI, S. & MOHAMMADI, B. 2015. Assessing the accuracy of multiple regressions, ANFIS, and ANN models in predicting dust storm occurrences in Sanandaj, Iran. *Natural Hazards,* 78**,** 879-893.

KADOMURA, H. 2009. Combating desertification and drought. *Land Use, Land Cover and Soil Sciences-Volume V: Dry Lands and Desertification***,** 233.

KAHN, R. A., GAITLEY, B. J., GARAY, M. J., DINER, D. J., ECK, T. F., SMIRNOV, A. & HOLBEN, B. N. 2010. Multiangle Imaging SpectroRadiometer global aerosol product assessment by comparison with the Aerosol Robotic Network. *Journal of Geophysical Research: Atmospheres,* 115.

KAHN, R. A., GAITLEY, B. J., MARTONCHIK, J. V., DINER, D. J., CREAN, K. A. & HOLBEN, B. 2005. Multiangle Imaging Spectroradiometer (MISR) global aerosol optical depth validation based on 2 years of coincident Aerosol Robotic Network (AERONET) observations. *Journal of Geophysical Research: Atmospheres,* 110.

KARIMI, N., MORIDNEJAD, A., GOLIAN, S., VALI SAMANI, J. M., KARIMI, D. & JAVADI, S. 2012. Comparison of dust source identification techniques over land in the Middle East region using MODIS data. *Canadian Journal of Remote Sensing,* 38**,** 586-599.

KIM, D., CHIN, M., BIAN, H., TAN, Q., BROWN, M. E., ZHENG, T., YOU, R., DIEHL, T., GINOUX, P. & KUCSERA, T. 2013. The effect of the dynamic surface bareness on dust source function, emission, and distribution. *Journal of Geophysical Research: Atmospheres,* 118**,** 871-886.

KISS, P., JANOSI, I. & TORRES, O. 2007. Early calibration problems detected in TOMS Earth-Probe aerosol signal. *Geophysical Research Letters,* 34.

KLINGMÜLLER, K., POZZER, A., METZGER, S., STENCHIKOV, G. L. & LELIEVELD, J. 2016. Aerosol optical depth trend over the Middle East. *Atmospheric Chemistry and Physics,* 16**,** 5063-5073.

KOK, J. F., PARTELI, E. J., MICHAELS, T. I. & KARAM, D. B. 2012. The physics of wind-blown sand and dust. *Reports on Progress in Physics,* 75**,** 106901.

KONATE, A. A., PAN, H., KHAN, N. & YANG, J. H. 2015. Generalized regression and feed-forward back propagation neural networks in modelling porosity from geophysical well logs. *Journal of Petroleum Exploration and Production Technology,* 5**,** 157-166.

KOTSIANTIS, S. B., ZAHARAKIS, I. & PINTELAS, P. 2007. Supervised machine learning: A review of classification techniques.

KOVEN, C. D. & FUNG, I. 2008. Identifying global dust source areas using high-resolution land surface form. *Journal of Geophysical Research: Atmospheres,* 113.

KUMAR, R., BARTH, M., PFISTER, G., NAJA, M. & BRASSEUR, G. 2014. WRF-Chem simulations of a typical pre-monsoon dust storm in northern India: influences on aerosol optical properties and radiation budget. *Atmospheric Chemistry and Physics,* 14**,** 2431-2446.

LECUN, Y., BENGIO, Y. & HINTON, G. 2015. Deep learning. *Nature,* 521**,** 436-444.

LEE, J. A., GILL, T. E., MULLIGAN, K. R., ACOSTA, M. D. & PEREZ, A. E. 2009. Land use/land cover and point sources of the 15 December 2003 dust storm in southwestern North America. *Geomorphology,* 105**,** 18-27.

LI, J., CARLSON, B. E. & LACIS, A. A. 2015. How well do satellite AOD observations represent the spatial and temporal variability of PM 2.5 concentration for the United States? *Atmospheric environment,* 102**,** 260-273.

LI, Y., LIU, Y. & WU, J. 2016. HIGH RESOLUTION AEROSOL OPTICAL DEPTH MAPPING OF BEIJING USING LANSAT8 IMAGERY. *ISPRS-International Archives of the Photogrammetry, Remote Sensing and Spatial Information Sciences***,** 1309-1312.

LIOU, K.-N. & CHOU, M.-D. 2008. *Recent Progress in Atmospheric Sciences: Applications to the Asia-Pacific Region,* World Scientific.

LIU, M., WESTPHAL, D. L., WALKER, A. L., HOLT, T. R., RICHARDSON, K. A. & MILLER, S. D. 2007. COAMPS real-time dust storm forecasting during Operation Iraqi Freedom. *Weather and forecasting,* 22**,** 192-206.

LIU, Y., DORIGO, W. A., PARINUSSA, R., DE JEU, R. A., WAGNER, W., MCCABE, M. F., EVANS, J. & VAN DIJK, A. 2012. Trend-preserving blending of passive and active microwave soil moisture retrievals. *Remote Sensing of Environment,* 123**,** 280-297.

LIU, Y. Y., PARINUSSA, R., DORIGO, W. A., DE JEU, R. A., WAGNER, W., VAN DIJK, A., MCCABE, M. F. & EVANS, J. 2011. Developing an improved soil moisture dataset by blending passive and active microwave satellite-based retrievals. *Hydrology and Earth System Sciences,* 15**,** 425.

LORENZ, R. D., BALME, M. R., GU, Z., KAHANPÄÄ, H., KLOSE, M., KURGANSKY, M. V., PATEL, M. R., REISS, D., ROSSI, A. P. & SPIGA, A. 2016. History and applications of dust devil studies. *Space Science Reviews,* 203**,** 5-37.

MA, X., BARTLETT, K., HARMON, K. & YU, F. 2013. Comparison of AOD between CALIPSO and MODIS: significant differences over major dust and biomass burning regions. *Atmospheric Measurement Techniques,* 6**,** 2391-2401.

MAHOWALD, N. M. & DUFRESNE, J. L. 2004. Sensitivity of TOMS aerosol index to boundary layer height: Implications for detection of mineral aerosol sources. *Geophysical Research Letters,* 31.

MARTICORENA, B. 2014. Dust production mechanisms. *Mineral Dust.* Springer.

MARTICORENA, B. & BERGAMETTI, G. 1995. Modeling the atmospheric dust cycle: 1. Design of a soil-derived dust emission scheme. *Journal of Geophysical Research: Atmospheres,* 100**,** 16415-16430.

MCTAINSH, G. & PITBLADO, J. 1987. Dust storms and related phenomena measured from meteorological records in Australia. *Earth Surface Processes and Landforms,* 12**,** 415-424.

MEARS, C. A., SCHABEL, M. C. & WENTZ, F. J. 2003. A reanalysis of the MSU channel 2 tropospheric temperature record. *Journal of Climate,* 16**,** 3650-3664.

MIDDLETON, N. & KANG, U. 2017. Sand and Dust Storms: Impact Mitigation. *Sustainability,* 9**,** 1053.

MORCRETTE, J. J., BOUCHER, O., JONES, L., SALMOND, D., BECHTOLD, P., BELJAARS, A., BENEDETTI, A., BONET, A., KAISER, J. & RAZINGER, M. 2009. Aerosol analysis and forecast in the European Centre for medium-range weather forecasts integrated forecast system: Forward modeling. *Journal of Geophysical Research: Atmospheres,* 114.

MORIDNEJAD, A., KARIMI, N. & ARIYA, P. A. 2015a. A new inventory for middle east dust source points. *Environmental monitoring and assessment,* 187**,** 1-11.

MORIDNEJAD, A., KARIMI, N. & ARIYA, P. A. 2015b. Newly desertified regions in Iraq and its surrounding areas: Significant novel sources of global dust particles. *Journal of Arid Environments,* 116**,** 1-10.

NABAVI, S. O., HAIMBERGER, L., ABBASI, R. & SAMIMI, C. 2017a. Prediction of Aerosol Optical Depth in West Asia using Dust Models and Machine Learning Algorithms. *Atmospheric Environment (in progress).*

NABAVI, S. O., HAIMBERGER, L. & SAMIMI, C. 2016. Climatology of dust distribution over West Asia from homogenized remote sensing data. *Aeolian Research,* 21**,** 93-107.

NABAVI, S. O., HAIMBERGER, L. & SAMIMI, C. 2017b. Sensitivity of WRF-chem predictions to dust source function specification in West Asia. *Aeolian Research,* 24**,** 115-131.

NOVLAN, D. J. A synoptic climatology of blowing dust events in El Paso, Texas from 1932-2005. 2007.

PARAJULI, S. P., YANG, Z. L. & KOCUREK, G. 2014. Mapping erodibility in dust source regions based on geomorphology, meteorology, and remote sensing. *Journal of Geophysical Research: Earth Surface,* 119**,** 1977-1994.

PINZON, J. E. & TUCKER, C. J. 2014. A non-stationary 1981–2012 AVHRR NDVI3g time series. *Remote Sensing,* 6**,** 6929-6960.

PROSPERO, J. M., GINOUX, P., TORRES, O., NICHOLSON, S. E. & GILL, T. E. 2002. Environmental characterization of global sources of atmospheric soil dust identified with the Nimbus 7 Total Ozone Mapping Spectrometer (TOMS) absorbing aerosol product. *Reviews of geophysics,* 40**,** 2-1-2-31.

QU, J. J., HAO, X., KAFATOS, M. & WANG, L. 2006. Asian dust storm monitoring combining Terra and Aqua MODIS SRB measurements. *IEEE Geoscience and remote sensing letters,* 3**,** 484-486.

RUDOLF, B., HAUSCHILD, H., RUETH, W. & SCHNEIDER, U. 1994. Terrestrial precipitation analysis: Operational method and required density of point measurements. *Global precipitations and climate change.* Springer.

RUDOLF, B. & SCHNEIDER, U. Calculation of gridded precipitation data for the global land-surface using in-situ gauge observations. Proc. Second Workshop of the Int. Precipitation Working Group, 2005. 231-247.

SAMADI, M., BOLOORANI, A. D., ALAVIPANAH, S. K., MOHAMADI, H. & NAJAFI, M. S. 2014. Global dust Detection Index (GDDI); a new remotely sensed methodology for dust storms detection. *Journal of Environmental Health Science and Engineering,* 12**,** 20.

SAYER, A., HSU, N., BETTENHAUSEN, C., JEONG, M., HOLBEN, B. & ZHANG, J. 2012. Global and regional evaluation of over-land spectral aerosol optical depth retrievals from SeaWiFS.

SAYER, A., HSU, N., BETTENHAUSEN, C. & JEONG, M. J. 2013. Validation and uncertainty estimates for MODIS Collection 6 "Deep Blue" aerosol data. *Journal of Geophysical Research: Atmospheres,* 118**,** 7864-7872.

SAYER, A., HSU, N., LEE, J., CARLETTA, N., CHEN, S. H. & SMIRNOV, A. 2017. Evaluation of NASA Deep Blue/SOAR aerosol retrieval algorithms applied to AVHRR measurements. *Journal of Geophysical Research: Atmospheres*.

SCHNEIDER, U., BECKER, A., FINGER, P., MEYER-CHRISTOFFER, A., RUDOLF, B. & ZIESE, M. 2011. GPCC full data reanalysis version 6.0 at 0.5: monthly land-surface precipitation from rain-gauges built on GTS-based and historic data. doi: 10.5676/DWD_GPCC. *FD_M_V6_050*.

SHAO, Y. 2008. *Physics and modelling of wind erosion*, Springer Science & Business Media.

SHAO, Y., ISHIZUKA, M., MIKAMI, M. & LEYS, J. 2011a. Parameterization of size-resolved dust emission and validation with measurements. *Journal of Geophysical Research: Atmospheres,* 116.

SHAO, Y., WYRWOLL, K.-H., CHAPPELL, A., HUANG, J., LIN, Z., MCTAINSH, G. H., MIKAMI, M., TANAKA, T. Y., WANG, X. & YOON, S. 2011b. Dust cycle: An emerging core theme in Earth system science. *Aeolian Research,* 2**,** 181-204.

SKAMAROCK, W., KLEMP, J., DUDHIA, J., GILL, D., BARKER, D., DUDA, M., HUANG, X., WANG, W. & POWERS, J. 2008. A description of the Advanced Research WRF Version 3, NCAR technical note, Mesoscale and Microscale Meteorology Division. *National Center for Atmospheric Research, Boulder, Colorado, USA*.

SMOYDZIN, L., TELLER, A., TOST, H., FNAIS, M. & LELIEVELD, J. 2012. Impact of mineral dust on cloud formation in a Saharan outflow region. *Atmospheric Chemistry and Physics,* 12**,** 11383-11393.

SU, L. & FUNG, J. C. 2015. Sensitivities of WRF-Chem to dust emission schemes and land surface properties in simulating dust cycles during springtime over East Asia. *Journal of Geophysical Research: Atmospheres,* 120.

SUN, W., HU, Y., MACDONNELL, D. G., WEIMER, C. & BAIZE, R. R. 2016. Technique to separate lidar signal and sunlight. *Optics express,* 24**,** 12949-12954.

TAHERI SHAHRAIYNI, H. & SODOUDI, S. 2016. Statistical modeling approaches for PM10 prediction in urban areas; A review of 21st-century studies. *Atmosphere,* 7**,** 15.

TAKEMI, T. & SEINO, N. 2005. Dust storms and cyclone tracks over the arid regions in east Asia in spring. *Journal of Geophysical Research: Atmospheres,* 110.

TAN, F., SAN LIM, H., ABDULLAH, K., YOON, T. L. & HOLBEN, B. 2015. AERONET data–based determination of aerosol types. *Atmospheric Pollution Research,* 6**,** 682-695.

THORSEN, T. J., FU, Q. & COMSTOCK, J. 2011. Comparison of the CALIPSO satellite and ground-based observations of cirrus clouds at the ARM TWP sites. *Journal of Geophysical Research: Atmospheres,* 116.

THORSTEINSSON, T., GÍSLADÓTTIR, G., BULLARD, J. & MCTAINSH, G. 2011. Dust storm contributions to airborne particulate matter in Reykjavík, Iceland. *Atmospheric environment,* 45**,** 5924-5933.

TIME MAGAZINE 2011. The 10 Most Air-Polluted Cities in the World.

TORRES, O., BHARTIA, P., HERMAN, J., AHMAD, Z. & GLEASON, J. 1998. Derivation of aerosol properties from satellite measurements of backscattered ultraviolet radiation: Theoretical basis. *Journal of Geophysical Research: Atmospheres (1984–2012),* 103**,** 17099-17110.

TUCKER, C. J., PINZON, J. E., BROWN, M. E., SLAYBACK, D. A., PAK, E. W., MAHONEY, R., VERMOTE, E. F. & EL SALEOUS, N. 2005. An extended AVHRR 8-km NDVI dataset compatible with MODIS and SPOT vegetation NDVI data. *International Journal of Remote Sensing,* 26**,** 4485-4498.

UNCCD 2001. *Global alarm: dust and sandstorms from the world's drylands*, United Nations Publications.

VAPNIK, V. N. 1995. Introduction: Four periods in the research of the learning problem. *The Nature of Statistical Learning Theory*. Springer.

VASILKOV, A., JOINER, J., SPURR, R., BHARTIA, P. K., LEVELT, P. & STEPHENS, G. 2008. Evaluation of the OMI cloud pressures derived from rotational Raman scattering by comparisons with other satellite data and radiative transfer simulations. *Journal of Geophysical Research: Atmospheres,* 113.

VUKOVIC, A., VUJADINOVIC, M., PEJANOVIC, G., ANDRIC, J., KUMJIAN, M., DJURDJEVIC, V., DACIC, M., PRASAD, A. K., EL-ASKARY, H. & PARIS, B. 2014. Numerical simulation of "an American haboob".

WAGNER, W., DORIGO, W., DE JEU, R., FERNANDEZ, D., BENVENISTE, J., HAAS, E. & ERTL, M. 2012. Fusion of active and passive microwave observations to create an essential climate variable data record on soil moisture. *ISPRS Annals of the Photogrammetry, Remote Sensing and Spatial Information Sciences (ISPRS Annals),* 7**,** 315-321.

WALKER, A. L., LIU, M., MILLER, S. D., RICHARDSON, K. A. & WESTPHAL, D. L. 2009. Development of a dust source database for mesoscale forecasting in southwest Asia. *Journal of Geophysical Research: Atmospheres,* 114.

WARD, D. & COTTON, W. 2011. A method for forecasting cloud condensation nuclei using predictions of aerosol physical and chemical properties from WRF/Chem. *Journal of Applied Meteorology and Climatology,* 50**,** 1601-1615.

WASHINGTON, R., TODD, M., MIDDLETON, N. J. & GOUDIE, A. S. 2003. Dust-storm source areas determined by the total ozone monitoring spectrometer and surface observations. *Annals of the Association of American Geographers,* 93**,** 297-313.

YU, Y., NOTARO, M., LIU, Z., WANG, F., ALKOLIBI, F., FADDA, E. & BAKHRJY, F. 2015. Climatic controls on the interannual to decadal variability in Saudi Arabian dust activity: Toward the development of a seasonal dust prediction model. *Journal of Geophysical Research: Atmospheres,* 120**,** 1739-1758.

ZHANG, J. & REID, J. 2010. A decadal regional and global trend analysis of the aerosol optical depth using a data-assimilation grade over-water MODIS and Level 2 MISR aerosol products. *Atmospheric Chemistry and Physics,* 10**,** 10949-10963.

ZHANG, W. & GOH, A. T. 2016. Multivariate adaptive regression splines and neural network models for prediction of pile drivability. *Geoscience Frontiers,* 7**,** 45-52.